

**HIGH DIELECTRIC CONSTANT POLYMER NANOCOMPOSITES
FOR EMBEDDED CAPACITOR APPLICATIONS**

A Dissertation
Presented to
The Academic Faculty

by

Jiongxin Lu

In Partial Fulfillment
of the Requirements for the Degree
Doctor of Philosophy in the
School of Materials Science and Engineering

Georgia Institute of Technology
December 2008

**HIGH DIELECTRIC CONSTANT POLYMER NANOCOMPOSITES
FOR EMBEDDED CAPACITOR APPLICATIONS**

Approved by:

Dr. C.P. Wong, Advisor
School of Materials Science and
Engineering
Georgia Institute of Technology

Dr. Z. L. Wang
School of Materials Science and
Engineering
Georgia Institute of Technology

Dr. Rina Tannenbaum
School of Materials Science and
Engineering
Georgia Institute of Technology

Dr. M. L. Liu
School of Materials Science and
Engineering
Georgia Institute of Technology

Dr. Karl Jacob
School of Polymer, Textile and Fiber
Engineering
Georgia Institute of Technology

Date Approved: Sept. 8, 2008

ACKNOWLEDGEMENTS

This doctoral dissertation is dedicated to my beloved parents for their love, encouragements, and support throughout my entire PhD life.

I am deeply indebted to my advisor, Dr. C.P. Wong, for his guidance and support throughout the course of this research. His profound knowledge and insights, dedication to research, enthusiasm for work, have been and will continue to be a great source of inspiration for me. Apart from the academic and technical training received in Dr. Wong's group, other important qualities and skills like self-motivation, time management, and leadership will always benefit me in my future career and life. I would like to extend my gratitude to Dr. Zhonglin Wang, Dr. Meilin Liu, Dr. Rina Tennenbaum and Dr. Karl Jacob for serving on my committee as well as providing invaluable insights and recommendations.

I would like to thank the faculty and staff members in the National Science Foundation Microsystems Packaging Research Center and the School of Materials Science and Engineering. They are Dr. Rao R. Tummala, Dr. Swapan Bhattacharya, Dr. Leyla Conrad, Dr. Isaac Robin Abothu, Dr. Raj Pulugurtha, Ms. Yolande Berta, Ms. Susan Bowman, Ms. Vicki Speights, Ms. Mechelle Kitchings, Ms. Karen Hutcheson, Mr. James Cagle, and Mr. Tim Banks.

My special thanks go to my fellow co-workers in Dr. Wong's group, for all the discussions and helps I received from Dr. Kyoung-Sik Moon, Dr. Zhuqing Zhang, Dr. Lianhua Fan, Dr. Jianwen Xu, Dr. Fei Xiao, Dr. Hai Dong, Dr. Yangyang Sun, Dr. Hongjin Jiang, Dr. Lingbo Zhu, Dr. Brian Englert, Mr. Suresh Pothukuchi, Dr. Lara

Martin, Dr. Yi Li, Mr. Yonghao Xiu, Ms. Guseul Yun, Mr. Qizhen Liang, Mr. Rongwei Zhang, Mr. Wei Lin, Mr. Owen Hildreth. I would also like to acknowledge my undergraduate research assistants who worked with me during the course of my PhD research. They are Mr. Sunil Smith, Mr. Danny Nguyen, Mr. Neil Patel and Mr. Robert Fee.

I would like to express my appreciation to Dr. Andrew Hunt and Dr. Zhiyong Zhao from nGimat Co. for their discussion and help with the high frequency test, to Mr. Mark Taylor and Mr. William Fox from TA Instruments for their help with the thermal analysis instruments.

This work was financially supported by the National Science Foundation through grant ECS-0203412 and grant ECS-0501405. Special thanks is extended to ALPS Electric, Inc., nGimat Co., Korean Institute of Science and Technology, and Oak-Mitsui Technologies for their interests and support of this work.

Once again, I would like to thank my parents for their unconditional love and continuous support. Without them, this dissertation would not be possible.

TABLE OF CONTENTS

	Page
ACKNOWLEDGEMENTS	iii
LIST OF TABLES	x
LIST OF FIGURES	xi
SUMMARY	xvi
 <u>CHAPTER</u>	
1 INTRODUCTION	1
1.1 Overview of Electronic Packaging	1
1.2 Passive Devices	5
1.3 Embedded Passives	6
1.3.1 Motivations	6
1.3.2 Capacitors	8
1.4 Dielectric Mechanisms	11
1.4.1 Capacitance, Dielectric Constant and Polarization	11
1.4.2 Dielectric Loss	15
1.5 Overview of Dielectric Material Options for Embedded Capacitors	16
1.5.1 Ferroelectric Ceramic Materials	17
1.5.2 Other Ceramic Materials	18
1.5.3 Polymer Materials	20
1.5.4 Ferroelectric Ceramic/Polymer Composites	21
1.5.5 Conductive Filler/Polymer Composites	23
1.5.6 All-Organic Polymer Composites	26
1.6 New Concepts and Current Trend	27
1.6.1 Nanocomposites	27
1.6.2 Nanodielectrics	36
1.6.3 Performance Enhancement of Hi-k Nanocomposites	37
1.7 Challenges for Embedded Capacitor Materials	43

1.8 Research Objectives	44
2 EXPERIMENTAL	46
2.1 Materials	46
2.1.1 Epoxy	46
2.1.2 Benzocyclobutene (BCB)	54
2.1.3 Polyaniline (PANI)	55
2.2 Preparation of Nanoparticles and Nanocomposites	59
2.2.1 Synthesis of Metal Nanoparticles	59
2.2.2 Preparation of Nanocomposites	61
2.3 Instrumentation and Characterization Procedure	61
2.3.1 Differential Scanning Calorimeter (DSC)	61
2.3.2 Thermogravimetric Analyzer (TGA)	62
2.3.3 LCR Meter	63
2.3.4 Surface Profiler	63
2.3.5 X-Ray Diffractometer	64
2.3.6 Scanning Electron Microscope (SEM) and Energy Dispersive X-Ray Spectroscopy (EDX or EDS)	64
2.3.7 Transmission Electron Microscope (TEM)	65
2.3.8 Fourier Transform Infrared Spectroscopy (FTIR)	66
2.3.9 Ultraviolet-visible (UV-Vis) Spectroscopy	66
2.3.10 X-ray Photoelectron Spectroscopy (XPS)	67
2.3.11 Proton Nuclear Magnetic Resonance (^1H NMR)	67
3 CONTROL OF DIELECTRIC LOSS OF HIGH-K COMPOSITES BY INCORPORATION OF METAL NANOPARTICLES AND THEIR SIZE AND SIZE DISTRIBUTION EFFECT	68
3.1 Introduction	68
3.2 Experimental	72
3.2.1 Materials	72
3.2.2 <i>In-Situ</i> Formation of Ag Nanoparticles in an Epoxy Matrix	72
3.2.3 Preparation of CB/Epoxy Composite and Ag/CB/epoxy Nanocomposite	73
3.2.4 Characterization	73
3.3 Results and Discussion	74

3.3.1	Two-Step Preparation of Ag/CB/Epoxy Nanocomposite	74
3.3.2	Effect of Capping Agent	77
3.3.3	Effect of Curing and Processing Procedure	80
3.3.4	Estimation of Filler Loading	82
3.3.5	Dielectric Properties of Ag/CB/epoxy Nanocomposites	84
3.4	Conclusions	90
4	SILVER/POLYMER NANOCOMPOSITES AS HIGH-K POLYMER MATRIX FOR DIELECTRIC COMPOSITES WITH IMPROVED DIELECTRIC PERFORMANCE	91
4.1	Introduction	91
4.2	Experimental	94
4.2.1	Materials	94
4.2.2	<i>In-situ</i> Photochemical Synthesis of Ag Nanoparticles	95
4.2.3	Preparation of Al/epoxy and Al/Ag-epoxy Composite	95
4.2.4	Characterization	95
4.3	Results and Discussion	97
4.3.1	Morphology and Composition	97
4.3.2	Dielectric Characterization	100
4.4	Conclusions	106
5	NANO-SCALE PARTICLE SURFACE MODIFICATION FOR TAILORING DIELECTRIC PROPERTIES OF POLYMER NANOCOMPOSITES	108
5.1	Introduction	108
5.2	Experimental	111
5.2.1	Materials	111
5.2.2	Surface Modification of Ag Nanoparticles	112
5.2.3	Preparation of SMN/Epoxy Composites	112
5.2.4	Material Characterization	113
5.2.5	Capacitor Prototype Fabrication and Dielectric Property Measurements	114
5.3	Results and Discussion	115
5.3.1	Characterization of Surface Modified Nanoparticles (SMN)	115
5.3.2	Characterization of Surface Modified Nanoparticles (SMN)/ Polymer Nanocomposites	120

5.3.3	Electrical and Dielectric Property Measurements	122
5.4	Conclusions	129
6	THE INFLUENCE OF CONNECTIVITY ON THE DIELECTRIC PROPERTIES OF NANOPARTICLE-BASED HIGH-K COMPOSITE MATERIALS	130
6.1	Introduction	130
6.2	Experimental	133
6.2.1	Materials	133
6.2.2	Preparation of Ag Nanoparticles with Different Morphology	133
6.2.3	Preparation of Ag/Epoxy Nanocomposites	133
6.2.4	Materials Characterization	134
6.3	Results and Discussion	135
6.3.1	Synthesis of Ag Nanoparticles with Varied Connectivity	135
6.3.2	Characterization of Synthesized Ag Nanoparticles	137
6.3.3	Dielectric Properties of Epoxy Nanocomposites Based on the Ag Nanoparticles with Varied Connectivity	139
6.4	Conclusions	141
7	ALL-ORGANIC HIGH-K POLYANILINE/EPOXY COMPOSITES VIA IN-SITU POLYMERIZATION	143
7.1	Introduction	143
7.2	Experimental	146
7.2.1	Materials	146
7.2.2	Preparation of PANI/Epoxy Composites by Simple Solution Mixing Method	146
7.2.3	Preparation of PANI/Epoxy Composites by <i>In-situ</i> Polymerization Method	146
7.2.4	Instrumental Analysis	148
7.3	Results and Discussion	149
7.3.1	PANI/Epoxy Composites Prepared by Simple Solution Mixing Method	149
7.3.2	PANI/Epoxy Composites Prepared by an <i>In-situ</i> Polymerization Method	150
7.3.3	Morphological Study of <i>In-situ</i> Formed PANI/epoxy Composites	155

7.3.4 Dielectric and Electrical Property Study of <i>In-situ</i> Formed PANI/Epoxy Composites	157
7.4 Conclusions	162
8 CONCLUSIONS AND SUGGESTED DIRECTIONS FOR FUTURE WORK	163
8.1 Conclusions	163
8.2 Suggested Directions for Future Work	168
8.2.1 Modeling of Structure and Dielectric Properties of New High- <i>k</i> Materials	168
8.2.2 Core-shell Structure via Layer-by-Layer (LbL) Assembly	169
APPENDIX A: AUTHOR'S AWARDS, PATENTS, AND PUBLICATIONS	173
REFERENCES	177

LIST OF TABLES

	Page
Table 1-1. Applications and properties of capacitors.	9
Table 1-2. Dielectric properties, specific capacitance and energy density of some common dielectrics.	15
Table 1-3. Summary of ceramic/polymer composite candidates.	23
Table 1-4. Summary of the conductive filler/polymer composite candidates.	25
Table 2-1. Typical filler types and potential property modifications in epoxy formulations.	53
Table 3-1. Size range of the Ag nanoparticles obtained.	80
Table 3-2. The electrical and dielectric properties of CB/Ag/epoxy nanocomposite.	85
Table 4-1. DC characteristic breakdown strength at 63.2 % failure probability (E_0) of Al/epoxy composites and Al/Ag-epoxy composites with different Al filler loadings.	106
Table 5-1. Data analysis from XPS spectra of SMN.	118
Table 5-2. Dielectric properties of SMN/epoxy nanocomposites containing SMN treated in different conditions.	126
Table 7-1. ^1H NMR data for Ani-CSA monomer in CDCl_3 .	152
Table 7-2. Dielectric properties of <i>in-situ</i> formed PANI/epoxy composites with different PANI contents @ 10 kHz.	158
Table 7-3. Comparison of the morphology of PANI/epoxy composites prepared by simple solution mixing method and <i>in-situ</i> polymerization method.	159
Table 7-4. Dielectric properties of 15 wt. % <i>in-situ</i> formed PANI/epoxy composites cured with various hardeners @ 10 kHz.	161

LIST OF FIGURES

	Page
Figure 1-1. Schematic representation of electronic packaging hierarchy.	3
Figure 1-2. Evolution of electronic packaging.	4
Figure 1-3. Schematic illustration of embedded passives integrated into the laminate substrate.	6
Figure 1-4. Schematic representation of the size advantages of the embedded passives as compared to discrete passives.	7
Figure 1-5. Distribution of capacitor values in typical portable consumer equipments.	8
Figure 1-6. Power supply and power distribution system without and with a decoupling capacitor.	10
Figure 1-7. Schematics of four major polarization mechanisms	13
Figure 1-8. (a) Diagram of an MLC capacitor: blue and yellow regions represent metallic and dielectric layers, respectively; (b) Diagram of a BLC capacitor: green areas represent reduced (semiconductor) ferroelectric grains while orange lines correspond to oxidized (insulator) grain boundaries; (c) Diagram of a percolative capacitor: blue and yellow regions represent metallic and dielectric material, respectively.	18
Figure 1-9. Schematic illustration of the dispersion and distribution states of nanofillers.	29
Figure 1-10. Morphologies of block copolymer-metal systems involving spherical micelle formation of the amphiphilic block copolymers: (a) cherry morphology, (b) raspberry morphology, (c) strawberry morphology, (d) proposed red currant morphology.	33
Figure 1-11. Schematic summary of nanoparticle modification.	34
Figure 1-12. Schematics of composite films based on micron-sized particles and nanoparticles.	37
Figure 1-13. Dielectric constant changes with BaTiO ₃ powder loading and size.	38
Figure 1-14. (a) HRTEM micrograph of a 100 nm Al particle with an oxide thickness about 2.8 nm and (b) dielectric properties of Al composites as a function of filler loading.	41

Figure 1-15. The dependence of dielectric constant and dielectric loss tangent values on silver volume fraction and frequency.	42
Figure 2-1. Chemical structures of liquid bisphenol A and cycloaliphatic epoxy resins.	47
Figure 2-2. Chemical structures of curing agents (a) MHHPA and (b) Anchor 1040.	49
Figure 2-3. Reaction mechanism of tertiary amine-catalyzed epoxy/anhydride reaction.	49
Figure 2-4. Reaction mechanism of a primary amine curing agent with an epoxy.	50
Figure 2-5. Reaction mechanism of an amine-boron trifluoride complex with an epoxy proposed by Harris et al.	51
Figure 2-6. Chemical structure of 1-methylimidazole and 2E4MZ-CN.	52
Figure 2-7. Reaction mechanism with imidazole catalyst.	52
Figure 2-8. Structure of BCB monomer.	55
Figure 2-9. General chemical formula of PANI.	56
Figure 2-10. Structural formula of undoped PANI _{EB} .	56
Figure 2-11. Bipolaron structure of doped PANI _{ES} .	57
Figure 2-12. Polaron structure of doped PANI _{ES} .	58
Figure 3-1. (a) TEM micrograph of carbon black; (b) dielectric constant and dissipation factor of carbon black/polymer composites as a function of filler loading.	69
Figure 3-2. TEM micrograph of Ag/CB/epoxy composite prepared by one-pot method.	77
Figure 3-3. TEM micrographs of Ag/epoxy composite (a) w/ APS (1 in molar ratio w.r.t. AgNO ₃) and (b) w/o APS.	78
Figure 3-4. TEM micrographs of uncured Ag/epoxy mixtures in the presence of a capping agent with [CA]/[AgNO ₃] ratio (a) R = 1, (b) R = 0.6, (c) R = 0.4 and (d) R = 0.2.	80
Figure 3-5. SEM images of cured Ag/epoxy nanocomposite for 16.08K magnification and the inset for 41.85K magnification.	81
Figure 3-6. XRD patterns of (a) Ag/epoxy composite and (b) Ag/CB/epoxy composite.	82
Figure 3-7. TGA studies of neat epoxy, Ag/epoxy mixture, CB/epoxy mixture and Ag/CB/epoxy mixture.	83

Figure 3-8. The dependence of (a) k and (b) $\tan\delta$ at 10 kHz on the loading level of Ag nanoparticles.	85
Figure 3-9. k and $\tan\delta$ values of (a) 4.2Ag/19.6CB/epoxy composites and (b) 6.2Ag/14.6CB/epoxy composites (dashed curve) with various concentrations of a capping agent ($R = [CA]/[AgNO_3]$).	87
Figure 3-10. (a) k and (b) $\tan\delta$ values of 5Ag/20CB/epoxy composites with various concentration of a capping agent ($R = [CA]/[AgNO_3]$) at different frequencies.	89
Figure 4-1. (a) TEM micrograph and (b) histogram of Ag nanoparticles synthesized by an in-situ photochemical reduction in epoxy resin.	98
Figure 4-2. SEM images of cured composites containing 70 wt. % Al filler: (a) Al/epoxy composite for 1 K magnification; (b) Al/epoxy composite for 5 K magnification; (c) Al/Ag-epoxy composite for 1 K magnification; and (d) Al/Ag-epoxy composite for 5 K magnification.	99
Figure 4-3. Dielectric constant (k) values of Al/epoxy and Al/Ag-epoxy composites as a function of Al filler loading (@ 10 kHz). Dielectric loss tangent ($\tan\delta$) values of Al/epoxy and Al/Ag-epoxy composites are displayed in the inset.	102
Figure 4-4. (a) k and (b) $\tan\delta$ values Al/epoxy composites and Al/Ag-epoxy composites with different Al filler loadings as a function of frequency.	103
Figure 4-5. Dielectric breakdown statistics of (a) Al/epoxy composites and (b) Al/Ag-epoxy composites with different Al filler loadings plotted as a Weibull distribution.	105
Figure 5-1. FTIR spectra of untreated nanoparticles and SMN treated in different conditions.	116
Figure 5-2. HRTEM micrographs of SMN.	117
Figure 5-3. XPS general survey and high resolution scan spectra of SMN.	118
Figure 5-4. XRD spectra of unmodified nanoparticles and SMN.	119
Figure 5-5. DSC isothermal curves of unmodified nanoparticles and SMN.	120
Figure 5-6. DSC curves and T_g s of cured unmodified nanoparticle/epoxy composite and SMN/epoxy composites with different SMN loadings.	121
Figure 5 7. SEM image of cured SMN/epoxy nanocomposite.	122

Figure 5-8. Dielectric properties of SMN/epoxy composites with different SMN loadings and different modification degree: (a) loading effects on k values, (b) loading effects on $\tan\delta$ values, and (c) frequency effects on k values.	124
Figure 5-9. Schematic representation of proposed mechanism of surface modification of Ag nanoparticles by APS.	127
Figure 5-10. I-V characteristics of unmodified nanoparticle/epoxy nanocomposite and SMN/epoxy nanocomposites with different SMN loadings and different modification degree.	128
Figure 6-1. Schematic representation of geometric morphologies of the nanofiller distribution in a two-phase material in (a) dispersed structure and (b) aggregated structure.	132
Figure 6-2. TEM images of Ag nanoparticles with different morphology: (a) Ag_a and (b) Ag_d.	136
Figure 6-3. FTIR spectra of synthesized nanoparticles Ag_a (solid line) and pure resorcinol (dashed line).	137
Figure 6-4. General survey XPS spectrum of Ag nanoparticle.	138
Figure 6-5. TGA curves of Ag nanoparticles with different morphology.	139
Figure 6-6. (a) k and (b) $\tan\delta$ values of Ag/polymer composites containing Ag nanoparticles with more aggregated structure (Ag_a) and more discrete structure (Ag_d).	140
Figure 7-1. Syntheses of aniline salt monomer Ani-CSA and PANI/epoxy composites via an <i>in-situ</i> polymerization of Ani-CSA in the epoxy matrix.	147
Figure 7-2. Dielectric properties of PANI-PTSA/epoxy composites with different PANI contents @ 10 kHz.	150
Figure 7-3. FT-IR spectra of (a) Ani-CSA monomer and (b) <i>in-situ</i> formed PANI/epoxy composite.	151
Figure 7-4. ^1H NMR spectrum of Ani-CSA monomer in CDCl_3 .	152
Figure 7-5. UV-Vis spectrum of an <i>in-situ</i> formed PANI/epoxy in DMSO.	153
Figure 7-6. DSC curves of neat epoxy and <i>in-situ</i> formed PANI/epoxy composites with different PANI contents.	154
Figure 7-7. TGA diagrams of <i>in-situ</i> formed PANI/epoxy composites with different PANI contents and neat PANI.	155

Figure 7-8. SEM micrographs of in-situ PANI/epoxy composites with (a) 8 wt. %, (b) 15 wt. %, (c) 20 wt. %, and (d) 25 wt. % PANI. 156

Figure 7-9. Frequency dependence of (a) k and (b) $\tan\delta$ of *in-situ* formed PANI/epoxy composites with different PANI contents. 160

Figure 8-1. Schematic of the LbL film deposition process using two typical polyions, the sodium salt of poly(styrene sulfonate) and poly(allyamine hydrochloride). 170

Figure 8-2. Schematic presentation of core-shell nanoparticle system formed via LbL assembly. 171

SUMMARY

Driven by ever growing demands of miniaturization, increased functionality, high performance and low cost for microelectronic products and packaging, new and unique solutions in IC and system integration, such as system-on-chip (SOC) and system-in-package (SiP), system-on-package (SOP), have been hot topics recently. Embedded passives will be one of the key emerging techniques for realizing the system integration. As an alternative to discrete components, embedded passives offer various advantages, including higher component density, increased functionality, improved electrical performance, increased design flexibility, improved reliability and reduced unit cost. Novel materials for embedded capacitor applications are in great demand, for which a high dielectric constant (k), low dielectric loss and process compatibility with printed circuit boards (PCBs) are the most important prerequisites. To date, no available material satisfies all these prerequisites and research is needed to develop materials for embedded capacitor applications. Conductive filler/polymer composites are likely candidate material because they show a dramatic increase in their dielectric constant close to the percolation threshold. One of the major hurdles for this type of high- k composites is the high dielectric loss inherent in these systems. This research designed and developed nanocomposites based on nanoparticles with controlled parameters to fulfill the balance between sufficiently high- k and low dielectric loss, which satisfied the requirements for embedded capacitor applications.

This work involved the synthesis of the metal nanoparticles with different parameters including size, size distribution, aggregation and surface properties, and an investigation on how these varied parameters impact the dielectric properties of the high-

k nanocomposites incorporated with these metal nanoparticles. The nanocomposites based on these varied nanoparticles were prepared using both *ex-situ* and *in-situ* techniques. The dielectric behaviors of the nanocomposites were studied systematically over a range of frequencies to determine the dependence of dielectric constant, dielectric loss tangent and dielectric strength on these parameters.

Silver (Ag) nanoparticles of different size and size distribution were *in-situ* formed in a polymer matrix by appropriate selection of capping agent and the ratio of capping agent to Ag precursor, and then incorporated into high- k composite materials. Study results suggest that the size and size distribution of Ag nanoparticles in the nanocomposite have significant influence on the dielectric properties of the composite system and result in different properties over different frequency ranges. It was found that Ag nanoparticles of small size and narrow size distribution had a low dielectric loss tangent while maintaining high dielectric constant.

The effect of high- k polymer matrix on the dielectric characteristics of polymer nanocomposites was also studied and the results suggest that the Ag-epoxy high- k polymer matrix effectively enhance the dielectric constant while maintaining the low dielectric loss of the high- k composites. By using an *in-situ* photochemical reduction method, uniformly dispersed Ag nanoparticles in the size of less than 15 nm were generated in polymer matrices. Self-passivated aluminum (Al) particles were incorporated into this Ag-epoxy matrix and the dielectric properties of the as-prepared composite materials were investigated. The composites showed more than 50% increase in k values as compared with an Al/neat epoxy composite with the same filler loading of

Al. The dielectric loss tangent of the Al/Ag-epoxy composites was below 0.1, which meets the requirement for embedded decoupling capacitors.

To better utilize the commercially available Ag nanoparticles, surface modification of nanoparticles was employed in order to change the surface chemistry and physical properties of nanoparticles and therefore improve dispersion of nanoparticles in the polymer matrix and tailor the dielectric properties of corresponding polymer nanocomposites. The surface coating layer formed via surface modification of the metal nanoparticle improves the dielectric performance of the nanocomposites by decreasing the dielectric loss, enhancing the dielectric breakdown strength. The experiments provided information about different surface modification conditions such as surface modification agent type and concentration, solvent media etc., which play complex roles in the quality and degree of the surface modification and allow for effective manipulation of the dielectric properties.

Apart from the size, size distribution and surface property effect, the effect of connectivity in terms of aggregation status of the metal nanoparticles on the dielectric properties of the nanocomposites was investigated as well. Ag nanoparticles with more discrete structure render much lower dielectric loss tangent compared to the nanocomposites with Ag nanoparticles of more aggregated structure. For an epoxy nanocomposite with 65 wt. % Ag nanoparticles of discrete structure, the k value reaches 96 and the $\tan\delta$ value remains as low as 0.036.

In addition to the metal conductive filler, the composites fabricated by dispersing an organic material possessing very high dielectric constant, such as polyaniline (PANI), in a polymer matrix were found to exhibit high- k as well. The *in-situ* polymerization of

an aniline salt within epoxy matrices successfully prepared PANI/epoxy composites with various PANI contents. A PANI/epoxy composite prepared in this fashion exhibited a high dielectric constant close to 3000, a dielectric loss tangent less than 0.5 at 10 kHz and at room temperature.

In summary, material and process innovations were explored to reduce the dielectric loss sufficiently while maintain the high- k of the nanocomposites, and correlations were sought between the metal nanoparticles parameters such as size, size distribution, connectivity in terms of aggregation status, surface properties etc. and the dielectric properties of nanocomposites with these metal nanoparticles incorporated.

CHAPTER 1

INTRODUCTION

1.1 Overview of Electronic Packaging

Ever since the invention of silicon integrated circuits (IC), the electronic industry has sustainably evolved and profoundly impacted the human life by providing new technology and products in the computer, telecommunication, automotive, and consumer electronics such as notebook computers, cellular phones, digital cameras, personal digital assistant (PDA) and more. As electronic products continue to miniaturize, increase in performance, and broaden in applications, it will be necessary to improve electronic packaging technologies to enable tomorrow's electronic systems. Consequently, electronic packaging becomes the focus of an intense development effort and the challenge of the microelectronics industry today.^{1,2}

Despite the different approaches taken to package the IC and electronic systems, the electronic packaging technology is, in essence, an art of interconnection, protection and ergonomic configuration of the system components with an aim of minimizing the profile and maximizing the performance of the IC and electronic system, while fulfilling these four major basic functions: (1) providing an electrical path to power the circuits; (2) distributing signals onto and off the IC chip; (3) removing the heat generated by the circuits; and (4) supporting and protecting the chips from hostile environments. Typical electronic systems are composed of several layers or levels of packaging, and each of them has distinctive types of interconnection devices associated with it. Figure 1-1

schematically represents the multi-level hierarchy of electronic packaging.³ The first level package establishes interconnection between an IC chip and a module. It must provide the required number of contacts for power and signal transmission, maintain thermal expansion compatibility between the chip and the second level package, and provide a thermal path for heat removal, while minimizing transmission delay and electrical noise. This is generally accomplished by three major techniques including wire bonding, flip-chip bonding, and tape automated bonding (TAB). The second-level packaging refers to the process of joining a module or packaged IC substrate with a circuit board or a card, the most common one being a conventional printed wiring board (PWB). The card contains the necessary power and signal lines to handle the communications between the chips and the third level package. The current second-level packaging technologies include pin through hole (PTH), peripheral surface mount technology (SMT), and surface-mount-array (SMA) technology. The third-level packaging is the process of placing the card onto a motherboard or interconnecting between PWBs. The emerging of new technology has blurred the distinction between different levels of packaging. For example, the chip-on-board (COB) technology, where an IC is directly attached onto a PCB, may be considered a level 1.5 package.⁴

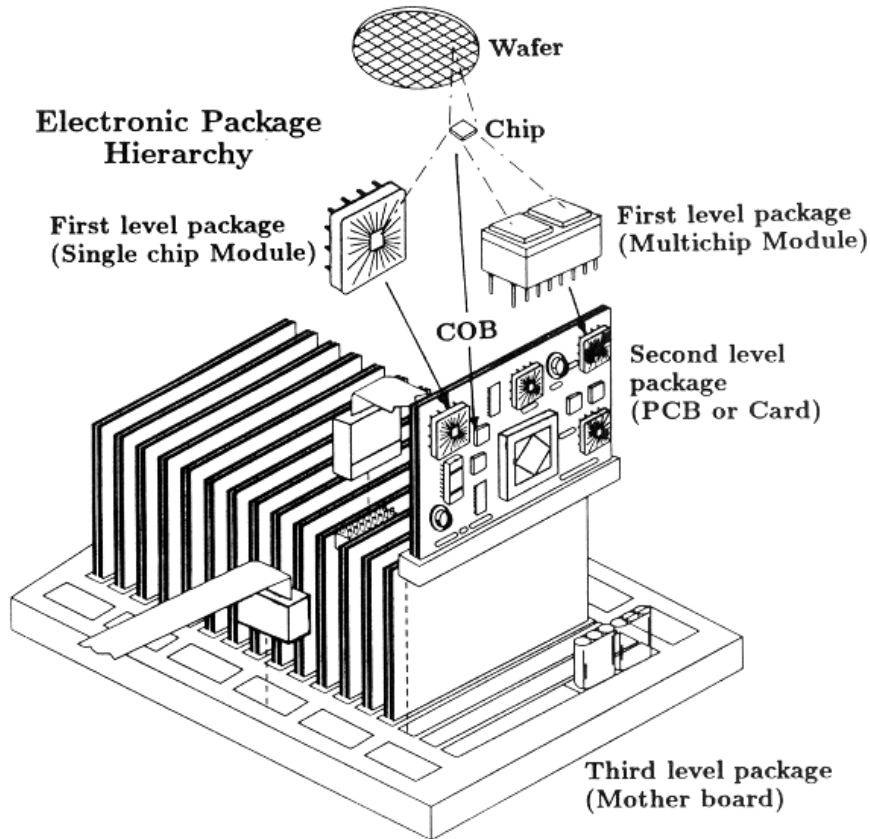


Figure 1-1. Schematic representation of electronic packaging hierarchy.³

The increase in transistor density of each successive generation of the semiconductor technology results in demands for corresponding increase of packaging interconnection density. To meet these demands there has been a continuous stream of new innovations and new developments in all aspects of electronic packaging: materials, processing, new designs, reliability and testing, metrology, modeling and simulation. Other driving forces including low cost, portability, high performance, multi-functionality, and environmental friendliness also fuel the development and introduction of the important packaging concept and technology revolutions of the last several decades. Figure 1.2 shows the evolution of electronic packaging technology. The shift from traditional through-hole packages started sometime in the 1980s when dual in line

package (DIP) began to be replaced in select applications by surface-mount packages (SMPs) like quad flat packages (QFPs), in response to a need for higher density PWBs. The early 1990s saw the emergence of both pin-grid array (PGA) and ball-grid array (BGA), primarily because of their high I/O density, minimized footprint, and shorter electrical path length and thereby better electrical performance. The BGA package evolved from flip-chip technology, also referred to as controlled-collapse chip connect (C4), pioneered by IBM for ICs in 1960s. In the mid 1990s, the BGA concept was applied to a second generation packaging technology referred to as chip scale packaging (CSP), which can increase the IC silicon efficiency 30-40%. The most advanced technology in packaging is called wafer-level packaging (WLP) or wafer-level chip scale package (WLCSP) began in the late 1990s, which involves building power and signal redistributions and packaging protections onto the wafer, representing the convergence of front-end and back-end processes in packaging. The next generation packaging technology will be a system-level integrated package and 3-dimensional (3D) packaging.⁵

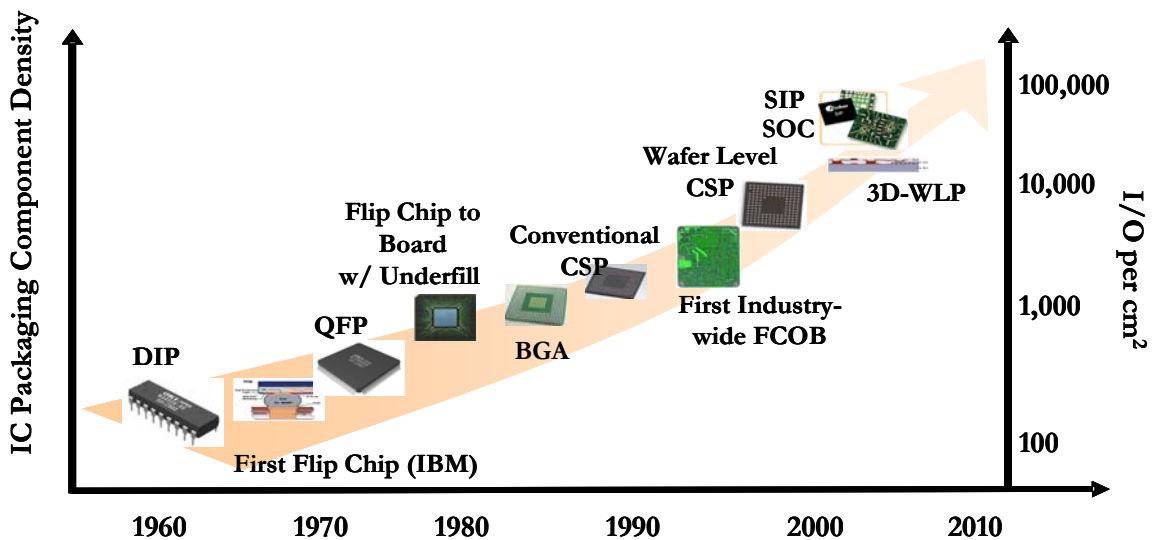


Figure 1-2. Evolution of electronic packaging.

1.2 Passive Devices

Passive devices refer to resistors, capacitors and inductors. They are present in all of the electronic system to provide impedance, current-to-voltage phase angle, and energy storage. Unlike active components, passives components are nonswitching, have no gain, and can not amplify. They can, however, use their impedance to decrease the signal current or voltage. Impedance is not a function of signal frequency for an ideal resistor, but decreases for an ideal capacitor and increase for an ideal inductor with increasing frequency. These sorts of behaviors are useful in many applications including filters, energy storage, voltage modification, current control, and line termination.⁵

As the total number of passives utilized increases over the years, passive technology switched from through-hole or “leaded” to surface-mount technology (SMT) components, then passive arrays, i.e. multiple passives in one surface-mount package, and finally, the concept of embedded passives in which the passive components are embedded within the board itself. In a high performance modern wireless microelectronic product such as cell phone, about 80 % of the electronic components are passive components which are unable to add gain or perform switching functions in circuit performance, but these surface-mounted discrete components occupy over 40 % of the printed circuit/wiring board (PCB/PWB) surface area, account for up to 30 % of solder joints and up to 90 % of the component placements required in the manufacturing process. Therefore, discrete passive components become the limiting factor in the form and mass of electronics, especially for analog and mixed-signal applications that use a larger number of passives than typical digital systems.^{5,6}

1.3 Embedded Passives

1.3.1 Motivations

The ever growing demands of miniaturization, increased functionality, better performance and low cost for microelectronic products and packaging have been the driving force for new and unique solutions in system integration, such as system-on-chip (SOC) and system-in-package (SiP). Embedded passives, an alternative to discrete passives, can address the issues associated with discrete parts by reducing substrate board space, cost, handling, assembly time and increasing yield. Figure 1-3 schematically shows an example of realization of embedded passive technology by building passive components directly into the laminate substrates.

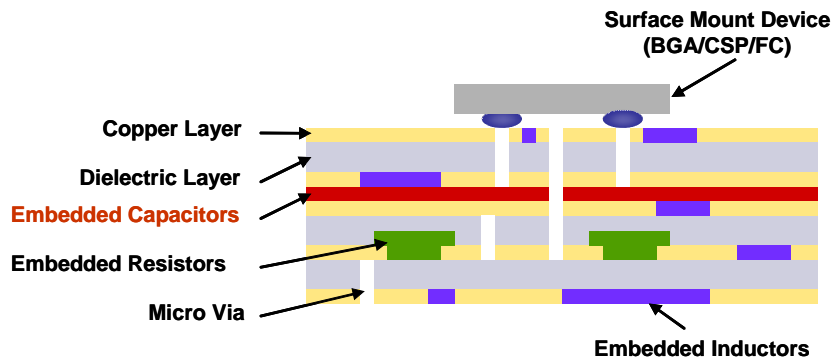


Figure 1-3. Schematic illustration of embedded passives integrated into the laminate substrate.

By removing these discrete passive components from the substrate surface and embedding them into the inner layers of substrate board, embedded passives can not only reduce the size and weight of the passives as shown in Figure 1-4, but can also have many other benefits such as increased reliability, improved electrical performance and reduced cost. Specifically, due to their simplified structure and lack of leads and contacts, embedded capacitors and resistors tend to have considerably less parasitic inductance

than their surface-mount counterparts. Also, short leads to the embedded capacitor or inductor can result in less parasitic resistance. As a result, electrical performance can be improved by employing embedded passive technology. Additional reliability advantage comes about because two solder joints per passive can be eliminated, which are a major failure point for systems with discrete components.⁶

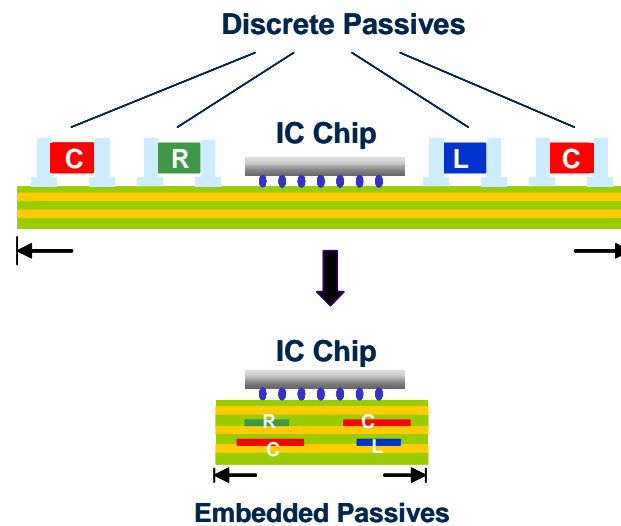


Figure 1-4. Schematic representation of the size advantages of the embedded passives as compared to discrete passives.

The benefits associated with embedded passives have driven a significant amount of research during the past decade for this technology. For instance, National Institute of Standards and Technology (NIST) launched its Advanced Embedded Passives Technology (AEPT) project in 1999 with a group of industrial partners, focusing on developing the materials, design and processing technology for embedded passive devices onto circuit board substrate. However, embedded passive technology has still not been commercialized for electronic packages due to materials and process issues. Therefore, to enable embedded passive technology it is necessary to develop materials

that satisfy the requirements of fabrication as well as electrical and mechanical performances.

1.3.2 Capacitors

All types of electronic systems are becoming more complex while simultaneously being required to be smaller and lighter. The number of passives per package is steadily increasing, and the required range of values is very wide. As stated previously, discrete passive component is the limiting factor in the form and mass of electronics, with capacitors dominating in numbers among different types of passive component and their wide applications.

The required capacitance range of capacitors in typical electronic systems is very wide as shown in Figure 1-5, which is an analysis of the capacitor distribution produced in two cell phones, two two-way radios and one global positioning system (GPS) receiver.

5

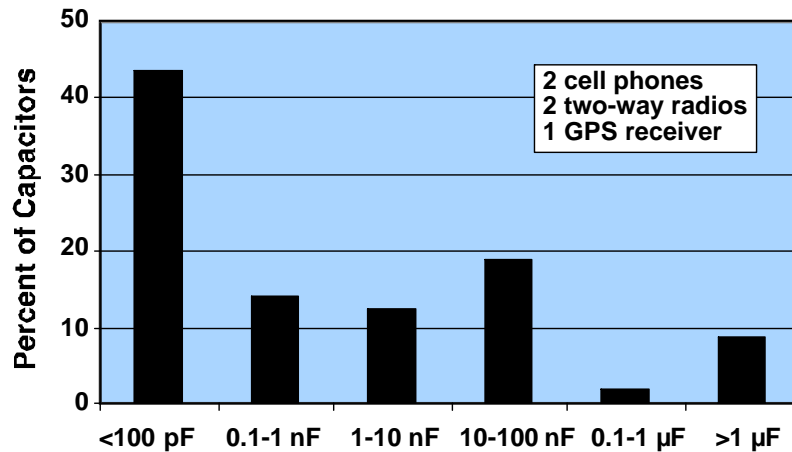


Figure 1-5. Distribution of capacitor values in typical portable consumer equipments.⁵

Table 1-1 shows a wide variety of applications and properties of capacitors, including filtering, timing, A/D conversion, termination, decoupling, and energy storage. Particularly, the development of microelectronics requires decoupling capacitors with higher capacitance and shorter distance from its serving devices.

Table 1-1. Applications and properties of capacitors.

Application	Value Range	Tolerance Required	Stability Required
Filtering, timing	1 pF – 100 pF	Moderate	Moderate
A/D conversion	1 pF – 10nF	Very high	Very high
Termination	50 – 200 pF	Low	Low
Decoupling	1nF – 100 nF	Low	Low
Energy Storage	1 μ F and up	Low	Low

Decoupling capacitors are present in all microelectronics, especially high-power logic and mixed signal devices, to decrease power supply requirements, remove noise from power/ground planes, and prevent false triggering. In modern microprocessors, high current ramping rate demands to chips cause voltage polarization over inductive leads and wires. The solution to this problem is to place decoupling capacitors across the power and ground distribution conductions, physically as close to the ICs as possible, to act as a short-time battery charger in between cycles and provide low impedance power to chips that cannot otherwise be supplied by the power supply due to the low-pass filtering action of the parasitic inductances. They are referred to as decoupling capacitors because they decouple the power distribution system from the current surges required by the IC as shown in basic form in Figure 1-6.⁵

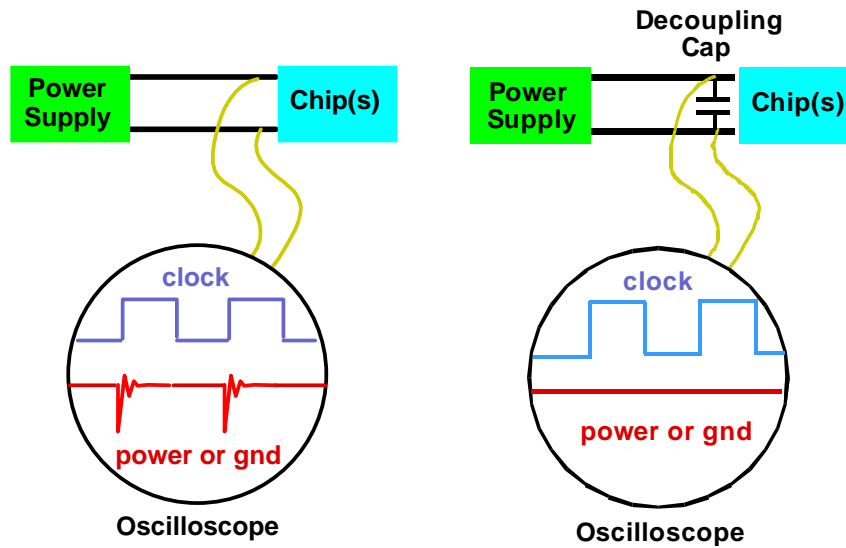


Figure 1-6. Power supply and power distribution system without and with a decoupling capacitor.

Decoupling capacitors are generally implemented at several levels: up to $10\ \mu\text{F}$ at the board's power pins; up to $100\ \text{nF}$ on the board near the chips; up to $100\ \text{pF}$ on the chips. Problems with today's discrete capacitor approach lie in that discrete components compete with chips for board space, their inherently inductive nature limits their ability to decouple at high frequencies, and the solder joints with discretes are easily to fail. As an alternative, the inherently low inductance of embedded capacitors and their ability to hide in the substrate near the chip make them ideal for this application.

However, capacitors are the major impediment to the implementation of embedded passives because the materials and processes of embedded capacitors which must be compatible with the substrate, interconnects and interlayer insulation layers are still unknown. Therefore, materials and fabrication for embedded capacitor applications are widely under development focusing on the research of dielectric material, film formation methods, and capacitor topography.

1.4 Dielectric Mechanisms

1.4.1 Capacitance, Dielectric Constant and Polarization

Capacitance (C) is a measure of how much electric charge can be stored in a capacitor. The relationship between capacitance C and dielectric constant $\epsilon_r(k)$ is given by the following equation:

$$C = \frac{\epsilon_0 \epsilon_r A}{t} \text{ Equation 1-1}$$

where ϵ_0 is the dielectric constant of the free space (8.854×10^{-12} F/m), A is the area of the electrical conductor, t is the thickness of the dielectric layer, and ϵ_r is the dielectric constant of the dielectric layer. It is evident that the larger the dielectric constant, the larger the capacitance which can be realized in a given space. Therefore, materials of high dielectric constant are favored in practical design of embedded capacitors for miniaturization. Under an alternate electric field, the dielectric constant of materials can be expressed by complex permittivities:

$$\epsilon^* = \epsilon' - j\epsilon'' = \epsilon_0 \epsilon_r - j\epsilon'' \quad \text{Equation 1-2}$$

where ϵ' is the real permittivity and ϵ'' is the imaginary permittivity.

The ability of the dielectric materials to store energy is attributed to the polarization, i.e. electric field-induced separation and alignment of the electric charges, which can result in an increase in capacitance. There are several molecular mechanisms associated with this polarization, including electronic, ionic, molecular (dipole), and interfacial (space-charge) polarization. In general, application of a field to each of these mechanisms in a normal state will cause a displacement of charge which results in a polarization in the direction of the field. This effect on each mechanism can be seen

schematically in Figure 1-7. For a given material, the sum of the contributions from each mechanism determines the net polarization, P , of the dielectric material.

$$P = P_{\text{electronic}} + P_{\text{ionic}} + P_{\text{molecular}} + P_{\text{interfacial}} \quad \text{Equation 1-3}$$

Electronic polarization occurs in neutral atoms when the electric field displaces the positive nucleus with respect to the electrons around it, thus induce dipole effect occurs in all materials. Magnitude of this mechanism is usually very small compared to other polarization mechanisms since the moment arms of these dipoles are very short. This mechanism would result in low k , perhaps up to 2-4, and can react to very high frequencies around 10^{15} Hz.

Atomic polarization occurs in substances made up of more than one type of nonionic atoms as the shifting of electron cloud toward the more electronegative atoms results in a permanent dipole under an applied electric field. The aligning of the permanent dipoles with the field creates enhanced capacitance. Therefore, k is a function of the material's structure and lattice flexibility as well as its composition. The magnitude of atomic polarization is usually quite small (one-tenth of that of electronic polarization) and cannot occur at very high frequencies because of the sluggish movement of heavy nuclei compared to electrons, as a result, it is not observed above infra-red frequencies.

Ionic polarization is similar to atomic polarization but involves the shifting of ionic species under the influence of the field. This shift can be considerable and lead to very high k , up to several thousand. Ionic conduction is the most prevalent mechanism at low frequencies but introduces losses into a system.

Molecular or dipolar polarization occurs in substances containing permanent dipole moment resulted from unbalanced sharing of electrons by atoms of a molecule.

And the rotations of the permanent dipoles to align with the external electric field cause orientation polarization to occur at around 10^{11} Hz to 10^{12} Hz.

Space charge or interfacial polarization occurs in heterogeneous systems such as multi-component materials or incompatible chemical substance containing materials when translating charge carriers are accelerated by an applied field until they are impeded by and trapped at the physical barriers in these heterogeneous systems. This build up of charge dictates the polarization of the material. Grain or phase boundaries and free surfaces are common barriers. The typical frequency range for this polarization is around 10^{-3} Hz to 10^3 Hz.

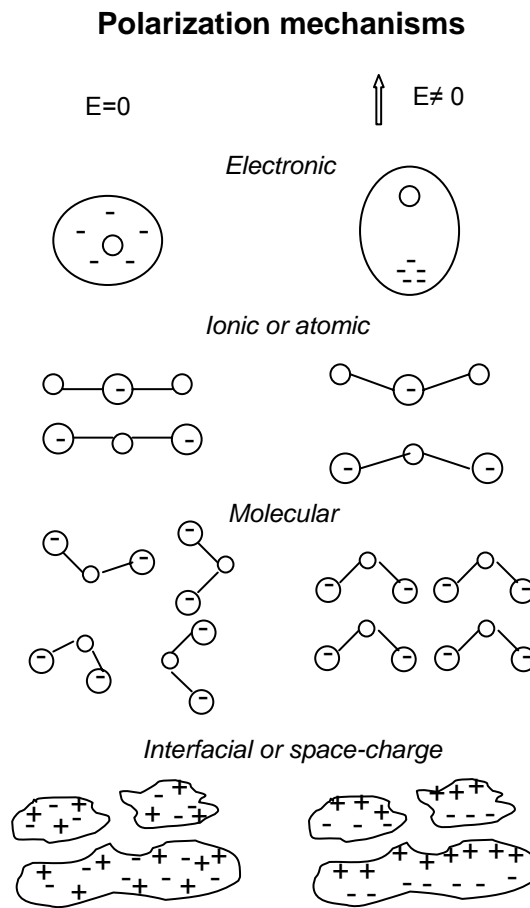


Figure 1-7. Schematics of four major polarization mechanisms

Ideally, the dielectric constant should be constant with regard to frequency, temperature, voltage, and time. However, each polarization mechanism has a characteristic relaxation frequency. Therefore, k values of most of the materials show a dependence on the frequency because slower mechanisms fail to respond and contribute to the dielectric storage when the frequency becomes large. The k values of dielectric materials can also vary with temperature, bias, impurity, and crystal structure to different extent according to materials types.^{6,7}

Because embedded capacitors are planar and area-ruled, the best way to express their value is as specific capacitance, i.e. capacitance per unit area, as expressed in Equation 1-4. The value of specific capacitance depends on two parameters, one is the dielectric material itself (k) and another one is its form (film thickness). Factors affecting film thickness are more specific to the type, processibility and reliability of the materials.

$$\text{Specific capacitance in } \frac{\text{nF}}{\text{cm}^2} = 0.885 \frac{k}{\text{Dielectric thickness in } \mu\text{m}} \quad \text{Equation 1-5}$$

The energy stored in a capacitor E is:

$$E = \frac{1}{2} CV^2 \quad \text{Equation 1-6}$$

where V is the voltage applied. The electric energy density in a dielectric material is limited to $kE_b^2/2$, where E_b is the breakdown strength, both large k and high breakdown strength are required for large electric energy storage.^{8,9}

Additionally, good high frequency performance is desirable for electronic products operating at ever increasing transmission data rates.

Table 1-2 shows the dielectric properties, specific capacitance and energy density that might be expected from some dielectric materials in attainable thickness.

Table 1-2. Dielectric properties, specific capacitance and energy density of some common dielectrics. ⁶

Dielectric	Dielectric Constant	Dissipation factor (%)	Thickness (μm)	Specific Capacitance (nF/cm^2)	Energy Density at 5 V ($\mu\text{J}/\text{cm}^2$)
Unfilled laminated polymer	4	0.1-1.5	25	0.14	0.002
Ferroelectric-filled polymer	50	<3	25	1.8	0.023
Spin-on BCB	2.7	0.1	2.0	1.2	0.015
SiO ₂	3.7	0.03	0.2	16	0.20
SiO	6	0.01	0.2	27	0.34
Al ₂ O ₃	9	0.4-1	0.2	40	0.50
Ta ₂ O ₅	24	0.2-1	0.2	110	1.40
TiO ₂	40	2-5	0.2	180	2.30
BaTiO ₃	~2000	5	1.0	1800	22

1.4.2 Dielectric Loss

The dielectric loss is a measure of energy loss in the dielectric during AC operation, which is a material property and does not depend on the geometry of capacitor. Usually the dielectric loss, expressed as the loss tangent ($\tan \delta$) or dissipation factor (Df) can be defined as

$$\tan \delta = \frac{\varepsilon''}{\varepsilon'} + \frac{\sigma}{2\pi f \varepsilon'} \quad \text{Equation 1-7}$$

where ε' , ε'' , σ are the real and imaginary part of the dielectric permittivity and the electrical conductivity of the materials, respectively, and f is the frequency.

In general, dielectric loss of the dielectric material is resulted from distortional, dipolar, interfacial, and conduction loss. The distortional loss is related with electronic

and ionic polarization mechanisms. The interfacial loss originates from the excessive polarized interface induced by the fillers and specifically the movement or rotation of the atoms or molecules in an alternating electric field. The conduction loss is attributed to the dc electrical conductivity of the materials, representing the flow of actual charge through the dielectric materials.^{10, 11}

The energy loss (W) refers to the energy dissipated in a dielectric material and is proportional to the dielectric loss tangent, which can be determined by the following equation:

$$W \approx \pi \epsilon' \xi^2 f \tan \delta \quad \text{Equation 1-8}$$

where ξ is the electric field strength and f is the frequency.¹² Therefore, a low dielectric loss is preferred in order to reduce the energy dissipation and signal losses, particularly for high frequency applications. Generally, a dissipation factor under 0.1% is considered to be quite low and 5% is high.⁶ Very low dissipation factor is desired for radio frequency (RF) applications to avoid signal losses, but much higher values can be tolerated for energy storage applications such as decoupling.

1.5 Overview of Dielectric Material Options for Embedded Capacitors

To meet the stringent materials requirements for dielectric materials to realize the embedded capacitor applications, considerable attention has been devoted to the research and development of the candidate high- k materials. To date, no one perfect dielectric material has yet been identified for embedded capacitor applications because they all compromise on certain issues including electrical and mechanical performance, or

processing constraints, however, a very wide range of material candidates are potentially available.

1.5.1 Ferroelectric Ceramic Materials

Ferroelectrics and paraelectrics are the two major classes of dielectric materials. The distinguishing feature is that ferroelectric materials do not lose all of their ionic polarization when the field is removed but paraelectrics do. The ions in ferroelectrics can be stabilized into configurations which do not revert back to the previous state once the field is removed because of lattice hindrances. While paraelectric materials cannot be left with a residual polarization once the field is removed due to the lack of mobile charged atoms with more than one stable lattice position.⁵ Ferroelectric ceramic materials such as BaTiO₃ (barium titanate), BaSrTiO₃ (barium strontium titanate), and PbZrTiO₃ (lead zirconium titanate) etc., have been used as dielectric materials for decoupling capacitors because these materials possess on the order of thousands. By far the highest specific capacitances, exceeding 1800 nF/cm², are achievable with these materials. BaTiO₃, the classic example of a ferroelectric, is a cubic crystal with a lattice constant of 4.01 Å and a k of paraelectric characteristics at around 15-40 above to its Curie temperature of 120 °C, but below this temperature converts to the tetragonal form with unequal side lengths: 3.98 and 4.03 Å, thereby with existence of permanent dipole moments and their mobile ionic charge resulting in a k in the thousands.^{6,13}

Traditionally, high-capacitance ceramic capacitors are made of thin layers of ferroelectric ceramic materials placed between conductive plates. MLCC (multilayer ceramic capacitors) and BLC (boundary layer capacitors) are two examples of the most efficient geometries for attaining high-density charge storage among those dispositions of

electrodes and dielectrics (See Figure 1-8 (a) and (b)).¹⁴ BLC based on perovskite oxides such as SrTiO₃ (strontium titanate) are normally processed in the reductive and particle oxidative atmosphere so that grains of the oxides becoming semiconducting while grain boundaries are insulating.

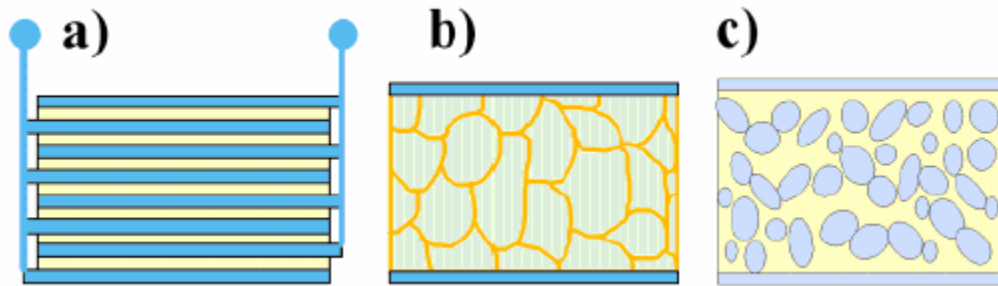


Figure 1-8. (a) Diagram of an MLC capacitor: blue and yellow regions represent metallic and dielectric layers, respectively; (b) Diagram of a BLC capacitor: green areas represent reduced (semiconductor) ferroelectric grains while orange lines correspond to oxidized (insulator) grain boundaries; (c) Diagram of a percolative capacitor: blue and yellow regions represent metallic and dielectric material, respectively.¹⁴

However, very high processing temperature in excess of 600 °C is required for sintering of these materials which make them unsuitable to process directly into low cost organic circuit boards. And the dielectric properties of ferroelectrics are typically a strong function of temperature, frequency, film thickness and bias, which results in significant nonlinearities in their performances.⁶

1.5.2 Other Ceramic Materials

As described in the preceding section, the high dielectric constants can be associated with ferroelectric properties for those oxides with the perovskite structure. However, the intrinsic problems of these capacitors due to strong temperature and frequency dependence make them undesirable for most applications. The introduction of

percolative capacitors with better electrical properties and simple production process could improve the applicability of ceramic capacitors.

Ceramic-metal composites (cermets) are considered as one of standard candidate for high capacitance percolative capacitors. Experimental evidence of and increase in the dielectric constant in the neighborhood of the percolation threshold has been reported. The fact that the effective dielectric constant of the mixture is much larger than those of the components can be understood as that there are many conducting particles isolated by thin dielectric layer at the percolation threshold (See Figure 1-8 (c)).^{14,15}

Pecharrómán et al. found BaTiO₃-nickle (Ni) composites with a high and frequency-independent dielectric constant ($\epsilon_r \approx 80,000$ at the percolation threshold) and designed, elaborated a new kind of electronic device. The device is based on the percolation theory and comprises an insulating ceramic matrix (BaTiO₃) and small, homogeneously distributed metallic particles (Ni). A high dielectric constant of 81,200 and a relatively low loss of 0.05 (measured at a frequency of 10 kHz) was achieved at metal volume concentration, f , close to 0.30 once the sample was annealed above the ferroelectric transition. This is one of the highest values reached for ceramic capacitors and can only be comparable with single-crystal values of ferroelectric and relaxor compounds at the Curie temperature.¹⁴

In addition, nonferroelectric and nonperovskite ceramics such as CaCu₃Ti₄O₁₂ (CCTO)^{16,17,18} and Li_{0.01}Si_xNi_{0.99-x}O (LSNO)¹⁹ can exhibit high- k as well which arises from the Maxwell-Wagner polarization (i.e. interfacial polarization) mechanism and thermally activated mechanism such as charge carrier transport rather than due to permanent dipoles.

1.5.3 Polymer Materials

Most polymers used in microelectronic industry such as epoxies, silicones, benzocyclobutenes (BCB), and polyimides (PI) are available for applications by spin-on or various coating methods followed by a moderate temperature cure. Therefore, these polymer dielectrics are compatible with the organic PWB manufacture. Generally speaking, polymers have low dielectric constant in the range of 2-5, e.g., ~ 2.5 for polystyrene, ~ 2.65 for BCB, ~ 2.7 for parylene, ~ 2.72 for silicone, and ~ 3.5 for epoxy and polyimide. These modest k values combined with relatively thick layers in 5-50 μm result in specific capacitances ranging from only 0.07 to 0.3 nF/cm^2 , which make polymer materials useful for embedding only the smallest valued capacitors into the board. It is also possible to deposit polymer dielectric layers ranging from 2 to 5 μm through coating and curing liquid resins, which can significantly increase their specific capacitance up to around 1.5 nF/cm^2 .⁵ Since polymers are paraelectric, the resulting capacitance is stable with regard to temperature, frequency, and the like. And also the dissipation factor of polymers is also very low, usually much lower than ferroelectric ceramics.

As one of the most primarily used polymers in electronic industry, epoxy resins have been of particular interest for embedded capacitor applications because of its compatibility with PWB manufacturing process. An epoxy system is basically composed of epoxy resin, hardener, and catalyst. The dielectric constant of epoxy can be adjusted by tailoring the components of epoxy system. For example, the dielectric constant of epoxy system can be increased significantly from 3.2 to 5.0 by proper choice of the catalyst such as metal acetylacetonate.²⁰

Compared with conventional polymers, ferroelectric polymers can have higher k values, above 10, because of its polar backbone.²¹ For example, pure polyvinylidene fluoride (PVDF) polymer has a k of about 11 at 1 kHz and 25 °C.^{22,23} Poly(vinylidene fluoride-trifluoroethylene) (P(VDF-TrFE)) copolymer, a class of relaxor ferroelectric, can have a relatively high k around 40 at room temperature after irradiation treatment.²⁴ As the irradiation process requires expensive and complicated equipment, Petchsuk et al.²⁵ and Yu et al.²⁶ synthesized polyvinylidene fluoride–trifluoroethylene–chlorotrifluoroethylene [P(VDF-TrFE-CTrFE)] terpolymers to obtain a similar structure as irradiated P(VDF-TrFE) copolymer by introducing CTrFE block in the polymer. It was found that P(VDF-TrFE-CTrFE) terpolymer with VDF:Tr-FE:CTrFE molar ratio of 65:35:9 exhibits a high k of about 60 (@ 1 kHz) at 33 °C, and its dielectric loss tangent is about 0.1. Its dielectric constant can be as high as 320 (@ 10 kHz) 145 °C. The above mentioned high- k polymers have non-conjugated backbones. In the case of a conductive polymer with conjugated backbone, the k can be even higher. For instance, polyaniline (PANI) was reported to possess a k value larger than 104 in a partially crystalline system for which an inhomogeneous disorder model was proposed.²⁷

1.5.4 Ferroelectric Ceramic/Polymer Composites

Study on ferroelectric ceramic/polymer composites with high- k has also been actively explored as a major material candidate for embedded capacitor applications. The methodology of this approach is to combine the advantages of the polymers which meet the requirements for the low cost organic substrate process, i.e. low temperature processibility, mechanical flexibility and low cost, with the advantages from the ferroelectric ceramic fillers, such as desirable dielectric properties.^{28,29,30,31,32,33,34,35,36} The

major advantage of this type of material lies in the processing, since the high temperature steps required to reach high k from the ferroelectric phase can be executed in advance of application to the organic substrate. Almost any high k ferroelectric material can be produced in quantity as submicron powders. Then these high k particles can be mixed with a polymer resin at up to 60 to 80% loading by volume, then screen printed, spun-on, or stenciled onto the substrate, and the polymer phase cured at temperatures tolerable to organic boards.

However, some challenging issues related to these polymer composites for high k applications remain to be solved, such as limited dielectric constants and capacitance density, and low adhesion strength which results in air gaps and lowers capacitance. The k of the final composite will be much closer to that of the low k material, which is generally the polymer with a k of about 3 to 5 according to the mixing rules for a two-phase combination of two materials with different k . Accordingly, most of the k values of ceramic/polymer composites developed to date are between 10 to 50 at room temperature. The corresponding film can be made in thickness of around 8 μm pinhole free by screen printing and delivers specific capacitance up to about 5 nF/cm².

Polar polymers can increase k of the composites at low frequencies. However, the presence of polar groups in the polymer matrix also increases dielectric losses, particularly within the intermediate and high-frequency ranges.³⁷ On the other hand, by employing polymer matrix with relatively high k , the k values of ceramic/polymer composites can be effectively enhanced because the k of polymer matrix shows very strong influence on the k of the final composites.^{29,34} For instance, Bai et al. prepared Pb(Mg_{1/3}Nb_{2/3})O₃-PbTiO₃/P(VDF-TrFE) composites with k values above 200.²⁹ Rao et

al. reported a lead magnesium niobate-lead titanate (PMN-PT)+BaTiO₃/high-*k* epoxy system (effective *k*: 6.4) composite with *k* value about 150, in which ceramic filler loading as high as 85 % by volume.²⁰ Studies have shown that the *k* of 0-3 connectivity type composite is dominated by the matrix, therefore, a relatively large volume fraction of high *k* ferroelectric inorganic phase is needed. And the high filler loading of ceramic powders is still the technical barriers for real application of ceramic/polymer composites in the organic substrate because it results in poor dispersion of the filler within the organic matrix, and almost no adhesion towards other layers in PWB as well due to the low polymer content.

Table 3-1 summarizes the type, composition and dielectric properties (room temperature values if not otherwise specified) of the ceramic/polymer composite material candidates for embedded capacitors.

Table 1-3. Summary of ceramic/polymer composite candidates.

Materials	Dielectric Constant	Dissipation Factor	Filler Size	Filler Loading	Ref.
Pb(Mg _{1/3} Nb _{2/3})O ₃ -PbTiO ₃ /P(VDF-TrFE)	~200 (10 kHz)	0.1 (10 kHz)	0.5 μm	50 vol%	29
PZT/PVDF	50	N/A	20 μm	50 vol%	31
BaTiO ₃ /epoxy	40 (1 Hz)	0.035	100-200 nm	60 vol%	32
bimodal BaTiO ₃ /epoxy	90 (100 kHz)	0.03 (100 kHz)	916 nm+60 nm	75 vol%	36
PMN-PT+BaTiO ₃ / high- <i>k</i> epoxy	~150 (10 kHz)	N/A	900nm /50 nm	85 vol%	20
CaCu ₃ Ti ₄ O ₁₂ /P(VDF-TrFE)	243 (1 kHz)	0.26 (1 kHz)	N/A	50 vol%	38
BaTiO ₃ / P(VDF-HFP)	37 (1 kHz)	< 0.07 (1 MHz)	30-50 nm	50 vol%	39

1.5.5 Conductive Filler/Polymer Composites

Conductive filler/polymer composites are another approach towards ultra-high k materials for embedded capacitors. Ultra-high k values have been observed with conductive filler/polymer composites when the concentration of the conductive filler approaches the percolation threshold, which can be explained by the percolation theory for conductor-insulator percolation system.¹⁵ For conductive filler/polymer composites, the effective electrical properties approaching the percolation threshold are determined by the scaling theory, which can be described as Equation 1-9 through Equation 1-11:

$$\sigma = \sigma_M (f - f_c)^t \quad f > f_c \quad \text{Equation 1-9}$$

$$\sigma = \sigma_D (f_c - f)^{-q} \quad f < f_c \quad \text{Equation 1-10}$$

$$\varepsilon = \varepsilon_D / |f - f_c|^q = \varepsilon_D (\sigma_M / \sigma_M)^s \quad \text{Equation 1-11}$$

where σ_M and σ_D are the electrical conductivity of conductive filler and polymer, respectively; f and f_c is the concentration and the percolation threshold concentration of the conductive filler within the polymer matrix, respectively; ε_D is the dielectric constant of the polymer matrix; and q , s and t are scaling constants, related to the material property, microstructure and connectivity of the phases in the conductive filler/polymer system.¹⁵

Sometimes the effective dielectric constant of the metal-insulator composite could be three or four orders higher than the dielectric constant of the insulating polymer matrix. This phenomenon can be interpreted in terms of a “supercapacitor network” with very large area and small thickness: when the concentration of the metal is close to the percolation threshold, large amount of conducting clusters are in proximity to each other, but they are insulated by thin layers of dielectric material. Furthermore, this percolative

approach requires much lower volume concentration of the filler compared to traditional approach of high- k fillers in a polymer matrix. Therefore, this material option represents advantageous characteristics over the conventional ceramic/polymer composites, specifically, ultra-high k with balanced mechanical properties including the adhesion strength. Various metal particles or other conductive fillers, such as silver (Ag), aluminum (Al), nickel (Ni), carbon black, have been used to prepare the polymer-conductive filler composites or three-phase percolative composite systems.^{40, 41, 42, 43, 44, 45, 46, 47, 48} High dielectric loss, low dielectric strength and narrow processing window are technical barriers for this category of materials. Because the highly conductive particles are easy to form a conductive path in the composite as the filler concentration approaches the percolation threshold. Currently much work has been focused to solve these problems of the conductive filler/polymer composites and much progress has been made. Details of some conductive filler/polymer composite materials reported in recent years are summarized in Table 1-4.

Table 1-4. Summary of the conductive filler/polymer composite candidates.

Materials	Dielectric Constant	Dissipation Factor	Filler Size	Filler Loading	Ref.
Ag flake/epoxy	~1000 (10 kHz)	0.02 (10 kHz)	1.5 μm	11.23 vol%	40
Al/epoxy	109 (10 kHz)	0.02 (10 kHz)	3 μm	80 wt%	41
Ni-BaTiO ₃ /PVDF	300 (10 kHz)	0.5 (10 kHz)	Ni: 0.2 μm , BT: 1 μm	Ni: 23 vol%, BT: 20 vol%	42
Ni-BaTiO ₃ /PMMA	150 (1 MHz)	N/A	Ni: 4 μm , BT: 1 μm	Ni: 12 vol%, BT: 20 vol%	43
Carbon black/epoxy	13000 (10 kHz)	3.5 (10 kHz)	~30 nm	15 vol%	45

Table 1-5 continued.

Ag/epoxy	~300 (1 kHz)	0.05 (1 kHz)	40 nm	22 vol%	46
Ag@C/epoxy	>300 (1 kHz)	< 0.05 (1 kHz)	80-90 nm core	25-30 vol%	48

1.5.6 All-Organic Polymer Composites

The composites fabricated by dispersing an organic filler material possessing very high dielectric constant in a polymer matrix can exhibit high- k as well. Zhang et al. used copper-phthalocyanine (CuPc) oligomer, a class of organic semiconductor materials with k as high as 10^5 , as high- k filler and dispersed in P(VDF-TrFE) matrix. The composite showed a k of 225 and a loss factor of 0.4 at 1 Hz.⁴⁹ The high dielectric loss is due to the long-range intermolecular hopping of electron. Wang et al. further chemically modified CuPc and bonded to P(VDF-TrFE) backbone to improve the dispersion of CuPc in polymer matrix. Dielectric loss was reduced and dielectric dispersion over frequency was weakened for chemically modified CuPc/P(VDF-TrFE) composites.⁵⁰ A k value above 1000 (@ 1 kHz) has been achieved by Huang et al. in an all-polymer high- k percolative composite material, fabricated by a combination of conductive polyaniline (PANI) with a poly (vinylidene fluoride-trifluoroethylene-chlorotrifluoroethylene) [P(VDF-TrFE-CTFE)] terpolymer matrix ($k > 50$).⁵¹ The possibility of all-organic composites as candidate high- k material for embedded capacitor requires further investigation and demonstration.

1.6 New Concepts and Current Trend

1.6.1 Nanocomposites

Nanocomposite materials are multi-constituent combinations of nano-dimensional phases with distinct differences in structure, chemistry, and properties. These materials typically contain an inorganic component in an organic host or vice versa, or consist of two or more inorganic/organic phases in some combinatorial form with the constraint that at least one of the phases or feature in the nanosize. In general, nanocomposite materials can demonstrate unique combinations of mechanical, electrical, optical, electrochemical, catalytic, and structural properties compared to those of each individual component and their micron-size filled counterparts by taking advantage of the different structure, composition and properties of their constituents.⁵²

1.6.1.1 Nanofillers

Nanofillers refer to those fillers of sub-100 nm size in at least one dimension. The primary driver for the usage of nanoparticle instead of micron-scale traditional fillers is the effect of particle size on their properties. The small size of the nanofillers can lead to unique and excellent electrical, magnetic, optical, catalytic, mechanical, chemical or biological properties, such as ultra-high modulus and conductivity of carbon nanotubes, Coulomb blockade effect of metal nanoparticles. Therefore, nanocomposite materials provide the possibility for enhanced functionality in contrast with their single-component counterparts. For example, nanocomposites with altered electrical or mechanical properties that retain their optical clarity can be obtained because very small nanoparticles do not scatter light significantly. Nanoparticles are also less likely to create

large stress concentrations and thereby can avoid the compromise of the material ductility while improve other mechanical properties.

In addition, the small size of the fillers leads to an exceptionally large interfacial area in the nanocomposites. Since nanoparticles have a much higher surface area per unit volume than larger particles, they possess a much greater interface with their surroundings. The interface controls the degree of interaction between the nanofiller and the polymer matrix, and thus controls the properties of the nanocomposites.

The method of synthesis often influences the size and properties of the nanoparticles. The nanoparticle size is dependent on the kinetics of nucleation and growth from a supersaturated solution as well as processes such as coarsening, oriented attachment, and aggregation, which tend to occur at longer times.⁵³ Due to the reduced lattice constants, the large surface energy and thermodynamic instability resulted from the large ratio of the surface to interior atoms, it is of the great challenges to stabilize nanoparticles. One method to prevent the nanoparticles from growth in size is to reduce the surface energy by insertion, i.e. adsorption and bonding, of surface active components into the particle surface. In addition, synthesis of nanoparticles in confined geometries and structured reaction media can yield anisotropic and size-controlled nanoparticles.

It is of paramount significance to understand, tailor and optimize properties by controlling the size, shape, volume fraction, interface, degree of dispersion or aggregation of nanoparticles to guide further development. The ability to manipulate the size, morphology and arrangements of nanoparticles in such a fashion that their unique optical, electrical and magnetic properties can be utilized for different applications remains a challenge.^{52,53,54}

1.6.1.2 Processing of Polymer Nanocomposites

Processing is one of the key limitations in the commercialization of nanocomposites. A major difficulty is proper dispersion of the nanofillers in the polymer matrix. Because, in the case of nanoparticles, aggregation or agglomeration occurs very easily due to the interparticle surface forces such as van der Waals forces, capillary forces and electrostatic forces, and often leads to undesirable materials properties.

The processing of polymer nanocomposites affects the state of the arrangement of nanofiller in the nanocomposites, which can be understood from the distribution and dispersion. Distribution of nanofiller describes the homogeneity throughout the sample, and dispersion of nanofiller describes the level of agglomeration. Figure 1-10 schematically illustrates the dispersion and distribution states of nanofillers as (a) good distribution but poor dispersion, (b) poor distribution and poor dispersion, (c) poor distribution but good dispersion and (d) good distribution and good dispersion. Without proper dispersion and distribution of the nanofillers, the high surface area which gives rise to unique properties of the nanofillers is compromised, and also the aggregates and agglomerations can act as defects and deteriorate the properties.

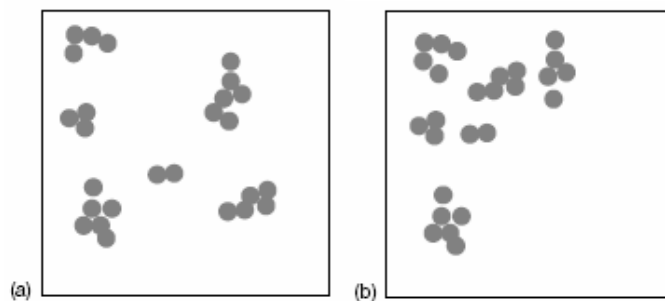


Figure 1-9. Schematic illustration of the dispersion and distribution states of nanofillers.⁵²

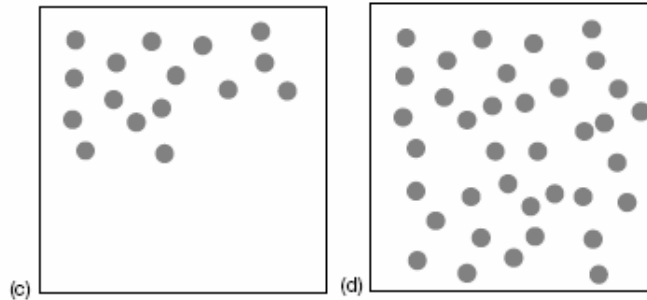


Figure 1-10 continued.

The quality of nanofiller dispersion in the polymer matrix directly correlates with its effectiveness for improving mechanical, electrical, thermal, impermeability and other properties. The properties of a composite are also intimately linked to the aspect ratio and surface-to-volume ratio of the filler.⁵⁵

There are three general methods of dispersing nanofillers in polymers. The first is direct mixing of the nanoparticle and the polymer either as discrete phases or in solution phase. The second is *in-situ* polymerization in the presence of the nanoparticles. And the third is *in-situ* formation of the nanoparticles and *in-situ* polymerization simultaneously. The latter can result in composites called hybrid nanocomposites because of the intimate mixing of the two phases.

(a) Direct Mixing

Direct mixing of the nanoparticle and the polymer can be carried out either as discrete phases or in solution phase.

Well established polymer processing techniques, melt-mixing or elastomeric mixing through roll mill, twin-screw extruder, Brabender high-shear mixer, or thermal spraying, can be used to direct mix the nanofillers and the polymer as discrete phases. The examples include nano silica (SiO₂)/polypropylene⁵⁶, nano alumina/poly(ethylene terephthalate) (PET) or low density polyethylene (LDPE)⁵⁷, nanoparticle-filled Nylon⁵⁸

etc. But the rapid increase of the viscosity with the addition of significant volume fractions of nanofiller limits the viability of this processing method.

Solution-phase mixing refers to dissolve or disperse the polymer and the nanoparticles in solution. The nanoparticle/polymer solution can be cast into a film or can be isolated from solution by solvent evaporation or precipitation. This allows modification of the particle surface without drying, which reduces particle agglomeration and thereby overcome some of the limitations of direct mixing. For instance, electrically conductive graphene/polymer nanocomposites was prepared by solution-phase mixing of the exfoliated phenyl isocyanate-treated graphite oxide sheets with polystyrene, followed by their chemical reduction. These composites feature individual graphene sheets well dispersed throughout the polymer matrix.⁵⁵

(b) *In-situ* Polymerization

In-situ polymerization means to disperse the nanofillers in the monomer or monomer solution followed by standard polymerization of the resulting mixture. A few examples are nano SiO₂/Nylon6⁵⁹, titania (TiO₂)/polymethylmethacrylate (PMMA)⁶⁰, calcium carbonate (CaCO₃)/PMMA⁶¹. One advantage of this method is the potential to graft the polymer onto the particle surface. Appropriate dispersion of the filler in the monomer is the key to this method, which often requires modification of the nanoparticle surface. Because the settling process is more rapid in a liquid than in a viscous melt although dispersion is easier.

(c) *In-Situ* Nanoparticle Processing/Formation

Another method for producing nanoparticle-filled polymers is an *in-situ* nanoparticle processing or formation. Ceramic/polymer composites can be prepared by

an *in-situ* processing of the SiO₂ and TiO₂ in a range of polymer matrices by mixing SiO₂ or TiO₂ precursor with a polymer followed by the sol-gel reaction.

Metal/polymer nanocomposites have also been processed via an *in-situ* formation of metal nanoparticles in the polymer matrix from suitable metal precursors. The presence of the protective polymer can prevent the agglomeration and limit the size of the nanoparticles. Mayer et al. reviewed parameters which affect the size, stability and morphology of as-formed nanoparticle.⁶² Primary parameters which control the nanoparticle size include the choice of metal precursor and the metal-polymer interaction. The nanoparticle size tends to be reduced if the polymer has a stronger interaction with the metal precursor because the precursors are prevented from phase separation.⁶³ The nanoparticle size is affected by the rate of reduction and faster reduction methods result in smaller nanoparticles.^{64,65}

Spherical micelle formation from amphiphilic block copolymers or crosslinked/gelled matrices can give specific control over nanoparticle size and morphology. Metal precursors either penetrate into the micelles or stabilize in the micelle corona and therefore metal nanoparticles can form either within the micelles or in corona after addition of the reducing agent, resulting in various morphologies shown schematically in Figure 1-11. Other block copolymer morphologies such as rods and layers can lead to interesting nanoparticle morphologies and thereby varied properties.⁶²

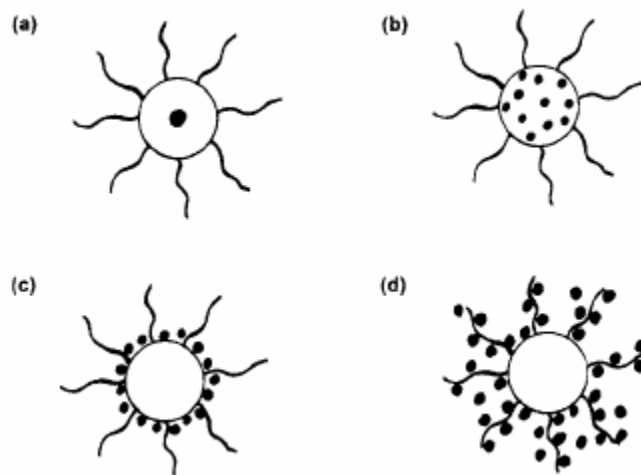


Figure 1-11. Morphologies of block copolymer-metal systems involving spherical micelle formation of the amphiphilic block copolymers: (a) cherry morphology, (b) raspberry morphology, (c) strawberry morphology, (d) proposed red currant morphology.⁶²

A wide range of conductive, semiconductive or magnetic nanoparticles including gold, silver, palladium⁶⁶, platinum, semiconductors, and metal oxides⁶⁷ can be formed by this method. It provides tremendous opportunity to tune the properties of these nanocomposite systems.

1.6.1.3 Modification of Nanoparticle Interfaces

The interfacial region within the polymer matrix possesses properties significantly different from those of the bulk polymer. The local chemistry, degree of cure, chain mobility, chain conformation, and degree of chain ordering or crystallinity can vary continuously from the filler/polymer matrix boundary to some point in the bulk polymer.⁵³ An understanding of the interfacial region is essential to understand the significant effects nanofillers exert on polymer behavior.

In addition to a specified size and shape, a controlled surface chemistry of nanoparticles is sometimes required to realize special advanced functionalities for various studies and applications. Encapsulation of nanoparticles endows them with important properties that bare uncoated nanoparticles lack. For instance, organic or inorganic coatings on metal or other inorganic particles enhance compatibility with organic ingredients, protect particle surfaces from oxidation, and hence improve dispersibility, chemical stability and so on. Consequently, nanofiller interface modification is important.

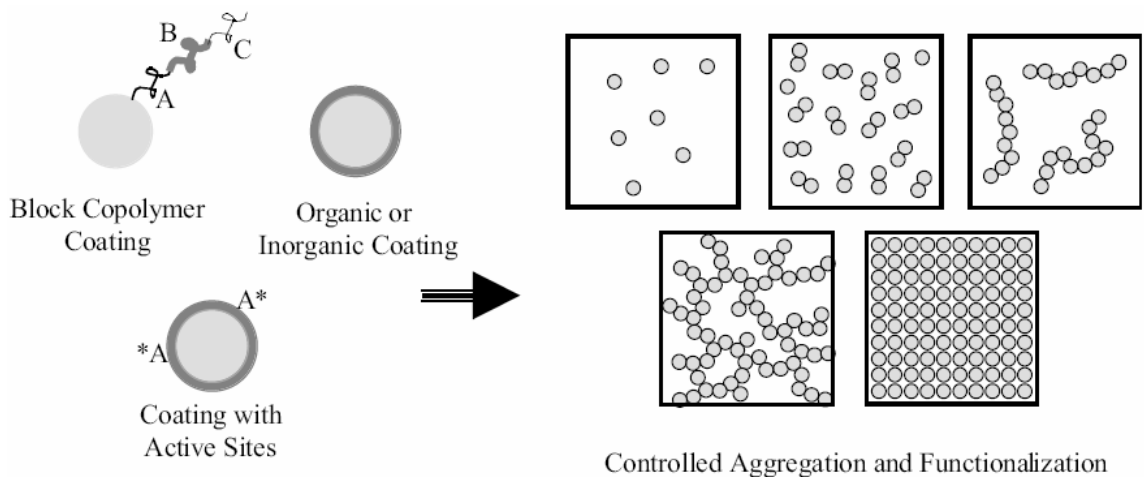


Figure 1-12. Schematic summary of nanoparticle modification.⁵²

(1) Organic Coatings

Two primary methods for modifying an inorganic nanoparticle surface with organic molecules are either connecting a short chain molecule onto the surface via grafting or strong hydrogen bonding, or applying a polymer coating onto the surface via polymerization. In general, these coatings can provide control over the compatibility of the modified nanoparticles with the polymer matrix and the strength of the interaction in between.

In the first method, hydroxyl groups on the metal and metal-oxide nanoparticle surface can react with a silane coupling agent. The large variety of functionalities attached to the silanol modifies the nanoparticle surface with long or short, hydrophilic or hydrophobic, linear or bulky chains. Hence, the strength of the interaction between the filler and the polymer matrix can be controlled from covalent bonding to repulsion, leading to increases or decreases in glass transition temperature, modulus, or other properties of nanocomposites.

Nanoparticles with controlled size and degree of aggregation are also the goal of many research efforts. As depicted in Figure 1-12, the coating layer with reactive sites on the nanoparticles could be used to bond particles together and lead to controlled aggregation of the nanoparticles.

As to the polymer coatings, they can be grafted or strongly adsorbed via hydrogen bonding onto the surface of the nanoparticles. Monomer adsorption and subsequent polymerization on the nanoparticle surface have been demonstrated on micrometerscale filler surfaces.⁶⁸ Another method involves grafting an initiator and then polymerizing a grafted polymer onto the nanoparticle surface.⁶⁹

Additionally, a multi-layer structure can be achieved on the nanoparticle surface by self-assembled polymer layers using layer-by-layer (LbL) colloid templating strategy. LbL assembly possesses the advantages of simplicity, universality, thickness control in nanoscale, low cost and being environmentally friendly. Uniform multilayers can be formed by this approach on a number of 3D objects due to the conformal nature of the polyelectrolyte adsorption process besides the 2D surfaces. The build-up of polyelectrolyte multilayers on colloidal surfaces ranging in size from several micrometers

down to nanometers has been demonstrated. A frequently utilized method to create nanoparticle-loaded thin film coatings on colloidal particles is via LbL assembly of a polyelectrolyte and preformed nanoparticles of an opposite surface charge.⁷⁰ This approach provides a simple route to create core-shell.

(2) Inorganic Coatings

Inorganic coatings have also been applied to nanoparticles via precipitation or deposition of the inorganic species onto the particle surfaces by a sol-gel type process. SiO₂, TiO₂, titanium nitride, and zirconia have been coated on nanoparticles, usually metal oxides, in this way.⁵²

1.6.2 Nanodielectrics

With the increased enthusiasm and activity toward the research on the nanotechnology, a new class of dielectric material, nanodielectric, is emerging. It is anticipated that nanocomposites are highly promising nanodielectrics.⁷¹ Polymer composite materials based on nanoparticles, one category of nanocomposites, provides a potential solution to meet the present and future technological demand in terms of the good processibility and mechanical properties of polymers combined with the unique electrical, magnetic or dielectric properties of nanoparticles.⁷² The heterogeneous inclusions, even if they are nonpolar, often cause heterogeneous dielectric polarization as a result of the accumulation of a virtual charge at the interface of two media with different permittivities or conductivities.

Additionally, nano-sized particles are preferred for high-*k* dielectric composite materials because they could help achieve thinner dielectric films leading to a higher

specific capacitance as shown in Figure 1-13. Therefore, more nanoparticles of ceramic, metallic or even organic semiconductor have been introduced to prepare high- k dielectric materials recently. Some of the examples can be referred to the materials candidates and corresponding properties as summarized in Table 1-3 and Table 1-4.

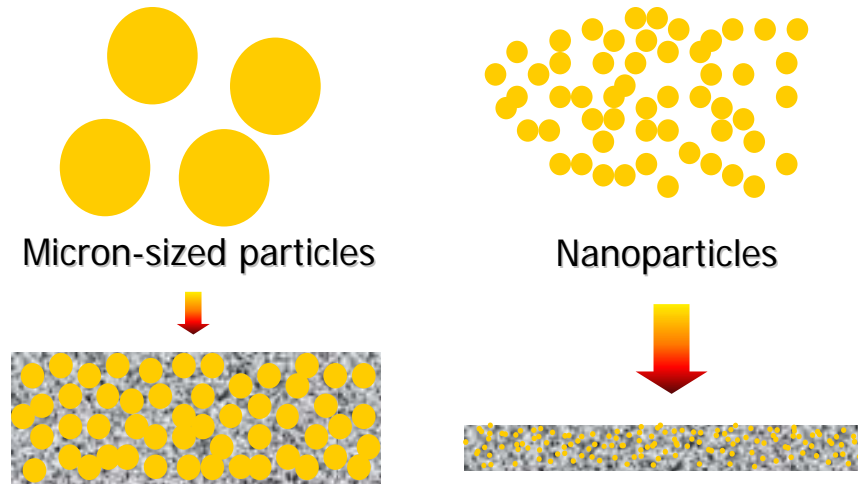


Figure 1-13. Schematics of composite films based on micron-sized particles and nanoparticles.

1.6.3 Performance Enhancement of High- k Nanocomposites

1.6.3.1 Filler Size Effect

It is worth to mention that there are several issues of nanoparticle-based dielectric composite materials need to be addressed. Although finer particle size is required to obtain a thin dielectric film and to increase the capacitance density, for ferroelectric ceramics, extremely fine particles may lead to the change of crystal structure from tetragonal, which results in the high permittivity, to cubic or pseudo-cubic. Generally speaking, the tetragonality and hence the permittivity of ceramic particles decreases with the particle size. Uchino et al.⁷³ and Leonard et al.⁷⁴ found that the tetragonality of

BaTiO₃ powders disappears finally when the particle size decreases to approximately 100 nm and 60-70 nm, respectively. Cho et al. prepared BaTiO₃/epoxy composite embedded capacitor films (ECFs) with average particle size of 916 nm (P1) and 60 nm (P2), the *k* values of ECFs made of P1 were higher than those made of P2. So the coarser particle is more useful than the finer particle to obtain high *k* of ECFs using unimodal powder in this case. But by adopting bimodal fillers, fine nanoparticle can effectively enhance the *k* values by maximizing packing density and removing the voids and pores formed in the dielectric films. A dielectric constant of about 90 was obtained at a frequency of 100 kHz using these two different size BaTiO₃ powders (see Figure 1-14).³⁶

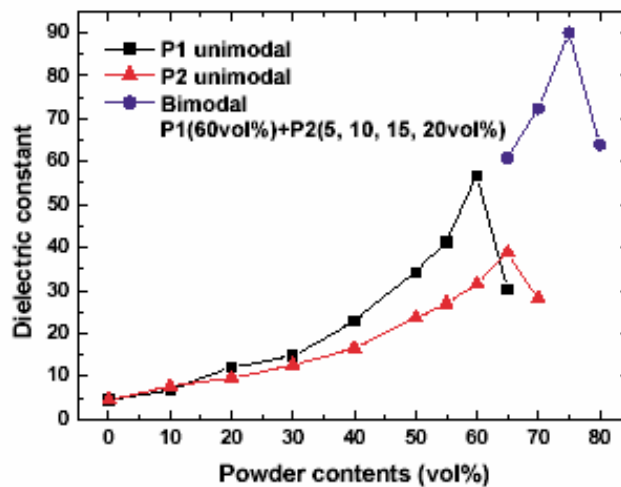


Figure 1-14. Dielectric constant changes with BaTiO₃ powder loading and size.³⁶

1.6.3.2 Controlled Dispersion

Uniform dispersion of nanoparticles in nanocomposite materials is required because nanoparticle agglomerates will lead to undesirable electrical or materials properties. Therefore, dispersion of nanoparticles is an extremely important contributor for achieving improved dielectric properties and reproducibility.

In a simple way, addition of surfactant or dispersant such as phosphate esters can improve the dispersion of nanoparticles in polymer matrix and thereby the overall film quality and dielectric performance of the nanocomposites.⁷⁵

Chemical modification of nanoparticles is also a useful approach to facilitate the dispersion of nanoparticles. For instance, Kim et al. reported that surface modification of BaTiO₃ and related perovskite-type metal oxide nanoparticles with phosphonic acid ligands leads to well-dispersed BaTiO₃/polymer nanocomposite films with high dielectric strength.³⁹ This methodology is straightforward and easily adapted to a wide range of systems by choosing appropriate ligand functionality. Another example is related with CuPc as discussed in section 1.5.6. Chemically modified CuPc can improve the dispersion of CuPc in polymer matrix. Compared to the simple blending method, the CuPc oligomer particulates in grafted sample are of relatively uniformly size in the range of 60-120 nm, which is about 5 times smaller than that of blended composite. Furthermore, dielectric loss was reduced and dielectric dispersion over frequency was weakened.⁵⁰

1.6.3.3 Control of Dielectric Loss for Conductive Filler/Polymer Nanocomposites

Conductive filler/polymer nanocomposites have been identified as a promising method to fulfill the material requirements for embedded capacitors. However, the dielectric loss of this type of materials is very difficult to control, because the highly conductive particles are easy to form a conductive path in the composite as the filler concentration approaches the percolation threshold. To solve this drawback, currently much work has been directed to the control of the dielectric loss of this system.

The direct contact of the conductive metal fillers will lead to high dielectric loss or even conduction for the conductive filler/polymer composites at or above percolation threshold. Therefore, core-shell structured filler was proposed to be utilized as fillers instead of using conductive filler directly because the non-conductive shell could serve as electrical barriers between the conductive cores to form a continuous interparticle barrier-layer network and thus achieve high- k and low loss. The core-shell structure can be formed either pristinely or by synthesis.

For instance, Al/polymer composite with low loss and relatively high k using self-passivating Al as the filler has been developed by Xu et al.⁴¹ This approach combines the advantages of ceramic/polymer and metal/polymer systems. Figure 1-15 (a) shows a high resolution TEM micrograph of a 100 nm Al particle, which has an oxide thickness about 2.8 nm. The self-passivated insulating aluminum oxide (Al_2O_3) layer on the Al metallic core showed significant effects on the dielectric properties of the corresponding composites. The nanoscale insulating oxide layer allows the Al/polymer composites to have a high dielectric constant as a percolation system; on the other hand, the insulating oxide layer confines the electrons within an Al particle, thus retaining a very low loss of the composites. The dielectric properties of Al/epoxy composites as a function of filler loading are shown in Figure 1-15 (b). A high k of 109 with low dissipation factor of 0.02 (epoxy-based resin has a loss factor of 0.02) has been obtained for a unimodal 80 wt. % Al (3 μm)/epoxy composite. For bimodal Al/epoxy composites, a much higher dielectric constant of about 160 has been accomplished.

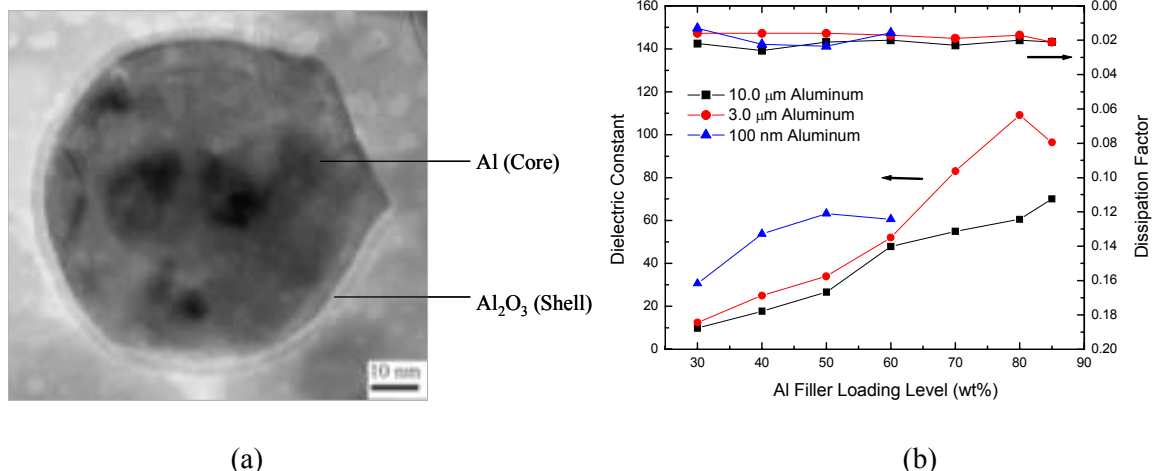


Figure 1-15. (a) HRTEM micrograph of a 100 nm Al particle with an oxide thickness about 2.8 nm and (b) dielectric properties of Al composites as a function of filler loading.

Most recently, Shen et al. reported a new polymer composite using synthesized core/shell hybrid particles with metal Ag cores coated by organic dielectric shells as fillers. The organic dielectric shells act as interparticle barriers to prevent the direct connection of Ag particles and facilitate the dispersion of fillers in the polymer matrix as well, leading to stable high k (>300) and rather low dielectric loss tangent (<0.05) for the polymer dielectric.⁴⁸

Similarly, attempts have been made to reduce the dielectric loss of the conductive filler/polymer nanocomposites by introducing surfactant layer coated on the metal filler surfaces during nanoparticle synthesis. The surfactant layer on the nanoparticle surfaces is expected to serve as a barrier layer to prevent the formation of conduction path to control the dielectric loss. For examples, Qi et al. reported a Ag/epoxy nanocomposite with 22 vol. % of Ag possessing a high k of 308 and a relatively low dielectric loss of 0.05 at a frequency of 1 kHz.⁴⁶ In this material system, 40 nm Ag nanoparticles coated with a thin layer of mercaptosuccinic acid were randomly distributed in the polymer matrix. As displayed in Figure 1-16, the k and dielectric loss increase with the filler

concentration up to 22 vol. %. The decrease of k after that point is not due to conduction, and this is attributed to the porosity as revealed from microstructure investigation. The introduction of porosity is possibly caused by the absorbed surfactant layer, which leaves space between Ag particles and the voids are not occupied by polymer. Another contributor could be micropores formed from solvent residue during curing, especially at a higher Ag content. In addition, no rapid increase of the dielectric loss tangent values was observed. Therefore, the observed highest k value was not considered as a real percolation threshold and the formation of a conducting filler network was prevented by the surfactant coating layer.

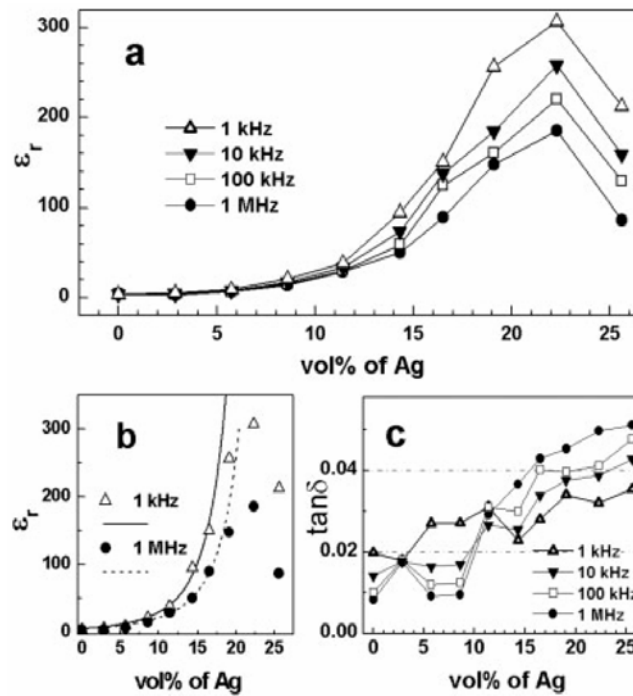


Figure 1-16. The dependence of dielectric constant and dielectric loss tangent values on silver volume fraction and frequency.⁴⁶

1.7 Challenges for Embedded Capacitor Materials

Past efforts, current status and recent advances in the field of high- k materials for embedded capacitor applications have been reviewed in previous sections. Generally speaking, high- k materials which meet the requirements for this application should possess high dielectric constant, low dissipation factor, high thermal stability, simple processibility, and good dielectric properties over broad frequency range. However, no such ideal materials that satisfy the above-mentioned prerequisites simultaneously have been realized till present. Polymer nanocomposite materials, arguably regarded as the most promising candidate material, have been studied extensively. Efforts to improve the overall dielectric performance of these materials have been devoted to maximize the dielectric constant and suppress the dielectric loss.

New insights into the unique properties of the nanoparticle filler, filler modification and the dispersion between filler and polymer matrix are anticipated to be gained for dielectric property enhancement of hi- k nanocomposites. Specifically, the required knowledge and technology include: (1) optimized formulation of dielectric materials with high filler loading of high- k ceramics for ceramic-polymer nanocomposites and appropriate loading level of conductive fillers in the neighborhood of percolation threshold for conductive filler-polymer nanocomposites; (2) improvement in microstructure of dielectric materials including filler size and distribution, morphology, degree of aggregation, packing, and dispersion in the polymer matrix; (3) enhancement of k values of nanocomposites by employing high- k polymer matrix; (4) modification of the filler interface to facilitate dispersion in the polymer matrix and suppress the dielectric loss of the composite materials etc.

1.8 Research Objectives

Novel materials for embedded capacitor applications are in great demands, for which high k , low dielectric loss and process compatibility with PCBs are the most important prerequisites. Dramatic increase of dielectric constant close to the percolation threshold observed in the conductor-insulator percolative system arouses interest of developing conductive filler/polymer composites as candidate materials for embedded capacitor applications. One of the major hurdles for this type of high- k composites is the associated high dielectric loss. However, the approaches to control the dielectric loss have not been studied thoroughly.

Accordingly, the overall objective of this research is to design and develop nanocomposites based on nanoparticles with controlled parameters to fulfill the balance between sufficiently high k and low dielectric loss, and satisfy the requirements to be a feasible option for embedded capacitor applications.

Specifically, this research involves the following aspects:

- Synthesize the metal nanoparticles with controlled parameters including size, size distribution, aggregation and surface properties.
- Prepare the nanocomposites based on these varied nanoparticles using both *ex-situ* and *in-situ* techniques.
- Investigate the dielectric behavior of the nanocomposites systematically over a range of frequencies to determine the dependence of dielectric constant, dielectric loss tangent and dielectric strength on these parameters. Provide information about the appropriate size, size distribution and aggregate status which might impact the

changes of the dielectric properties and allow for effective enhancement of the dielectric properties of the high- k nanocomposites.

- Employ surface modification of metal nanoparticles to change the surface chemistry and physical properties of nanoparticles and therefore to improve dispersion of nanoparticles in the polymer matrix and tailor the dielectric properties of corresponding polymer nanocomposites. Explore different surface modification conditions such as modification agents and their concentrations, solvent media etc., which may play complex roles in the quality and degree of the surface modification.
- Explore an *in-situ* photochemical method to prepare metal nanoparticle-polymer composite as high- k polymer matrix in which metal nanoparticles were generated by photochemical reduction of a metallic precursor within the polymer matrix. The as-prepared high- k polymer matrix can be used to host various fillers such as conductive metal or ferroelectric ceramic fillers to achieve both high k and relatively low dielectric loss.
- Explore an approach to incorporate organic conductive element in the polymer matrix. Investigate the possibility of all-organic composites as a high- k material candidate for embedded capacitor.

CHAPTER 2

EXPERIMENTAL

2.1 Materials

2.1.1 Epoxy

To ensure low-temperature and low-cost processibility, high- k dielectric nanocomposites for embedded capacitor applications in this research was based on polymer matrices. Specifically, epoxy-based composites were the focus of this research because of its good compatibility with the sequential build-up processes of organic substrates.

An epoxy generally refers to a molecule containing one or more reactive epoxy (1,2-epoxide or oxirane) groups, which are three-member ring consisting of a oxygen bonded to two carbon atoms. In the cured resin, all of epoxy groups may have reacted and it no longer contains any epoxy group, but the cured resin is still called epoxy. Most common epoxy resins are produced from a reaction between epichlorohydrin and bisphenol-A. The first commercial attempts to prepare resins from epichlorohydrin were made in 1927 in the United States. Because of the strained nature of the three-member ring, epoxies are highly reactive. The chemistry of epoxies and the range of commercially available variations allow them to be produced with a very broad range of properties. In general, epoxies are known for their excellent adhesion, chemical and heat resistances, good to excellent mechanical properties and very good electrical insulating properties,

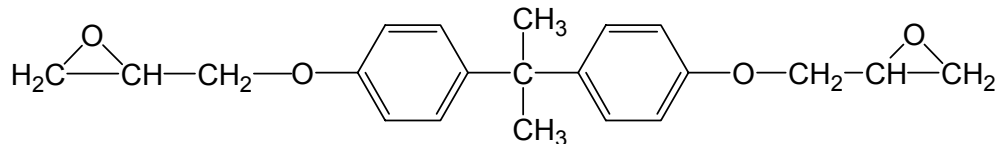
which make them cover extensive applications including coatings, adhesives and composite materials such as those using carbon fiber and fiberglass reinforcements. It is also predominating thermosetting resin for electronic packaging.

An epoxy is typically composed of an epoxy resin, a hardener, a catalyst, and some necessary additives and modifiers.

2.1.1.1 Epoxy Resins

The base epoxy resins are very important in that many ultimate material properties such as viscosity, adhesion, toughness, moisture absorption, and electrical properties are mainly determined by the base epoxy resins. The commonly used epoxy resins can be categorized in two groups: diglycidyl ether type and cycloaliphatic type. The chemical structures of bisphenol-A type epoxy and cycloaliphatic epoxy used in this research are show in Figure 2-1.

Bisphenol A (EPON 828):



Cycloaliphatic (ERL 4221)

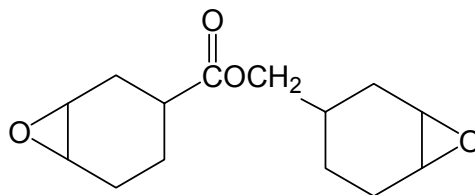


Figure 2-1. Chemical structures of liquid bisphenol A and cycloaliphatic epoxy resins.

The bisphenol-A epoxy (EPON 828) with an equivalent epoxide weight (EEW) of 187 g was supplied by Shell. The cycloaliphatic epoxy (ERL 4221) with an EEW of 134 g was supplied by Union Carbide.

2.1.1.2 Curing Agents

The curing agents (hardeners, crosslinkers) are necessary to promote crosslinking or curing of epoxy resins to convert them into hard, infusible three-dimensional thermoset networks. The curing process is by either homopolymerization initiated by a catalytic curing agent or polyaddition/copolymerization with a multifunctional curing agent.⁷⁶ The epoxy resin curing agents can be divided into three categories⁷⁷:

(1) Active hydrogen compounds include polyamines, polyacids such as carboxylic acids and anhydrides, polymercaptans, and polyphenols. Epoxy resins are cured by polyaddition reactions via the compound containing the active hydrogen and the terminal carbon of the epoxide group, with a stabilization of the epoxide into a hydroxyl group.

(2) Ionic initiators can be subdivided into anionic initiators (such as metal hydroxides, secondary amines, and tertiary amines) and cationic initiators (such as metal halides, boron-trifluoride complexes, and coordination catalysts, i.e., metal alkoxides, metal chelates, and metal oxides). They initiate homopolymerization and cure an epoxy resin through ionic or coordination polymerization.

(3) Hydroxyl crosslinkers, which couple through the secondary hydroxyls of the high molecular weight bisphenol A-type epoxy resin, are represented by a broad range of melamine-, phenol-, and urea-formaldehyde resins.

In this research, a carboxylic anhydride (4-methylhexahydrophthalic anhydride, MHHPA, Aldrich Chemicals), a polycycloaliphatic amine (Ancamine 2167 from Air

2.1.1.3 Catalysts/Accelerators

The pot-life, curing temperature and time, and processability of an epoxy system are mainly determined by the curing catalysts. Tertiary amines, imidzaoles, and ureas are the most frequently used curing catalysts. Tertiary amines, which react with epoxy resins at low temperature as curing agents, can also be used catalytically as accelerators in elevated temperature cured system, e.g. anhydride/bisphenol-A type epoxy system. Imidazoles are efficient accelerators for anhydrides and dicyandiamide, and can act as catalytic epoxy curing agents at moderate to high temperatures also. The imidazole catalysts used in this research are 1-methylimidazole from Aldrich Chemicals and 1-cyanoethyl-2-ethyl-4-methylimidazole (2E4MZ-CN) from Shikoku Chemicals, whose chemical structures are shown in Figure 2-7. They react at the 3-N position with a molecule of epoxy ring to form a highly reactive alkoxide ion, which initiates rapid anionic polymerization of epoxy resin, as shown in Figure 2-8.⁷⁶

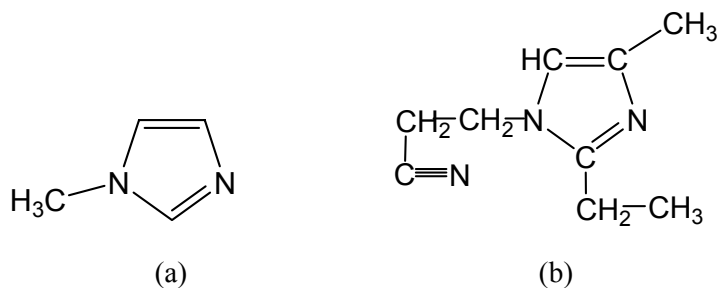


Figure 2-7. Chemical structure of 1-methylimidazole and 2E4MZ-CN.

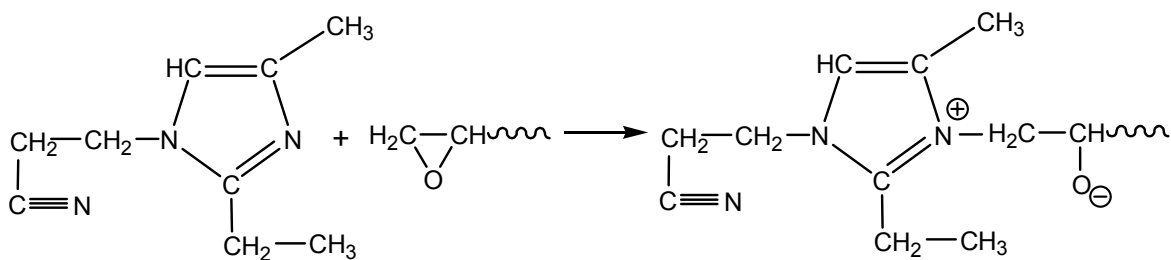


Figure 2-8. Reaction mechanism with imidazole catalyst.

2.1.1.4 Fillers

Fillers are the most common formulatory ingredient employed in the majority of epoxy formulations besides the resin and curing agents. Various filler type can provide a wide range of characteristic modifications on the properties and characteristics of epoxies for many applications. Some of the most important fillers and potential property modifications employed in epoxy formulations are summarized in Table 2-1. Despite this beneficial effect, fillers can cause some disadvantageous characteristics such as an increased density together with an increase in viscosity.

Table 2-1. Typical filler types and potential property modifications in epoxy formulations.

<i>Filler</i>	<i>Property modification</i>
Aluminum	Machinability, impact resistance, thermal conductivity, mechanical properties, dimensional stability
Alumina	Abrasion resistance, electrical resistivity, dimensional stability, toughness, thermal conductivity
Calcium carbonate	Extender, pigmentation, dimensional stability, machinability, mechanical properties
Carbon black	Reinforcement, pigmentation, thermal conductivity, electrical conductivity, thermal resistance
Copper	Electrical conductivity, thermal conductivity, mechanical properties
Colloidal fumed silica	Thixotropy
Fibrous glass	Impact strength
Graphite	Lubricity, pigmentation, thermal conductivity, electrical conductivity, abrasion resistance
Mica	Electrical resistance, dielectric properties, chemical resistance, toughness, moisture resistance, lubricity
Quartz	Electrical properties, dimensional stability, extender
Fused silica	Abrasion resistance, electrical properties, dimensional stability, extender, thermal conductivity, moisture resistance
Silver	Electrical conductivity, thermal conductivity
Titanium dioxide	Pigmentation, dielectric properties, extender

In this research, with an aim to prepare high- k conductive filler/polymer composite materials, the fillers incorporated in the epoxy composites are metal fillers, specifically Ag nanoparticles, either synthesized in our lab or supplied by nGimat Co., and Al particles supplied by Alfa-Aesar Chemical Co.

2.1.1.5 Additives and Modifiers

In addition to the main ingredients of an epoxy formulation introduced above, many other formulatory materials are available and frequently employed to modify the characteristics and properties of epoxies. For the filled epoxy systems, coupling agents are often used to improve the adhesion between epoxy resin and filler. In addition to adhesive bonding, the coupling agents have also been employed to enhance the properties of filled epoxy systems, such as moisture resistance, mechanical properties and so on. Organo-silanes, mercapton compounds, titanate, and aluminum chelates can be used as coupling agents, but the most popular ones are organo-silane compounds.⁷⁹ Dispersing agents are used to effectively disperse fillers into the epoxy resin and thereby the epoxy resin composition thus prepared has high dispersion stability and exhibits improved properties. Acidic phosphate ester BYK 9010 from BYK Chemie is copolymer with acidic groups.

2.1.2 Benzocyclobutene (BCB)

Benzocyclobutene (BCB)-based polymeric materials have recently attracted growing attention and research interest in the area of structural and electronic applications because of the versatile chemistry of benzocyclobutene as well as the combined advantages of processability and properties such as a low dielectric constant

and dissipation factor, a high T_g , very low water uptake, and a high degree of planarization. BCB, siloxane-crosslinked polymeric materials, obtained via thermal ring-opening at elevated temperatures ($\sim 200\text{ }^\circ\text{C}$) to provide reactive o-quinodimethane and successive 1,4 addition via Diels-Alder cycloaddition/polymerization of the divinyltetramethyl-disiloxane-bis(benzocyclobutene) monomers (see Figure 2-9). BCB needs to be cured under nitrogen purging in a Lindberg furnace to avoid oxidation.

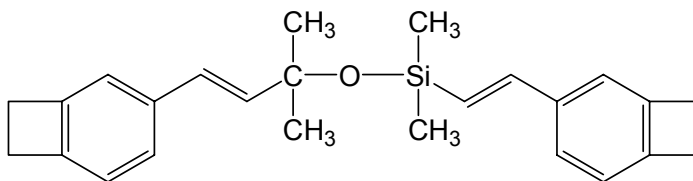


Figure 2-9. Structure of BCB monomer.

BCB has been developed as a thin film dielectric for microelectronics applications because it possesses many of the requisite dielectric properties. It has a low dielectric loss tangent of 0.001 and a low k of about 2.7. The leakage current is low and the dielectric breakdown strength is found to exceed 5 MV/cm, which is about one magnitude higher than epoxy resins. And also it is processible pin-hole free down to a few nanometers. BCB (Cyclotene 3022-35) from Dow Chemical Company is used in this research.

2.1.3 Polyaniline (PANI)

The composites fabricated by dispersing an organic conductive material possessing very high k in a polymer matrix can exhibit high k as well. The possibility of all-organic composites as candidate high- k material for embedded capacitor was investigated in this work as well. As one of the most widely used conductive polymer, polyaniline (PANI) was used in this work.

Polyaniline was first prepared by Letheby in 1862 by anodic oxidation of aniline in sulphuric acid.⁸⁰ PANI is regarded as one of the most promising electrically conductive polymers (ECP) owing to its high polymerization yield, good environmental stability combined with moderate electrical conductivity and relatively low cost. ECPs are able to conduct electricity because of their conjugated *p*-bond system, which is formed by the overlapping of carbon *p* orbitals and alternating carbon-carbon bond structure. In PANI, nitrogen *p_z* orbitals and C rings are also part of the conjugation system. The conjugated double bonds permit easy electron mobility throughout the molecule due to the delocalization of the electrons, making the polymer electrically conductive.²⁷

Figure 2-10 displays general chemical formula of PANI. PANI can exist in three forms of oxidation states: fully reduced leucoemeraldine ($x = 0$, only benzenoid amine structures), partially reduced and partially oxidized emeraldine ($x = 0.5$, neutral), and fully oxidized pernigraniline ($x = 1$, only quinoid imine structures).

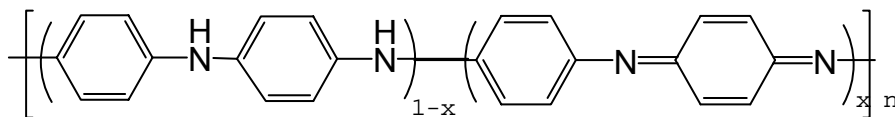


Figure 2-10. General chemical formula of PANI.

The emeraldine-base (EB) form of PANI (PANI_{EB}) is easily processed and widely used. The emeraldine-based form of PANI is also the most stable of the three states as shown in Figure 2-11.

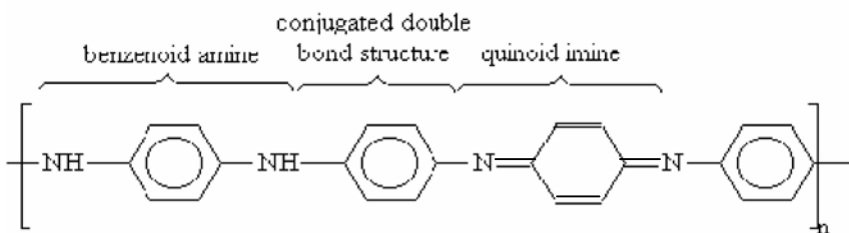


Figure 2-11. Structural formula of undoped PANI_{EB}.

Simple acid-base chemistry can be employed to control the physical and structural properties of the EB form of PANI. PANI_EB can be transformed to emeraldine-salt (ES) form (PANI_ES) by doping them with oxidative/reductive substituents through acid/base protonation or by donor/acceptor radicals through charge transfer reactions.⁸⁰ This process will increase the polymer's ability to conduct electricity because of the increased concentration of charge carriers. For instance, the electrical conductivity of PANI could be selectively tailored from 10^{-10} - 10^{-8} S/cm to 10^{+1} S/cm, which depends on the redox state, the doping level, solvent and solvent vapors, and moisture content of the polymer.^{81,82} The conductivity can be increased because doping process can form a polaron/bipolaron structure which will increase PANI's charge due to increased delocalization. When PANI_EB is protonated with acid, the bipolaron structure is formed via the attachment of the hydrogen ions to the quinoid nitrogen atoms. This structure is highly unstable because of the high energy this structure possesses. Thus, the C=N bonds of the quinoid imine structure will break, transforming the quinoid ring into a more stable benzenoid ring with lower energy, by aromatization, creating the bipolaron structure of doped PANI_ES (see Figure 2-12).

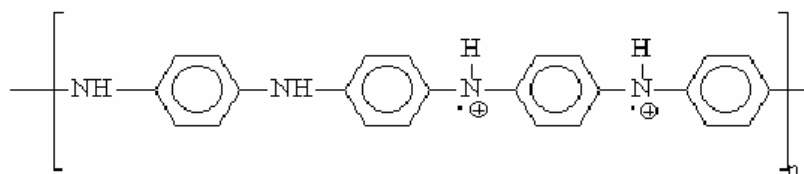


Figure 2-12. Bipolaron structure of doped PANI_ES.

The new benzenoid ring, although more stable than the initial structure, still has high energy because of the repulsion force between the adjacent positive charges. In order to stabilize this structure, the positive charge of one of the hydrogen ions will

neutralize the charge by attracting electrons from the neighboring benzene ring. As such, two new positively charged nitrogen groups with a neutral nitrogen atom in between are formed. The increased distance between the two positive charges results in the isolated polaron structure (see Figure 2-13), which has a lower energy level than the bipolaron structure.

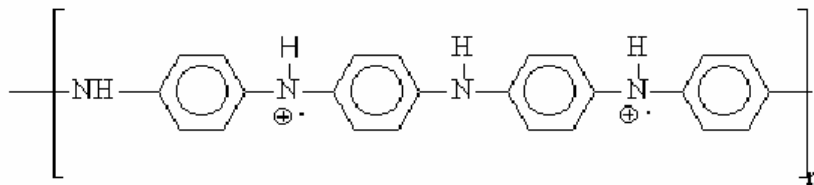


Figure 2-13. Polaron structure of doped PANI_ES.

One of the problems which limit the application of PANI is its poor processibility caused by poor solubility in the conducting emeraldine salt form. Many researchers have attempted to alleviate this problem by substitution of aromatic ring of PANI with $-CH_3$, $-OCH_3$, $-SO_3$, or long alkyl chain to increase its solubility in organic solvents because of decreased polymer chain stiffness and interaction between polymer chains. However, it is still difficult to dissolve PANI in the conducting ES form. Furthermore, steric hindrance induced by the substituents, increased interchain length and decreased conjugation length will cause the conductivity decreament.⁸³ Recently, Cao et al. reported that doping PANI by functionalized protonic acid, like camphorsulfonic acid (CSA) and dodecylbenzenesulfonic acid (DBSA) etc., renders the solubility of PANI in the conducting ES form in common nonpolar or weakly polar organic solvents. This counter-ion induced processability not only enables the processing of PANI_ES in common organic solvents, but also facilitates the preparation of PANI polymer blends in other bulk polymers because most commercial polymers can be codissolved in these solvents.⁸⁴

2.2 Preparation of Nanoparticles and Nanocomposites

2.2.1 Synthesis of Metal Nanoparticles

Due to the extremely small sizes and large specific surface areas of nanoparticles, they usually exhibit exceptional electrical, optical, magnetic, physical and chemical properties and are potentially favored for various application such as electronic, optical and mechanical devices, magnetic recording media, superconductors, high-performance engineering materials, dyes and pigments, adhesives, drug delivery, and so on. Many approaches have been developed to prepare and stabilize metal nanoparticles, including gas evaporation, sputtering, sol-gel, hydrothermal, microemulsion, polyols, laser pyrolysis, photochemical or sonochemical synthesis, chemical (co-)precipitation, and so on. These methods could be generally divided into top-down and bottom-up approaches. The top-down methods broadly employed in semiconductor technology (lithography) are mainly based on milling of metal materials. But this method does not allow produce desired particle size and shape. The bottom-up methods build the nanostructures from atoms, molecules or atom clusters using physical deposition or chemical methods. For chemical methods, nanoparticles are prepared by chemical reactions from appropriate precursors with stabilizers, such as ionic or nonionic surfactant and polymers, in the form of a colloid solution. Among these reported methods, the chemical (co-)precipitation is considered one of the most promising one because of its simplicity and productivity.

The chemical (co-)precipitation, i.e. homogeneous and heterogeneous nucleation of metal nanoparticles, is based on the super-saturation of reactant solutions comprised of precursors (metal salts), reducing agent, stabilizers, co-stabilizers and various additives. The super-saturation state can be reached by the reduction in temperature to convert

highly soluble chemicals into less soluble chemicals. The sufficient high temperature of the solution initiates the chemical reaction of the reagents and forms a super-saturation of species in solution. Upon nucleation of primary particles, the concentration of these species drops below the critical nucleation concentration, and so further material can only add to the existing nuclei. The size distribution is determined by the time over which the nuclei are formed. A general scheme for preparing mono-dispersed metal nanoparticles requires a single, temporally short nucleation followed by slower growth on the existing nuclei. Polydispersity increases as a result of the second nucleation as well as Ostwald ripening. In the process of Ostwald ripening, the large nanoparticles grow on the expense of the small ones as the high surface energy of the small particles promotes their dissolution and the afterwards dissolved material is redeposited on the large ones. In general, the particle size increases with increasing reaction time and temperature. The particle dispersions can be stabilized and isolated from their growth solutions if the interaction between the capping groups and the solvent is favorable, providing an energetic barrier to counteract the van der Waals and other attractions between nanoparticles. Consequently, the particle size could be controlled by systematic adjustment of the reaction conditions including time, temperature, concentration and chemistry of reagents and stabilizers.^{53, 85,86,87}

2.2.2 Preparation of Nanocomposites

Two main challenges remain for the development of polymer nanocomposite materials after the desired nanoparticle has been selected for the polymer of interest. One is an interfacial interaction and/or compatibility between the choice nanoparticles with the polymer matrix. The other is the proper processing technique required to uniformly

disperse and distribute the nanoparticles or nanoparticle aggregates within the polymer matrix.

In this research, varied high-*k* nanocomposites were prepared using both *ex-situ* and *in-situ* techniques. For *ex-situ* formation of commercially available Ag nanoparticles, they are processed into composites using solution-phase mixing method. An *in-situ* formation of Ag nanoparticle in a polymer matrix was also used to prepare polymer nanocomposite because the *in-situ* method could obtain smaller particle size and achieve better control of the dispersion of the nanoparticles in polymers compared to a simple mixing method.

2.3 Instrumentation and Characterization Procedure

2.3.1 Differential Scanning Calorimeter (DSC)

The differential scanning calorimeter (DSC) can be used to investigate the curing profiles and glass transition temperature of polymers and polymer nanocomposites as polymer curing and glass transition process involve heat-related events. From DSC thermograph, the curing onset temperature, peak temperature, end temperature, heat capacity, degree of curing, and glass transition temperature can be obtained. A modulated DSC (Model 2920, TA Instruments) was used to obtain cure information of the polymer formulations and the glass transition temperature (T_g) of cured polymer and polymer nanocomposites.

In DSC studies, a polymer sample of ~10 mg was placed in a hermetic DSC sample pan. For curing kinetics studies, the sample and a reference were heated in the DSC cell at a rate of 5 °C/min from room temperature to 300 °C under standard mode.

Heat was transferred through the disk up into the sample and reference. The difference in the heat between the sample and reference was measured as differential heat flow. The differential heat flow as a function of time and temperature was recorded. For the study of the glass transition temperature of a cured formulation, the sample and a reference were then heated to 250 °C at a rate of 5 °C/min under modulated mode in order to separate the reversible and non-reversible events. N₂ purging was applied during all experiments. The purging rate was 40 ml/min for DSC cell and 110 ml/min for refrigerated cooling system (RCS).

2.3.2 Thermogravimetric Analyzer (TGA)

A thermogravimetric analyzer (TGA, Model 2050, TA Instruments) was used to characterize the material mass change, either as a function of temperature, or isothermally as a function of time, in a controlled atmosphere. TGA can be used to characterize any material that exhibits a weight change due to decomposition, oxidation, or dehydration. In this research, TGA was used to investigate the oxidation (weight gain) of filler particles, degradation (weight loss) of materials coated on filler particle surfaces, and thermal stability (weight loss) of cured high-*k* composite formulations. In a TGA measurement, the weight of sample, temperature, and time were recorded. A platinum sample pan was used for characterization of non-metal fillers and formulations; and a ceramic sample pan was used for characterization of metal fillers. About 20 mg sample was placed in the TGA sample pan and then heated from room temperature to desired temperature (up to 800°C) at a rate of 10°C/minute in a nitrogen or air atmosphere. TGA curve showed the sample mass as a function of temperature or time, from which the

weight change at a certain temperature can be obtained and the onset temperature of weight change can be defined.

2.3.3 LCR Meter

The capacitance and conductance of the nanocomposites in this research with parallel plate prototype was measured by a HP 4275 Multi-Frequency LCR Meter. The measurement was conducted at middle frequency range from 10 kHz to 4 MHz. The k values of the nanocomposites were calculated from capacitance measurements. Dielectric constant and dielectric loss tangent ($\tan\delta$) can be calculated from the capacitance and conductance measured by Equation 1-1 and Equation 2-1:

$$\tan \delta = \frac{G}{2\pi fC} \text{ Equation 2-1}$$

where C is the capacitance, G is the conductance, f is the frequency at which the capacitance and conductance are measured.

2.3.4 Surface Profilometer

In this research, the thicknesses of dielectric materials were measured by a KLA-Tencor P-15 profilometer. The P-15 profilometer is a highly sensitive surface profiler that accurately measures step height up to 326 μm . Measurements were made electro-mechanically by moving the sample beneath a diamond-tipped stylus. The sample beneath the stylus was moved according to the desired scan length, speed, and stylus force. Surface variations caused the stylus to be translated vertically and the instrument detected this motion.

2.3.5 X-Ray Diffractometer

X-ray diffraction (XRD) is a powerful and nondestructive technique used primarily for crystallographic characterization of solid materials, based on the basic principles that the angle of reflection of X-rays from a sample is related to the crystal structure and composition of the material. XRD can provide structural information of bulk materials and thin film, and also the composition of crystallographic phases present in a sample, the extent of defects, size and orientation of grains, and so on. The depth of analysis is in the range of 100 to 1000's Å.⁵ The XRD patterns of filler particles were characterized by an X-ray powder diffractometer (PW 1800, Philips Co.). The measurement was conducted at a scanning rate of 0.02°/s in the 2θ range from 10° to 110° with a Cu-K α radiation ($\lambda \sim 0.154$ nm). In this research, XRD was used to investigate the crystal structure of filler particles and calculate the size of particles.

2.3.6 Scanning Electron Microscope (SEM) and Energy Dispersive X-Ray Spectroscopy (EDX or EDS)

Scanning electron microscope (SEM) analysis involves detection of secondary and backscattered electrons from a sample rastered with a focused primary electron beam and leads to a surface image with a great depth of field. In addition to revealing morphological characteristics of a surface, an energy dispersive X-ray spectrometer (EDX or EDS) attachment can detect the X-rays emitted from the sample which is irradiated with the primary electron beam and provide information about the chemical composition of a specimen. A thermally-assisted field emission (TFE) scanning electron microscope (SEM, Model LEO1530) was used to investigate the microstructure of high- k nanocomposite materials. LEO 1530 is a state-of-the-art SEM, yielding 1 nm resolution

at 20 kV and 3 nm at 1 kV. The SEM was used to study the dispersion uniformity of the filler particles, the size of the agglomerate, and the connectivity between filler particles. The dispersion of nanofiller particles had dramatic affect on the electric and dielectric properties of high- k nanocomposite. For SEM characterization, the cross section of samples was polished before observation. For non-conductive dielectric samples, a thin layer of gold was sputter coated on the sample surface in order to obtain good images.

2.3.7 Transmission Electron Microscope (TEM)

Transmission electron microscopy (TEM) is a microscopy technique whereby a beam of electrons is transmitted through an ultra thin specimen, interacting with the specimen as it passes through it, magnified and focused by an objective lens and produces an image. In this work, JEOL 100CX II transmission electron microscope, operating at 100 kV, was used to observe the particle size and size distribution of nanoparticle synthesized or nanofiller incorporated in the epoxy formulation. A JOEL 4000EX high-resolution transmission electron microscope (HRTEM) was also used to analyze the particle size of core-shell particles and the thickness of the shell layer operating at 400 KV. The JOEL 4000 EX has a point-to-point image resolution of 0.18 nm, and it uses a top-entry specimen stage for high mechanical stability. Spatially resolved EDS attached with the HRTEM was used to confirm the presence and element composition of a thin layer of shell around the nanoparticles after surface modification.

2.3.8 Fourier Transform Infrared Spectroscopy (FTIR)

Infrared (IR) spectroscopy is a chemical analytical technique which detects the vibration characteristics (stretch, contract and bend etc.) of chemical functional groups in

a sample as an infrared light interacts with the matter (mostly organic). Based upon the wavelength (wavenumber) of light, infrared light can be categorized as far infrared ($4\sim 400\text{ cm}^{-1}$), mid infrared ($400\sim 4,000\text{ cm}^{-1}$) and near infrared ($4,000\sim 14,000\text{ cm}^{-1}$). The mid infrared, approximately $30\sim 1.4\text{ }\mu\text{m}$ in wavelength, may be used to study the fundamental vibrations and associated rotational-vibrational structure. In this work, the organo-functionalized surface chemistry of filler nanoparticles was characterized by a Nicolet Magna-IR 560 FTIR spectrometer. The filler particles were first dried in an oven at 100°C for 2 hours, and then KBr pellets were prepared with the dried particles. The spectrum was collected in the range from 4000 to 400 cm^{-1} .

2.3.9 Ultraviolet-visible (UV-Vis) Spectroscopy

Ultraviolet-visible spectroscopy is used to analyze compounds in the UV (200 to 400 nm) and visible (400 to 800 nm) region of the electromagnetic spectrum. The absorption in these regions corresponds to electronic transitions between different molecular orbitals of the systems. In particular, UV-Vis spectroscopy is of most use for identifying conjugated systems since transitions involving π orbitals and lone pairs tend to have stronger absorptions. In this work, the UV-Vis spectra of varied materials were recorded on a Beckman DU 520 General purpose UV-Vis spectrophotometer from the wavelength of 300 to 800 nm. The purpose of this characterization and sample preparation for different systems will be discussed in each chapter involved specifically.

2.3.10 X-ray Photoelectron Spectroscopy (XPS)

X-ray photoelectron spectroscopy (XPS), also known as electronic spectroscopy for chemical analysis (ESCA), is a sensitive nondestructive analysis technique for the

elemental composition and chemical state of the top 5 to 100 Å of a surface with a sensitivity of 0.1% of a monolayer.⁵ It operates on the basic principle as X-ray irradiation of sample results in emission of photoelectrons whose energy is related to binding energy of the electrons, providing elemental and chemical state information of the specimen. In this study, XPS was employed to investigate the surface chemistry characteristics of the Ag nanoparticles. XPS analysis was performed on a Model 1600 XPS with 46.95 eV X-rays from an Al K α source (1486.6 eV) with spectrometer resolution \sim 1.0 eV for survey scans and \sim 0.1 eV for high-resolution scans. It is equipped with an electron flood gun to neutralize charge build up and an Argon ion gun to etch and clean samples for depth profiling.

2.3.11 Proton Nuclear Magnetic Resonance (^1H NMR)

Proton nuclear magnetic resonance (^1H NMR) spectroscopy is a powerful method for determining the structure of organic compounds via their chemical shifts. The ^1H NMR spectrum of an organic compound provides information concerning the number of different types of hydrogens present in the molecule, the electronic environment of different types of hydrogens and the number of hydrogen "neighbor" a hydrogen atom has. The ^1H NMR spectrum of aniline salt Ani-CSA monomer was obtained on a 300 MHz Varian Mercury Vx 300 NMR spectrometers.

CHAPTER 3

CONTROL OF DIELECTRIC LOSS OF HIGH-K COMPOSITES BY INCORPORATION OF METAL NANOPARTICLES AND THEIR SIZE AND SIZE DISTRIBUTION EFFECT

3.1 Introduction

The increasing requirements for electronic circuit miniaturization and higher performance electronic device have driven the research and development of embedded passive components which possess more advantages over traditional discrete ones, including higher component density, increased functionality, improved electrical performance, increased design flexibility, improved reliability and reduced unit cost. Novel materials for embedded passive applications are in urgent demands, for which high k , low dielectric loss and process compatibility with the PCBs are the most important prerequisites.⁸⁸ Polymer composites provide an ideal solution to combine the dielectric or electrical properties of the ceramic or metal fillers and the low-temperature (<250 °C) processability and mechanical properties of polymer matrix.

For conductor-insulator composite percolative systems with dramatic increase of k close to the percolation threshold, besides the well reported metal/polymer composites,^{40,41,42,43,46,48} the carbon black (CB)/epoxy composite has also been considered as a candidate material for embedded capacitors due to its ultra-high k .^{44,45} Carbon black was selected as the filler due to its large surface area and its wide range of electrical properties

based on its particle size and aggregate structure. The dielectric properties of CB/polymer composites are strongly dependent on the particle size, aggregate structure, and conductivity of the carbon blacks. For example, for a highly conductive carbon black, a high k over 13,000 (@10 kHz) was observed, and for a relatively low conductivity carbon black, dielectric constant in thousands (@10 kHz) was easy to achieve.⁴⁵ Figure 3-1 (a) shows the TEM micrograph of carbon black powders (CBC2), with large primary particle size about 70 nm and not highly aggregated structures. Figure 3-1 (b) displays the dielectric properties of CBC2/epoxy and CBC2/silicone composites as a function of filler loading. It was found that the change of polymer matrix does not have a very significant influence on the dielectric properties of their composites as the charge transfer between aggregates cause high dielectric loss and the carbon black dominates the dielectric properties.

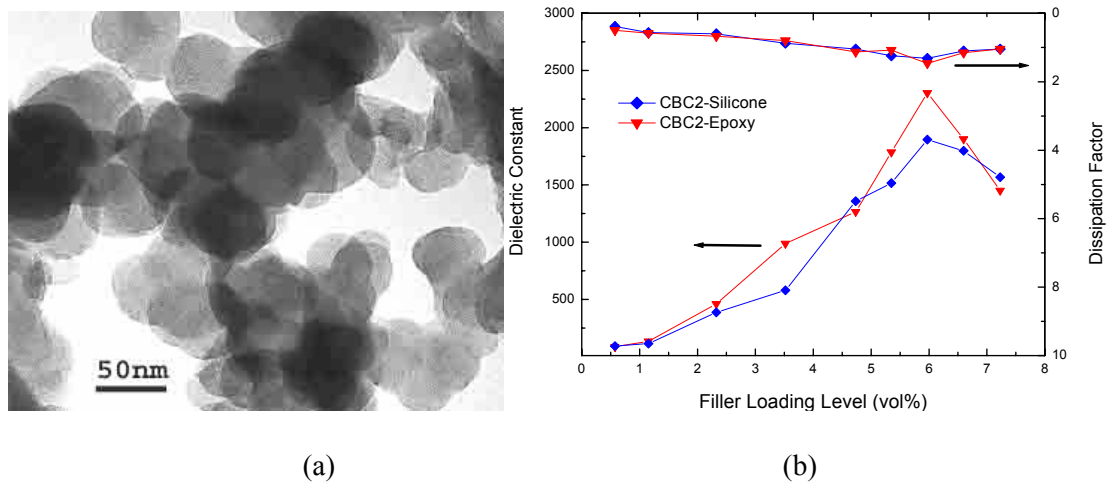


Figure 3-1. (a) TEM micrograph of carbon black; (b) dielectric constant and dissipation factor of carbon black/polymer composites as a function of filler loading.

Since the CB filler loading required to reach high k is much lower than that of ceramic/polymer composites, higher adhesion of carbon black composites to the substrates compared to that of the ceramic composites can be obtained. Although

CB/polymer composites can give extremely high k , the dielectric loss tangent of CB composites is also very high. The high dielectric loss is one key issue of this system that needs to be addressed for the embedded capacitor applications.

Materials based on nano-sized metals provide a potential solution to meet the present and future technological demand in virtue of the novel properties (plasmon absorption, superparamagnetism, Coulomb blockade etc.) and unique property combination of metal nanoparticles.⁷² The Coulomb blockade effect is one of the well-known quantum effects of metal nanoparticles. If the size of metal nanoparticle or so-called “Coulomb island” is small, the tunneling electron creates an additional barrier due to the charging energy $e^2/2C$ (where e is the electron charge unit, and C is the capacitance of metal island) to the further transfer of electrons. When the charging energy exceeds the thermal fluctuation energy $k_B T$ (where K_B is the Boltzman constant, and T is absolute temperature), the Coulomb blockade will occur, which inhibits the charge transfer through the small island below a certain voltage threshold and leads to an increase in resistance.^{89,90,91} Feng et al. studied the dielectric properties of Ag/PVA nanocomposites and found that the composite with 20-30 nm Ag particles has a higher resistivity and breakdown voltage than its matrix.⁹¹ Ideally, due to the Coulomb blockade effect, metal nanoparticles in a polymer matrix may reduce the electron tunneling and increase the resistivity of composites. Thus the conduction loss of the dielectric system might be mitigated to some extent. Tang et al. reported the effect of dispersed Ag nanoparticles on the dielectric properties of Ag/PbTiO₃ composite films and found that the dielectric constant of the films increases and the dissipation factor of the films decreases with the

addition of Ag nanoparticles into PbTiO₃ films at some loading level of Ag, but no mechanism were discussed.⁹²

On the other side, uniform dispersion of nanoparticles in the nanocomposites is required because clumps of particles inside the polymer matrix lead to deteriorated electrical or dielectric properties. However, uniformly dispersed ultrafine particles in a polymer matrix may not be easily achieved by incorporating pre-made nano-size particles into a polymer due to the easy agglomeration of nanoparticles and high viscosity of polymers, while the *in-situ* formation of metal nanoparticles in a polymer matrix could facilitate a more uniform dispersion of nanoparticles in polymers.^{72,93, 94,95} Moreover, much smaller particle size obtained by *in-situ* reduction than commercially available micron or nano-size Ag particles can help achieve thinner dielectric films leading to a higher capacitance density, and also more evident Coulomb blockade effects.⁹⁰

In this work, the *in-situ* formed Ag nanoparticles in a neat epoxy resin and Ag/CB/epoxy nanocomposites based on as-synthesized Ag/epoxy nanocomposite and CB/epoxy composite were investigated. The *in-situ* formed nanoparticles in the epoxy resins were characterized by transmission electron microscopy (TEM) and the nanocomposites were studied by scanning electron microscopy (SEM), X-ray diffraction (XRD) and thermogravimetric analysis (TGA). In addition, the dielectric properties of the nanocomposites filled with the *in-situ* formed Ag nanoparticles are discussed and correlated with the structure and morphology of the composites. The size, size distribution and loading level of metal nanoparticles in the nanocomposite were found to have significant influence on the dielectric properties of the nanocomposite system.

3.2 Experimental

3.2.1 Materials

A cycloaliphatic type epoxy resin ERL 4221E (Shell Chemicals Co.), an anhydride type curing agent hexahydro-4-methylphthalic anhydride (HMPA, Lindau Chemical Co.) and an imidazole type catalyst 1-methylimidazole (Aldrich Chemical Co.) were used. Silver nitrate (AgNO_3) and hydroquinone (both from Aldrich Chemical Co.) were selected as a metal precursor and a reducing agent, respectively. Heptanoic acid (Aldrich Chemical Co.) was employed as capping agent. A low aggregate structure carbon black (Columbia Chemical Co.) was used. Acetonitrile (Alfa Aesar Chemical Co.) was chosen as the solvent because of its low boiling point (82 °C) and capability of dissolving all other chemical ingredients.

3.2.2 *In-Situ* Formation of Ag Nanoparticles in an Epoxy Matrix

A cycloaliphatic epoxy resin ERL 4221E was selected as the polymer matrix in the dielectric formulations due to its low viscosity and low ionic contamination, and moreover, the presence of carboxylate groups of this epoxy matrix might interact with the silver ions and atoms and thus have some beneficial effects as regards to the final silver particle size and dispersion. The Ag nanoparticles were *in-situ* synthesized in the epoxy matrix via chemical reduction, specifically reduction of AgNO_3 with hydroquinone.⁹³ Epoxy resin and hardener were mixed in a 1:1 weight ratio in solvent. Different amounts of capping agents with respect to AgNO_3 were introduced to the reaction mixture to prevent the Ag nanoparticles from agglomeration. Then hydroquinone and AgNO_3 were dissolved in the mixture sequentially. The amount of hydroquinone was equivalent to 1.2

times the stoichiometric requirement (each mole of silver nitrate requires a half mole of hydroquinone for reduction). Finally the solvent was evaporated at room temperature for 30 min using a rotary evaporator under reduced pressure.

3.2.3 Preparation of CB/Epoxy Composite and Ag/CB/epoxy Nanocomposite

CB/epoxy composites were prepared by adding carbon black into the mixture of the epoxy resin and hardener. The carbon black was dispersed in the epoxy resin by an ultrasonicator for 1 hr, and then further mixed through a three-roll-mill for 10 runs. The Ag/CB/epoxy composite was prepared by mixing the *in-situ* formed nano Ag/epoxy mixture and CB/epoxy mixture via stirring for 15 min and then ultrasonication for 2 hr. Variation of Ag/epoxy and CB/epoxy compositions led to Ag/CB/epoxy nanocomposites with different loading levels of CB and Ag. The loading levels of fillers were estimated from remaining amounts in TGA tests.

3.2.4 Characterization

A JEOL 100C transmission electron microscope (TEM) was used for analyzing the size and size distribution of nanoparticles. Scanning electron microscopy (SEM) measurements were carried out on a JEOL 1530 equipped with a thermally assisted field emission gun operated at 10 KeV. Spatially resolved energy-dispersive X-ray spectroscopy (EDS) attached with the SEM was also used to confirm the presence of silver.

The X-ray diffraction (XRD) patterns of Ag/epoxy and Ag/CB/epoxy composites were recorded at a scanning rate of $0.02\text{ }^{\circ}\text{s}^{-1}$ in the 2θ range of 10° - 80° using an X-ray powder diffractometer (PW 1800, Philips Co.) with Cu-K α radiation ($\lambda \sim 0.154\text{ nm}$).

XRD was used to calculate the size of Ag nanoparticles in Ag/epoxy composite and Ag/CB/epoxy composite by the Scherrer method.⁹⁶

Thermogravimetric analysis was conducted on a TA Instruments 2050 TGA under a nitrogen atmosphere. The procedure was set as heating at 100 °C for 15 min and at 125 °C for 1 hr and with 5 °C/min ramping over the whole temperature range.

The capacitance and dielectric loss tangent of the Ag/CB/epoxy composites were determined using parallel plate capacitor type test coupons. Thick film of Ag/CB/epoxy mixture was made onto the copper clad FR-4 board with a doctor-blade. Then the samples were cured in the thermal oven at 100 °C for 0.5 hr and 125 °C for 1 hr. Finally, a DC sputter was used to deposit a thin layer of copper as the top electrode (about 3000 Å in thickness and 3.4 mm in diameter) onto the cured material through a shadow mask. The capacitance and dissipation factor of the capacitor were then measured with a HP 4263A LCR meter. The thickness of the dielectric film was measured with a profilometer (Alpha-Step Co.) and used to calculate the dielectric constant of the sample.

3.3 Results and Discussion

3.3.1 Two-Step Preparation of Ag/CB/Epoxy Nanocomposite

An attempt to *in-situ* form nano Ag in a CB/epoxy mixture was made, where the precursor and the reducing agent with solvent were added to the mixture. From this attempt, however, no uniform dispersion of Ag nanoparticles but only agglomerates of Ag near CB were obtained, which might be due to strong adsorption nature of CB. Therefore, a two-step method was used to prepare Ag/CB/epoxy composites. The

CB/epoxy mixture and *in-situ* formed nano Ag/epoxy mixture were prepared separately. Then the Ag/CB/epoxy nanocomposites were prepared by mixing various amounts of the pre-synthesized Ag/epoxy and CB/epoxy mixtures. TEM, SEM and XRD results indicated that ultrafine Ag nanoparticles were obtained in the Ag/epoxy mixture and their size and dispersion were retained in the final Ag/CB/epoxy composites. Therefore, this two-step method was effective in preparing the desired composites and all the samples investigated below were prepared in this fashion.

3.3.1.1 Preparation of a Ag/Epoxy Nanocomposite by an *In-situ* Reduction

One of the conventional avenues was to form the composites by mechanically mixing the polymer matrix and the metal nanoparticles which were prepared separately. However, it is extremely difficult to achieve the homogeneous dispersion of the nanoparticles in the polymer matrix in this way due to the easy agglomeration of nanoparticles and the high viscosity of polymer. To assure the well dispersion of the nanoparticles in the composite which is highly required to achieve high k and low loss, an *in-situ* synthesis of metal nanoparticles in the presence of the polymer matrix was employed to obtain Ag/epoxy nano-composites. The Ag nanoparticles were prepared by hydroquinone reduction of silver precursor AgNO_3 in a homogeneous mixture of epoxy resin, hardener and acetonitrile with appropriate capping agent. Then the solvent acetonitrile was evaporated at room temperature (20 °C) in the rotary evaporator under a reduced pressure. The size and distribution of Ag particles in obtained composite was observed via TEM by dispersing a small amount of composite in organic solvent.

3.3.1.2 Two Methods of Ag/CB/Epoxy Nanocomposite Preparation

Two different methods were tried to introduce Ag nanoparticles into a CB/Epoxy composite to form a Ag/CB/Epoxy nanocomposite. A relatively easy one-pot method was tried initially. The *in-situ* formation of Ag nanoparticles was attempted by reduction of AgNO₃ directly in a mixture of CB/epoxy composite and hydroquinone in acetonitrile. Then the solvent was evaporated at room temperature (20 °C) in the rotary evaporator under reduced pressure. However, Ag nanoparticles could not be obtained in the composite according to the observation of TEM micrograph of as-formed composite (see Figure 3-2). The reason might be that the reduced Ag failed to nuclear and grow as individual nanoparticles but covering the surface of CB when CB is present in the system. And also the re-agglomeration of CB occurred in the mixture once the CB/epoxy composite was dispersed in the solvent. Therefore, the one-pot method is not suitable to obtain the ideal dispersed Ag nanoparticles as well as CB in the composites. As such, the preparation of the Ag/CB/epoxy composite by a two-step method was carried out. Firstly, the CB/epoxy composite and Ag/epoxy nanocomposite were prepared separately. Then the Ag/CB/epoxy nanocomposite was prepared by mixing the as-formed Ag/epoxy nanocomposite and CB/epoxy composite via hand mixing and ultrasonication. Various loading of Ag/epoxy composite and CB/epoxy composite can lead to Ag/CB/epoxy nanocomposites with different loading level of CB and Ag.

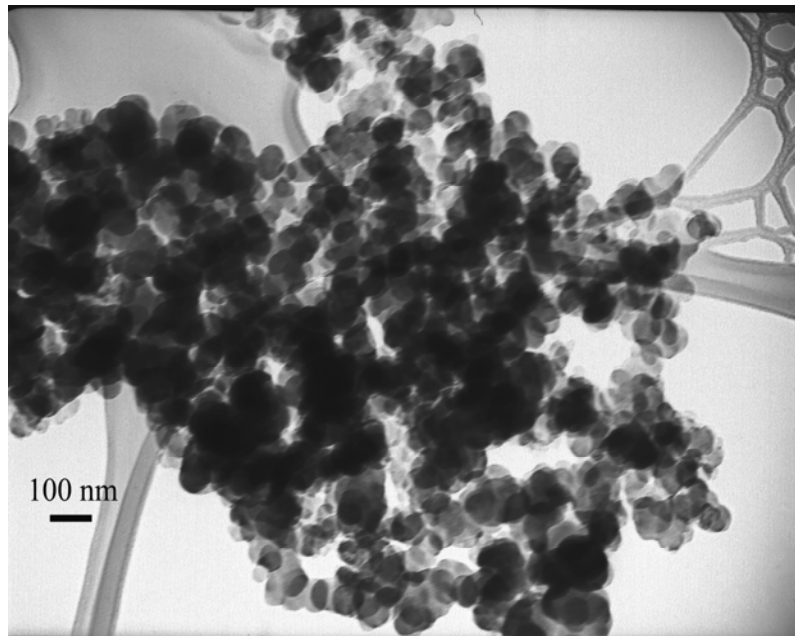
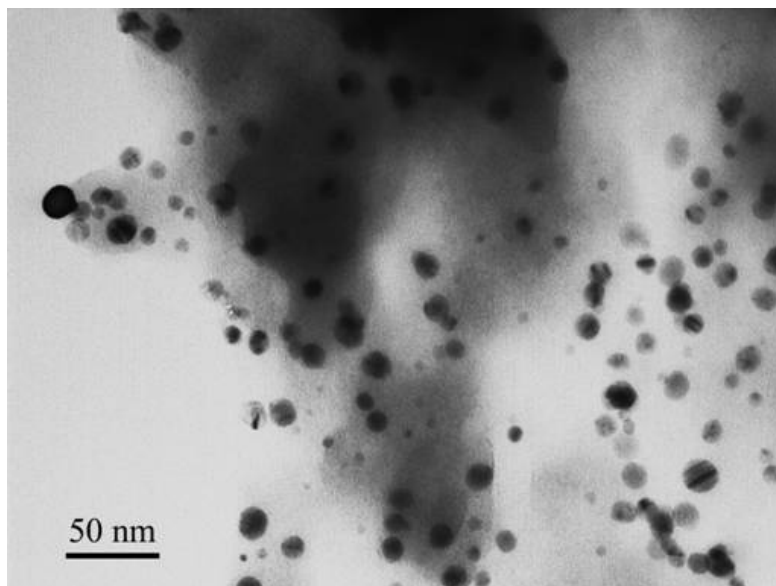


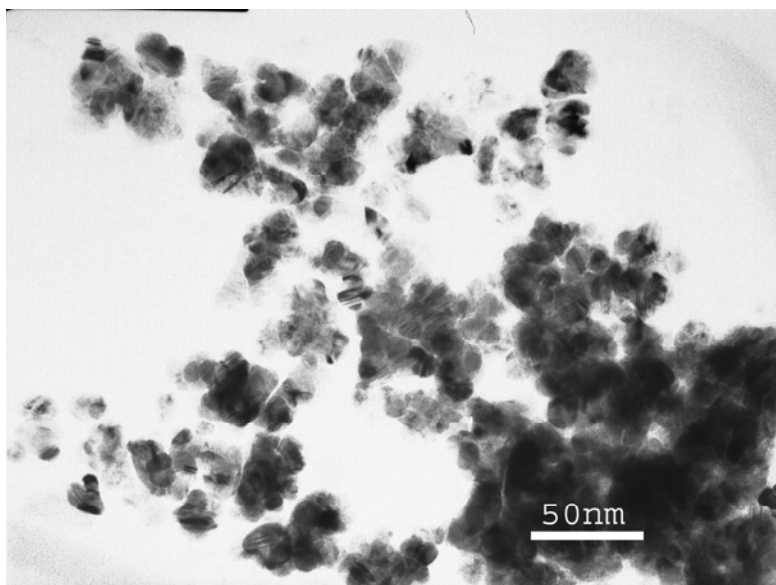
Figure 3-2. TEM micrograph of Ag/CB/epoxy composite prepared by one-pot method.

3.3.2 Effect of Capping Agent

To obtain smaller size and better dispersion of Ag nanoparticles in the polymer matrix, different capping agents were incorporated during the preparation of Ag/epoxy nanocomposites. Silane coupling agent and carboxylic acids of various chain lengths were tried to prevent the Ag nanoparticles from agglomeration. The influence of capping agents on the size and distribution of the resulting particles was studied. 3-aminopropyltrimethoxysilane (APS), a type of silane coupling agent, is demonstrated to be one of the effective capping agents for well dispersion of the Ag nanoparticles as compared from the TEM micrographs of obtained Ag/epoxy nanocomposite (see Figure 3-3). The nanoparticles are in the range of 15-20 nm while the smaller ones can be down to 3-5 nm. The stabilization effect can be attributed to the complexation of amino groups in APS to Ag nanoparticles.



(a)



(b)

Figure 3-3. TEM micrographs of Ag/epoxy composite (a) w/ APS (1 in molar ratio w.r.t. AgNO_3) and (b) w/o APS.

Furthermore, heptanoic acid was tried as a capping agent to control the size and size distribution of Ag nanoparticles in the polymer matrix. The influence of the capping agent concentration on the size and size distribution of the resulting particles was studied by TEM. Heptanoic acid was found to be effective in trapping small particles and render

uniform dispersion of Ag nanoparticles in the epoxy matrix. The affinity of carboxylic acid moiety of the capping agent to the Ag nanoparticles is responsible for the capping effect which retards extensive agglomeration of Ag nanoparticles.

Attempts to vary the amount of heptanoic acid relative to the silver precursor were made to further explore the effect of heptanoic acid on controlling the size distribution of Ag nanoparticles. Figure 3-4 shows the TEM micrographs of the *in-situ* formed nano Ag/epoxy mixture in the presence of a capping agent (CA) with different ratios to Ag precursor (R denotes $[CA]/[AgNO_3]$ ratio, i.e. the ratio of the capping agent to $AgNO_3$). The size range and average size of the Ag nanoparticles are summarized in Table 3-1. Nanoparticles of roughly two size ranges formed in all mixtures while the mixtures with higher concentrations of the capping agent showed the narrower size distribution. In the case of $R = 1$ and 0.6 (see Figure 3-4 (a) and Figure 3-4 (b)), Ag nanoparticles in size of 1-3 nm were well-dispersed, and some larger ones in size ranging from 6 to 8 nm. In the case of samples with $R = 0.4$ and 0.2 , both small and large particles in size of 1-3 nm and 30-45 nm, respectively, were observed simultaneously (see Figure 3-4 (c) and (d)). The average sizes of large particles were determined from the histograms to be 7.0 nm, 7.4 nm, 36.3 nm and 37.0 nm for samples with R values of 1, 0.6, 0.4 and 0.2, respectively. This might indicate that the nucleation and growth of Ag nanoparticles were influenced and controlled by the presence of the capping agent which helps inhibit the further growth and agglomeration of nanoparticles.

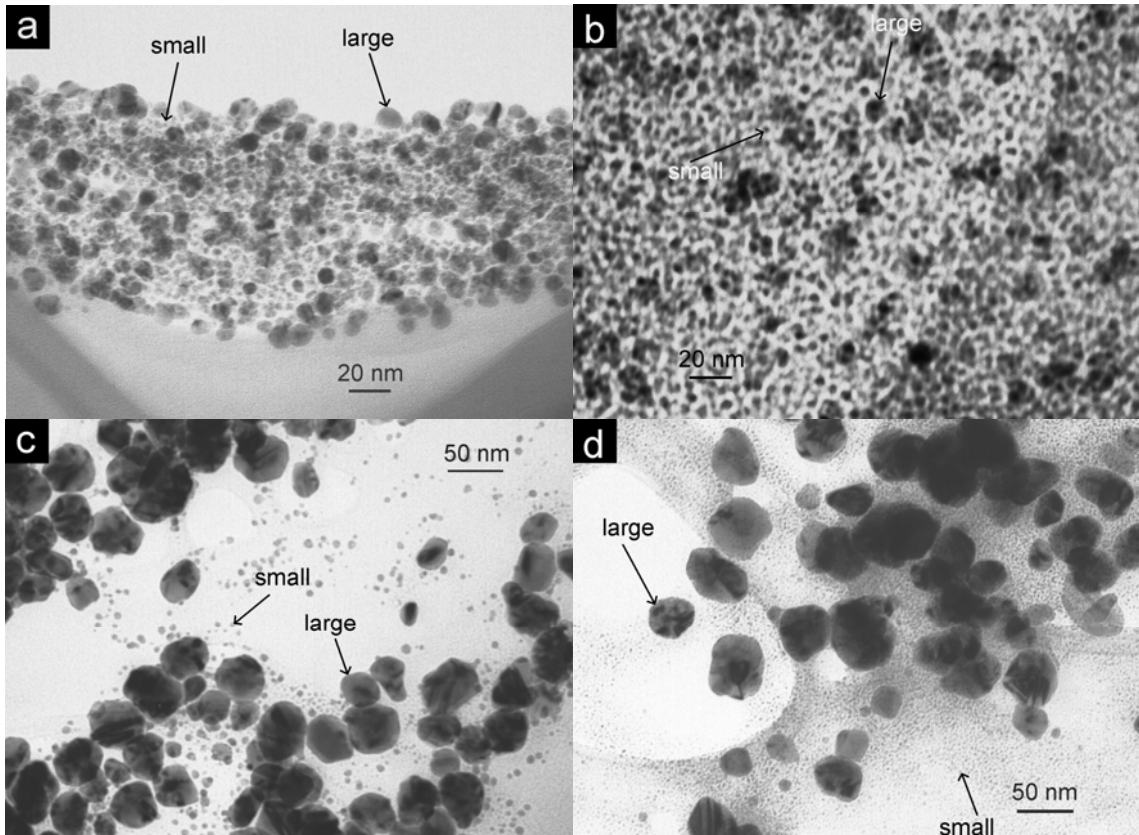


Figure 3-4. TEM micrographs of uncured Ag/epoxy mixtures in the presence of a capping agent with $[CA]/[AgNO_3]$ ratio (a) $R = 1$, (b) $R = 0.6$, (c) $R = 0.4$ and (d) $R = 0.2$.

Table 3-1. Size range of the Ag nanoparticles obtained.

		(a)	(b)	(c)	(d)
$R = [capping\ agent]/[Ag\ precursor]$ ratio		1	0.6	0.4	0.2
Size range	Small	1-3 nm	1-3 nm	1-3 nm	1-3 nm
	Large	6-12 nm	6-12 nm	30-45 nm	30-45 nm
Average size of large particles		7.0 nm	7.4 nm	36.3 nm	37.0 nm

3.3.3 Effect of Curing and Processing Procedure

The curing condition for Ag/epoxy and Ag/CB/epoxy composites was set to be 100 °C for 0.5 hr and 125 °C for 1 hr. The size and dispersion status of Ag nanoparticles in the composite after curing were characterized by SEM, EDS and XRD in order to

investigate whether high temperature curing process causes the nanoparticles to agglomerate and grow further. The SEM images in Figure 3-5 shows that the nanoparticles of ultrafine size were embedded in the polymer matrix. The EDS result indicated the presence of Ag nanoparticles in the epoxy matrix.

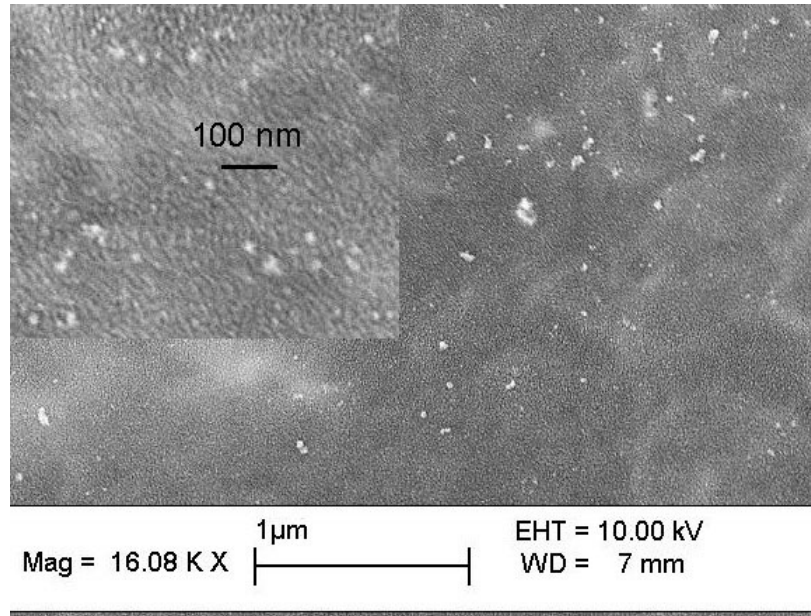


Figure 3-5. SEM images of cured Ag/epoxy nanocomposite for 16.08K magnification and the inset for 41.85K magnification.

The X-ray diffraction patterns of cured Ag/epoxy and Ag/CB/epoxy nanocomposites are shown in Figure 3-6. The XRD spectrum of the Ag/epoxy composite shows well defined four strong peaks at $2\theta = 38.4, 44.3, 64.7$ and 77.6° , corresponding to the (111), (200), (220) and (311) of the face-centered cubic (fcc) Ag phase (JCPDS No.4-0783), respectively. By using the Scherrer's equation, the average size of the Ag nanoparticles of the Ag/epoxy composite with $R = 0.6$ was estimated to be 11 nm. Furthermore, no obvious narrowing of the diffraction peaks was observed for the sample of the Ag/CB/epoxy composite compared to Ag/epoxy composite. The average

size of the Ag nanoparticles of the Ag/CB/epoxy composite with $R = 0.6$ was estimated to be 13 nm. This indicates that the mixing process of Ag/epoxy composite with CB/epoxy composite and the thermal curing procedure did not affect the average crystallite sizes of the in-situ formed Ag nanoparticles significantly.

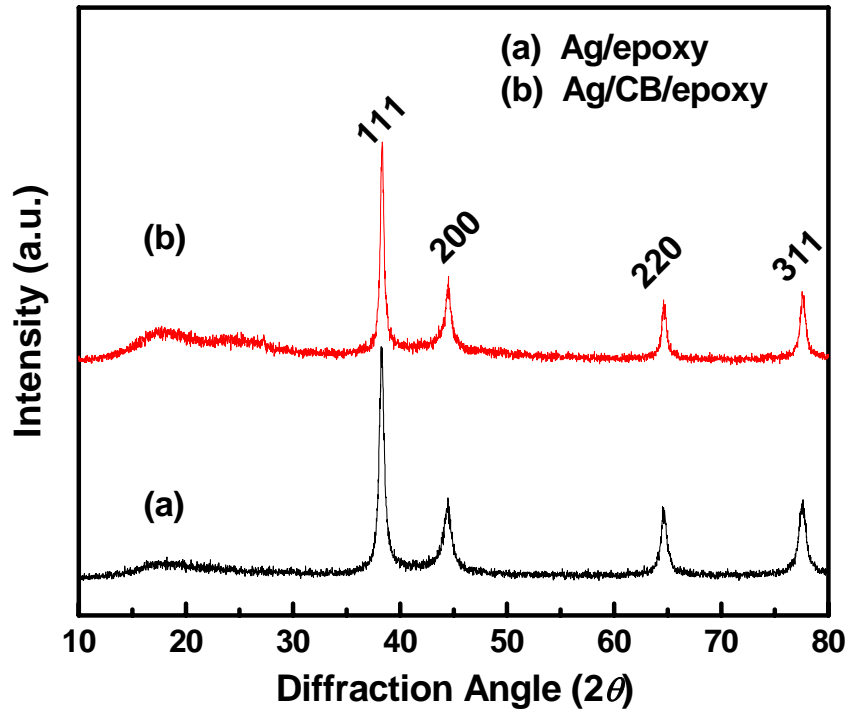


Figure 3-6. XRD patterns of (a) Ag/epoxy composite and (b) Ag/CB/epoxy composite.

3.3.4 Estimation of Filler Loading

Figure 3-7 displays TGA curves of neat epoxy, Ag/epoxy mixture, CB/epoxy mixture and Ag/CB/epoxy mixture all in uncured state initially. To estimate the compositions of the Ag/CB/epoxy mixtures, an isothermal and dynamic combined procedure was set as heating at 100 °C for 15 min and at 125 °C for 1 hr and ramping over the entire temperature range at 5 °C/min. The two weight loss regions at 100 °C and 125 °C are due to the volatilization of hardener for all mixtures and volatilization/

decomposition of various chemicals including the solvent residue, the capping agent and benzoquinone resulted from the oxidation of hydroquinone for Ag/epoxy mixture and Ag/CB/epoxy mixture. It can be seen that the neat epoxy resin was almost degraded above 450 °C. The residue in the CB/epoxy composite at 600 °C was attributed to carbon black which accounts for 29.57 wt. %. The residues in the Ag/CB/epoxy composite at 600 °C can be attributed to Ag and CB and thus was used to estimate the content of Ag and CB in the Ag/CB/epoxy nanocomposites.

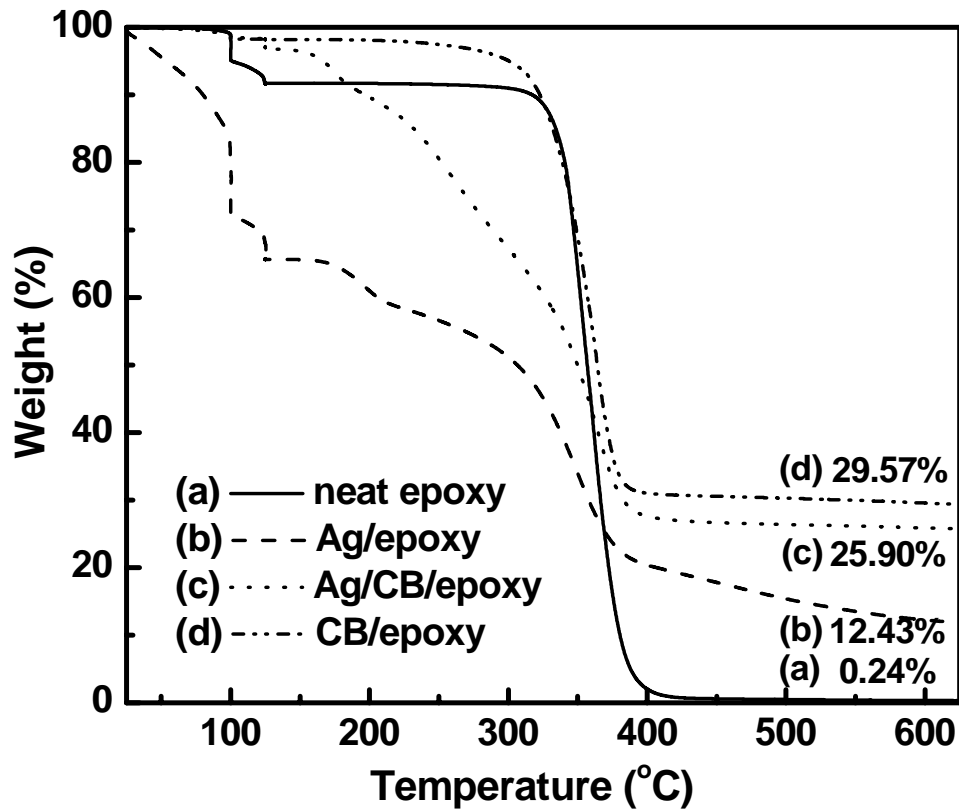


Figure 3-7. TGA studies of neat epoxy, Ag/epoxy mixture, CB/epoxy mixture and Ag/CB/epoxy mixture.

3.3.5 Dielectric Properties of Ag/CB/epoxy Nanocomposites

3.3.5.1 Effect of Ag loading

Table 3-2 and Figure 3-8 show the dielectric constants and dielectric loss tangent of Ag/CB/epoxy composites with different loading levels of Ag nanoparticles at 10 kHz. The k value increased and $\tan\delta$ decreased with the increase of the loading of Ag nanoparticles. The k value of sample with 3.7 wt. % Ag showed a k of 2259 while the $\tan\delta$ was maintained at around 0.43, which is much lower than the sample without Ag nanoparticles (k : 1560, $\tan\delta$: 0.7). The remarkable increase of k may be due to the piling of charges at the extended interface and/or more conducting particles based on the percolation theory. In general, dielectric loss of the dielectric material is resulted from distortional, dipolar, interfacial, and conduction loss. The distortional loss is related with electronic and ionic polarization mechanisms. The interfacial loss is originated from the excessive polarized interface induced by the fillers and specifically the movement or rotation of the atoms or molecules in an alternating electric field. The conduction loss is attributed to the dc electrical conductivity of the materials, representing the flow of actual charge through the dielectric materials. It is believed that the conduction loss contributes significantly to the high $\tan\delta$ of carbon black composites especially at low frequency due to the conducting properties of carbon black. The decreased $\tan\delta$ with the incorporation of metal nanoparticles might be explained as the Coulomb blockade effect. The Ag nanoparticles of ultrafine size might cause a high charging energy for the tunneling electrons and inhibit the charge transfer through the small metal island, reducing the conduction loss which represents the flow of charge through the dielectric materials. Single-electron charging effect or Coulomb blockade transport have been observed at

room temperature in gold nanocluster structure⁹⁷, gold nanoparticles assembled on a biopolymer template⁹⁸. Unfortunately, the Coulomb blockade effect is still difficult to be experimentally demonstrated in our system so far due to the lack of the art of experiment and instrument.

Table 3-2. The electrical and dielectric properties of CB/Ag/epoxy nanocomposite.

<i>Ag loading loading</i>	<i>k</i> (@10 kHz)	<i>tan δ</i> (@10 kHz)	<i>Specific Capacitance</i> (nF.cm ⁻²)
0	1560	0.70	17.14
1.2 %	2002	0.48	25.55
2.4 %	2030	0.46	20.53
3.7 %	2259	0.43	24.39
4.2 %	2421	0.45	25.44

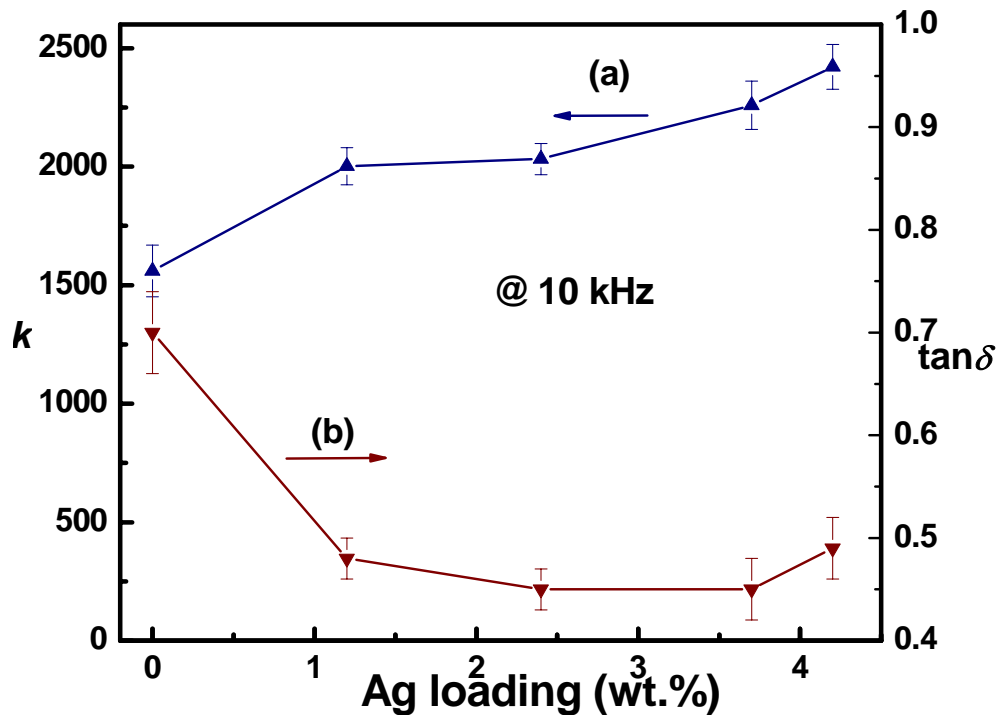


Figure 3-8. The dependence of (a) k and (b) $\tan \delta$ at 10 kHz on the loading level of Ag nanoparticles.

3.3.5.2 Effect of Size and Size Distribution of Ag Nanoparticles on Dielectric properties of Ag/CB/epoxy Composites

Figure 3-9 indicates that k and $\tan\delta$ values of Ag/CB/epoxy composites with Ag nanoparticles of different size and size distribution varied considerably. For Ag/CB/epoxy composites containing 4.2 wt. % Ag and 19.6 wt. % CB (denoted as 4.2Ag/19.6CB/epoxy composite, see Figure 3-9 (a)), compared with the control sample (~20 wt. % CB only, without Ag nanoparticles), increased k and decreased $\tan\delta$ observed for samples in which average size of large Ag nanoparticles are 7.0 nm and 7.4 nm, while the $\tan\delta$ values for samples in which average size of large Ag nanoparticles are 36.3 nm and 37.0 nm increased. This phenomenon may be due to the effect of the size and distribution of Ag nanoparticles on the dielectric properties of the dielectric materials. Smaller size and narrower size distribution of Ag nanoparticles, obtained from the presence of larger amounts of a capping agent, resulted in more evident single-electron charging by Coulomb blockade effect and thus reduced conduction loss.

The increase of k with the increase of Ag nanoparticle concentration is monotonic while the decrease of $\tan\delta$ was not. For Ag/CB/composites containing 6.2 wt. % Ag and 14.6 wt. % CB (denoted as 6.2Ag/14.6CB/epoxy composites) shown in Figure 3-9 (b), no decreased $\tan\delta$ is observed even for samples with better dispersion and narrower size distribution. A plausible explanation may be that the interfacial loss due to newly induced interface is higher than the suppressed conduction loss by incorporation of metal nanoparticles, therefore the overall dissipation factor is still increased for samples with a higher concentration of metal nanoparticles.

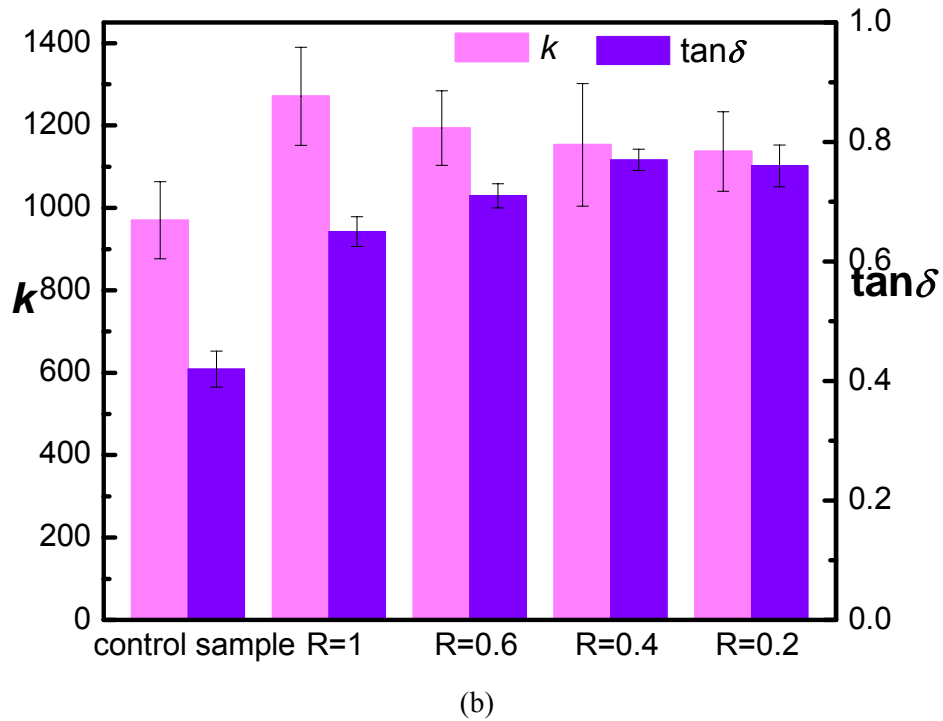
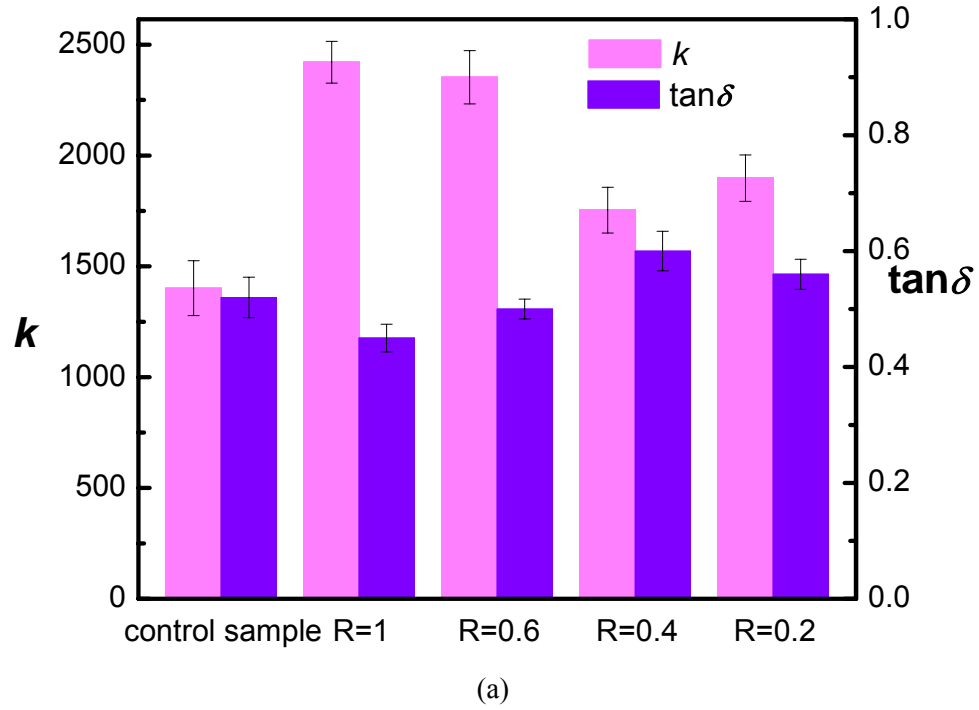


Figure 3-9. k and $\tan\delta$ values of (a) 4.2Ag/19.6CB/epoxy composites and (b) 6.2Ag/14.6CB/epoxy composites (dashed curve) with various concentrations of a capping agent ($R = [CA]/[AgNO_3]$).

3.3.5.3 Effect of Frequency on Dielectric properties of Ag/CB/epoxy Composites

Figure 3-10 illustrates the dielectric properties of the nanocomposites measured at different frequencies. The k values of nanocomposites containing Ag nanoparticles are larger than those of a control sample without Ag in the whole frequency range (see Figure 3-10 (a)). The decreased $\tan\delta$ for nanocomposites containing Ag nanoparticles is observed in the low frequency range (10 kHz and 100 kHz in Figure 3-10 (b)) only. These observations might be explained as the fact that the conduction loss, which is related to the dc electrical conductivity of the materials, contributes to the entire $\tan\delta$ value less significantly as the frequency increases (see Equation 3-1).

$$\tan \delta = \frac{\varepsilon''}{\varepsilon'} + \frac{\sigma}{2\pi f \varepsilon'} \quad \text{Equation 3-1}$$

where ε' , ε'' , σ are the real and imaginary part of the dielectric constant and the electrical conductivity of the materials, respectively, and f is the frequency. Therefore, the effect of metal nanoparticles on suppressing dielectric loss is not obvious at higher frequency. Additionally, the contribution of interfacial loss is more evident in the high frequency range. Accordingly, the $\tan\delta$ values of nanocomposites containing Ag nanoparticles are higher than those without Ag nanoparticles at higher frequencies (1 MHz and 10 MHz in Figure 3-10 (b)).

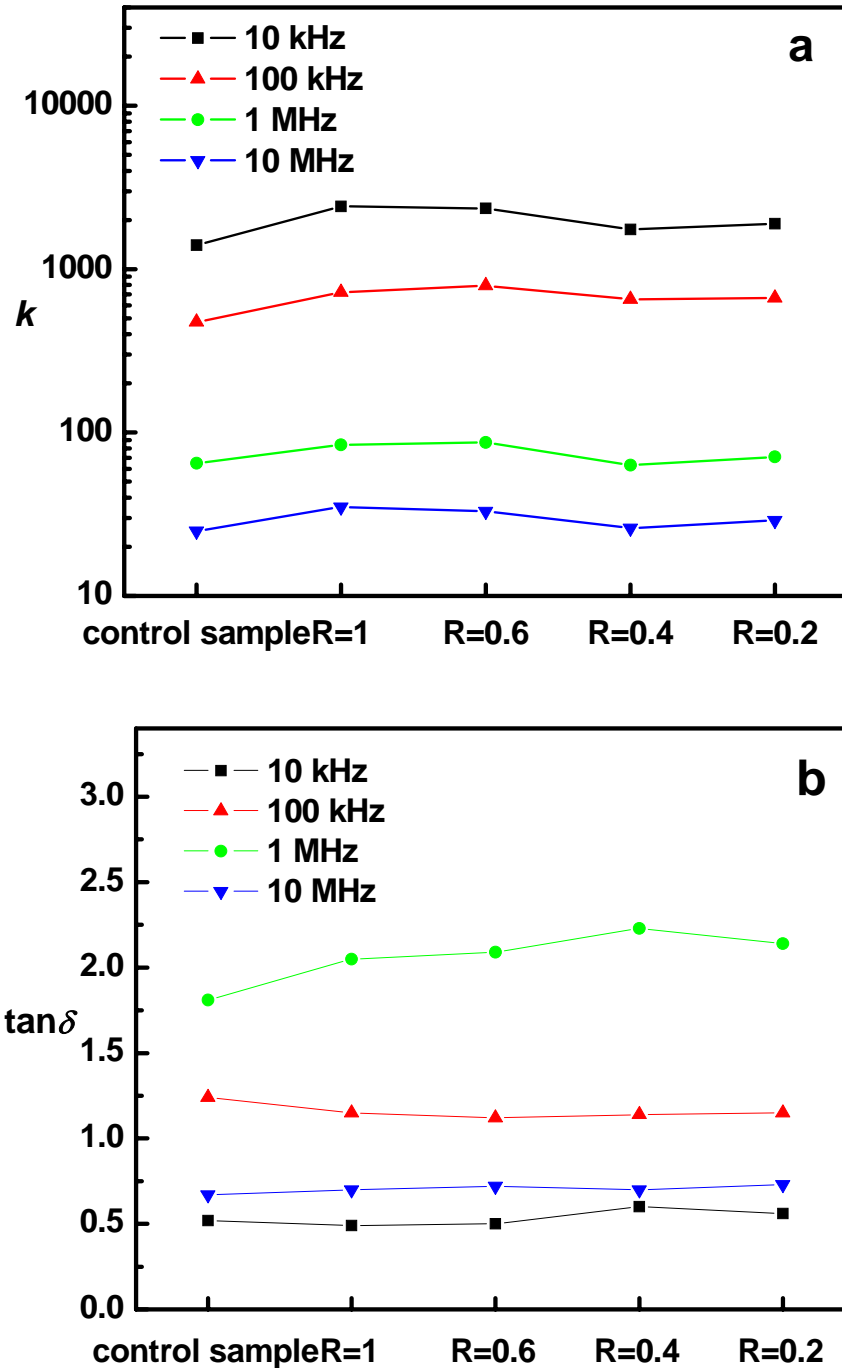


Figure 3-10. (a) k and (b) $\tan \delta$ values of 5Ag/20CB/epoxy composites with various concentration of a capping agent ($R = [CA]/[AgNO_3]$) at different frequencies.

3.4 Conclusions

The Coulomb blockade effect of metal nanoparticles, a novel method to control dielectric loss of ultra high- k polymer composite materials for embedded passives was explored in this study. The Ag nanoparticles were *in-situ* formed in polymer matrix and then incorporated into dielectric composite materials. The size and distribution of nanoparticles were controlled by the appropriate selection of a capping agents and the ratio of capping agent to Ag precursor. The increased dielectric constant and decreased dielectric loss tangent were observed by the incorporation of Ag nanocomposites. The increased dielectric constant is due to the piling of charges at the extended interface which normally results in increased conductivity and higher loss. However, the reduced dielectric loss was observed in the high- k composite materials containing Ag nanoparticles in virtue of Coulomb blockade effect, the well-known quantum effect of nanoparticles, which reduces the electron tunneling. As such, it reduces the conduction loss part from the total dielectric loss of the dielectric composite systems. This Coulomb blockade process can be an effective approach to achieve the high dielectric constant and low dielectric loss simultaneously at low frequency. The size, size distribution and a loading level of Ag nanoparticles in the nanocomposite have significant influence on the dielectric properties of the composite system and supply different effects at different frequency range as well.

CHAPTER 4

SILVER/POLYMER NANOCOMPOSITES AS HIGH-K POLYMER MATRIX FOR DIELECTRIC COMPOSITES WITH IMPROVED DIELECTRIC PERFORMANCE

4.1 Introduction

High dielectric constant (k) materials have received increasing interest in the recent years as they are attractive as potential materials for various applications including gate dielectrics⁹⁹, high charge-storage capacitor²⁹ and electroactive materials⁴⁹. For instance, high dielectric constant and low dielectric loss materials are imperative to realize the real applications of embedded capacitor, which is one of the emerging and important technologies for electronic packaging to provide the advantage of size reduction and system performance enhancement. A wide variety of materials have been extensively investigated as candidates for this application, such as ferroelectric ceramic⁶, ferroelectric ceramic/polymer composite²⁹ and conductive filler/polymer composite⁴⁰. Conductive filler/polymer composite materials, identified as conductor-insulator percolative system, have been recognized as a promising method to achieve high k . According to the scaling theory, the effective k of the percolative composite can be dramatically enhanced at filler loadings approaching the percolation threshold as described through the Equation 4-1.

$$k = \frac{k_m}{|f - f_c|^q} \quad \text{Equation 4-1}$$

where k_m is the dielectric constant of the polymer matrix; f and f_c are the concentration and the percolation threshold concentration of the conductive filler within the polymer matrix, respectively; q is scaling constant, related to the material property, microstructure and phase connectivity of the conductive filler/polymer composites.⁴⁰ And also this percolative approach requires a much lower volume concentration of the filler compared to the traditional approach of dispersing ferroelectric ceramic particles in polymer matrix to achieve high k . Therefore, this material option represents advantageous characteristics over the conventional ceramic/polymer composites, specifically, ultra-high k with balanced mechanical properties and good adhesion strength. Various conductive fillers, such as silver (Ag), nickel (Ni), carbon black, have been used to prepare the polymer-conductive filler composites or three-phase percolative composite systems.^{40,42,43,44,46} Although these composites were reported with high k values at the percolation threshold, they still cannot be considered as effective materials for embedded capacitor applications because of the accompanied high dielectric loss and low resistance at a high filler loading level due to the conductive nature of the filler. During the past few years, much effort has been dedicated to creating low loss dielectric materials. Some researchers use semiconductor fillers to achieve relatively low conductivity at the percolation threshold as compared to conductive fillers.¹⁰⁰ Additionally, the inter-particle barrier layer formed intrinsically or extrinsically by an insulating surface coating or shell around the conducting metal core could effectively reduce the dielectric loss of the conductive filler-polymer composites. It has also been demonstrated by Xu et al. that the insulating oxide layer outside the aluminum (Al) powders could prevent the direct contact of conducting

metal cores and thus endow the Al/epoxy composites with low dielectric loss.⁴¹ However, the k values of this system were limited due to the passivation layer on the conductive filler. An effective attempt to reduce the dielectric loss of the conductive filler/polymer nanocomposites was reported by Qi et al. to introduce surfactant layer coated on the metal filler surfaces during nanoparticle synthesis.⁴⁷ Shen et al. reported a polymer composite with synthesized core/shell hybrid particles using metal Ag cores coated by organic dielectric shells.⁴⁸

On the other hand, the k values of ceramic/polymer composites (usually below 50) can be effectively enhanced by employing the relatively high- k polymer matrix.^{2,17} For instance, using poly(vinylidene fluoride-trifluoroethylene) (P(VDF-TrFE)) copolymer, a class of relaxor ferroelectric with high k (~ 40), Bai et al. prepared $\text{Pb}(\text{Mg}_{1/3}\text{Nb}_{2/3})\text{O}_3\text{-PbTiO}_3/\text{P}(\text{VDF-TrFE})$ composites with k values above 200.²⁹ In addition to the intrinsic high- k polymer matrix, the effective k of polymer matrix can be increased by introducing additives with large dipoles such as β -diketone chelating agents. Rao et al. developed a high- k epoxy-cobalt (III) acetylacetonate matrix with effective k of 6.4 and the lead magnesium niobate-lead titanate (PMN-PT)+ BaTiO_3 /high- k epoxy system composite achieved a k value about 150.²⁰ As the k of polymer matrix shows very strong influence on the k of the composites, the effective k of the conductive filler/polymer composite are expected to be further enhanced by increasing the k value of the polymer matrix according to Equation 4-1.

Therefore, we would like to take advantage of the high- k polymer matrix to achieve a simultaneously high- k and low dielectric loss conductive filler/polymer composite. In this study, a uniformly dispersed metal nanoparticle-polymer composite

was developed as a high- k polymer matrix adopting a relatively low concentration of conductive Ag nanoparticles to enhance the k values while maintaining acceptable levels of dielectric loss. The *in-situ* formed metal-polymer nanocomposite can be employed as a high- k polymer matrix to host various fillers, such as conductive metal or ferroelectric ceramic fillers to achieve both high k and relatively low dielectric loss. In this case, self-passivated Al particles were incorporated in the as-prepared Ag-epoxy nanocomposite with aim to prepare high k and low loss dielectric materials. Capacitor prototype was fabricated based on the developed materials and the dielectric properties were studied to find out the benefits of the incorporation of the Ag nanoparticles in the high- k polymer matrix. The frequency dependence of the dielectric behavior and the dielectric breakdown strength of the composite materials were investigated. The dielectric properties were correlated with the composition and the morphology of the composites and discussed in details.

4.2 Experimental

4.2.1 Materials

A cycloaliphatic epoxy resin ERL-4221E (Shell Chemical Co.), an anhydride type curing agent hexahydro-4-methylphthalic anhydride (Lindau Chemical Co.) and an imidazole type catalyst 1-methylimidazole (Aldrich Chemical Co.) were used. Silver nitrate (AgNO_3) (Aldrich Chemical Co.) and Triton-100 (formula weight: 646.85, Acros Chemical Co.) were selected as a metal precursor and a reducing agent, respectively. The metal filler used in the formulations were aluminum particles in micron size (Alfa-Aesar

Chemical Co.). Acetonitrile (Fischer Chemical Co.) and propylene glycol monomethyl ether acetate (PGMEA, Aldrich Chemical Co.) were used as received.

4.2.2 *In-situ* Photochemical Synthesis of Ag Nanoparticles

The Ag nanoparticles were *in-situ* synthesized in the epoxy resin through reduction of AgNO₃. Triton-100 was used as reducing agent and nanoparticle stabilizer simultaneously. The epoxy resin, hardener, reducing agent and silver precursor were dissolved in acetonitrile homogeneously and then exposed to the 295 nm UV source (ELC-2541 power supply with ELC-4001 light curing unit, Electro-Lite Corp.) for 30 min. Finally the solvent was evaporated in a rotary evaporator under a reduced pressure.

4.2.3 Preparation of Al/epoxy and Al/Ag-epoxy Composite

The Al/epoxy and Al/Ag-epoxy composites was prepared by mixing the Al particles in the epoxy resin and *in-situ* formed Ag-epoxy matrix, respectively, for 15 min and sonication for 1 hr. PGMEA is added to disperse filler at high loading level for Al/epoxy composites. Variation of the ratio of Ag-epoxy matrix to Al powders led to Al/Ag-epoxy composites with different loading levels of Al and Ag. The Al/epoxy composites and the Al/Ag-epoxy composites were cured under a two-step curing profile: 100 °C for 15 min then 150 °C for 90 min, and a three-step curing profile: 100 °C for 15 min then 150 °C for 30 min and finally 190 °C for 90 min, respectively.

4.2.4 Characterization

A JEOL 100C transmission electron microscopy (TEM) was used for observing the morphology and analyzing the size of *in-situ* formed Ag nanoparticles. Scanning electron microscopy (SEM) measurements were carried out on a JEOL 1530 equipped

with a thermally assisted field emission gun operated at 10 KeV to observe the morphology of Al/Ag-epoxy and Al/epoxy composites.

Thermogravimetric analysis was conducted on a TGA (TA Instruments 2050) at a heating rate of 10 °C/min under a nitrogen atmosphere to estimate the composition of *in-situ* formed Ag nanoparticle-epoxy mixture.

Parallel plate capacitors based on the formulated high-*k* composite materials were fabricated on a copper clad FR-4 board and copper top electrodes were coated by DC sputtering. First, a thick film of the high-*k* composites was made onto the copper clad FR-4 board with a doctor-blade. Then the sample was cured in a thermal oven. Finally, the DC sputter was used to deposit a thin layer of copper (about 3000 Å) as the top electrode onto the cured material through a shadow mask. The capacitance and dielectric loss tangent ($\tan \delta$) of the capacitor were then measured with a HP 4263A LCR meter at room temperature. Dielectric breakdown voltage measurements of Al/epoxy and Al/Ag-epoxy composites were conducted through current-voltage characteristics using a KEITHLEY 6517A high resistance meter at room temperature. Two samples with twelve data points for each wt. % of the composites were investigated. The thickness of the dielectric films was measured with a profilometer (Alpha-Step Co.) and used to calculate the dielectric constant and dielectric breakdown strength of the sample.

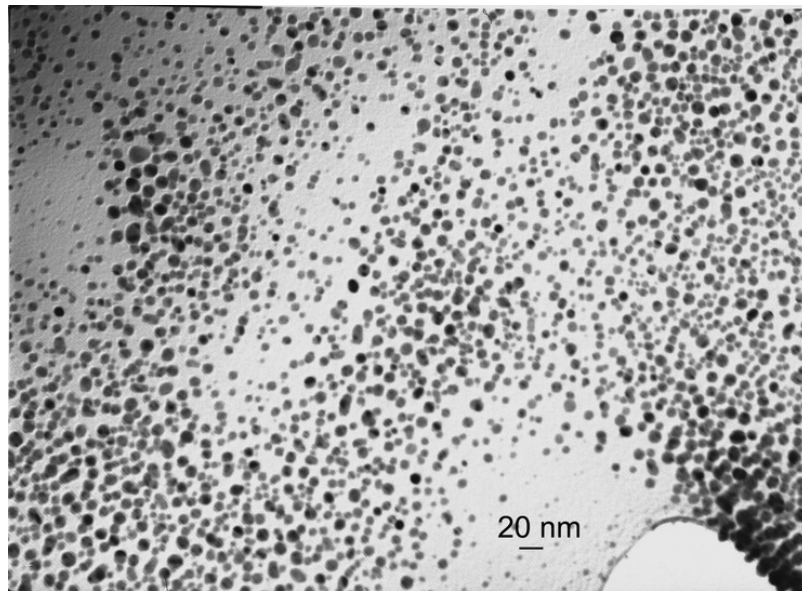
4.3 Results and Discussion

4.3.1 Morphology and Composition

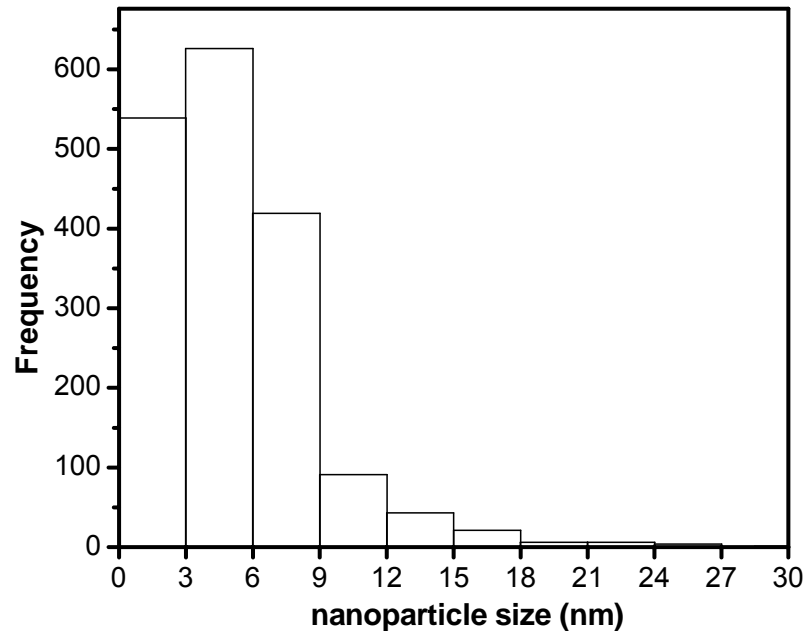
The quality of nanofiller dispersion in the polymer matrix directly correlates with its effectiveness for improving the properties of the nanocomposites. It is believed that uniformly distributed metal nanoparticles within the polymer matrix are desired to achieve a relatively high- k and low dielectric loss matrix. Compared with *ex-situ* techniques, *in-situ* techniques could facilitate a more uniform dispersion of nanoparticles in polymers.⁷² And the photochemical approach provides the advantages of simplicity, reproducibility, versatility, selectivity and ability of larger scale synthesis.^{101,102,103,104} Therefore, the Ag-epoxy mixture was prepared via an *in-situ* photochemical method, in which Ag nanoparticles were generated by chemical reduction of a metallic precursor upon UV irradiation. Triton-100 in this system serves as reducing agent and capping agent simultaneously. The reduction of the silver ion is induced by hydroxymethyl radical which is generated from the photolysis of Triton-100. Stabilization of the nanoparticles is rendered by its capping property because of the micelle/reverse micelle forming ability. The exact structure of the Triton-100 in this system can be investigated through cryo-TEM in conjunction with small angle X-ray scattering (SAXS) technique.

This simple process produced Ag-epoxy mixture with uniform dispersion and narrow size distribution of nanoparticles, which was confirmed by TEM characterization. Figure 4-1 displays TEM micrograph and histogram of Ag nanoparticles synthesized via an *in-situ* photochemical reduction in epoxy resin. The particle size analysis was performed and the results show that well-dispersed Ag nanoparticles with the size mostly smaller than 15 nm in polymer matrix were obtained. The average size was calculated as

5.2 nm. The composition of *in-situ* formed nanoparticles in the whole mixture was estimated at around 10 wt. % according to the TGA test.



(a)



(b)

Figure 4-1. (a) TEM micrograph and (b) histogram of Ag nanoparticles synthesized by an *in-situ* photochemical reduction in epoxy resin.

It has been demonstrated that the insulating oxide layer outside the Al powders could prevent the direct contact of conducting metal cores and thus render the Al/epoxy composites with low dielectric loss.⁴¹ Therefore, these self-passivated Al fillers were incorporated into the *in-situ* formed Ag-epoxy matrix. Various properties of the as-prepared Al/Ag-epoxy composites were investigated. For comparison, Al/epoxy composites were also prepared and studied by mixing the Al filler in the neat epoxy matrix instead of Ag-epoxy matrix. SEM observation was performed on the cryogenically fractured surface of cured Al/epoxy and Al/Ag-epoxy composites as displayed in Figure 4-2. There was no obvious difference in morphology between these two sets of composites. The size of Al fillers was in the range 1-5 microns. The *in-situ* formed Ag nanoparticles could not be seen in the SEM images of Ag/Ag-epoxy composites due to the ultrafine size of the nanoparticles and limited resolution of SEM.

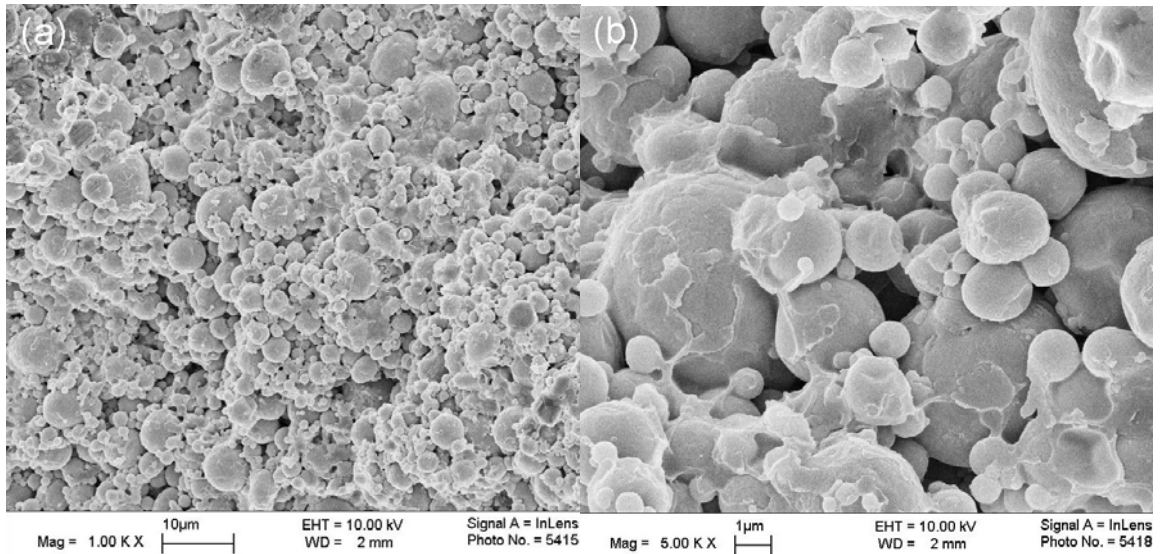


Figure 4-2. SEM images of cured composites containing 70 wt. % Al filler: (a) Al/epoxy composite for 1 K magnification; (b) Al/epoxy composite for 5 K magnification; (c) Al/Ag-epoxy composite for 1 K magnification; and (d) Al/Ag-epoxy composite for 5 K magnification.

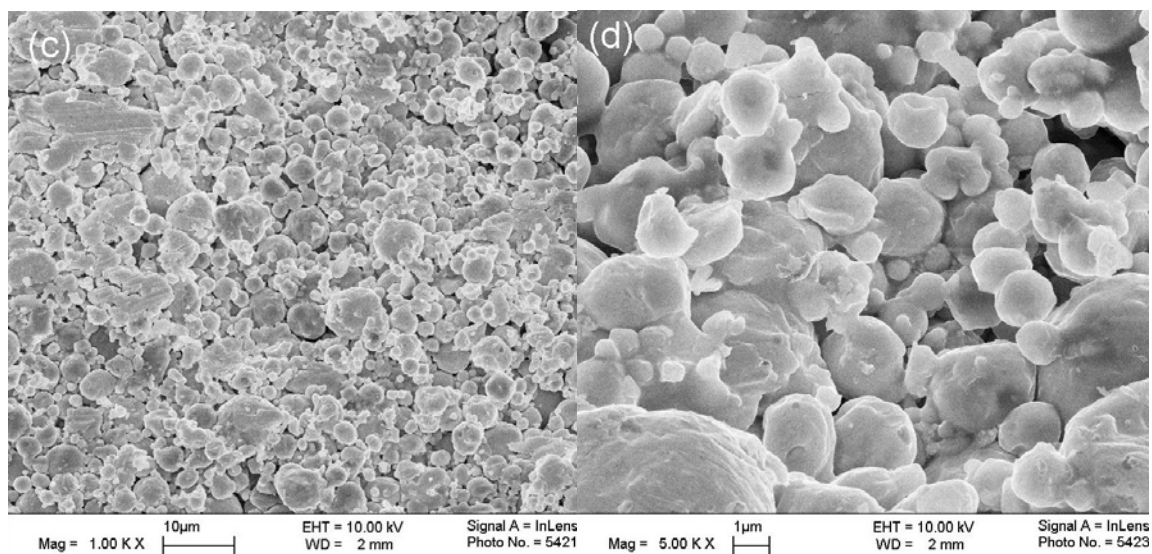


Figure 4-3 continued.

4.3.2 Dielectric Characterization

Dielectric behaviors of Al/Ag-epoxy composites together with Al/epoxy composites were studied and analyzed for comparison. For each wt.% of the composites, two samples with twelve data points ranging in thickness from 50 μm to 90 μm were investigated. The tests show good reproducibility for each data point. Figure 4-4 shows the dielectric properties of Al/epoxy composites and Al/Ag-epoxy composites as a function of Al filler loading at a frequency of 10 kHz. The Al/Ag-epoxy composites exhibit more than 50% increase in k values compared with Al/epoxy composites with the same filler loading of Al, which demonstrated that the incorporation of well-dispersed Ag nanoparticles in the polymer matrix delivers a huge impact on the dielectric constant enhancement. It is also notable that the dielectric loss tangent values (see the inset of Figure 4-4) for Al/Ag-epoxy composites with different Al filler loadings are all below 0.1, which is tolerable for some applications such as decoupling capacitors. The low

dielectric loss can be attributed to the good dispersion of Ag nanoparticles in the polymer matrix together with the thin self-passivated aluminum oxide layer forming an insulating boundary outside of the Al particles. The results suggest that the metal-polymer nanocomposites via an *in-situ* photochemical approach can be employed as a high- k polymer matrix to enhance the k value of the composites while maintaining the relatively low dielectric loss tangent.

The trends of the dielectric properties with the variation of filler loadings behaved differently for Al/epoxy composites and Al/Ag-epoxy composites. For Al/Ag-epoxy composites, the k values increased considerably with the increase of Al filler loading as a result of interfacial and space charge polarization. The k values at 10 kHz of the Al/Ag-epoxy composites were 92, 112, 160 and 196 for samples containing 60 wt. %, 70 wt. %, 80 wt. % and 90 wt. % of the Al filler, respectively. But for Al/epoxy composites, the k value decreased at a 90 wt. % Al filler loading due to voiding from imperfect filler packing and solvent evaporation, because solvent is required to disperse filler at high loading level.¹⁴ As to the dielectric loss tangent value of Al/Ag-epoxy composites, it did not show a monotonic increase with the Al filler loading, instead, it decreases from 0.082 to 0.045 as the Al filler loading is increased from 60 to 80 wt. % and then increases again at 90 wt. %. This phenomenon can be explained in terms of the origins and mechanisms of the dielectric loss of the heterogeneous conductive filler/polymer composite material. The measured dielectric loss tangent at a given frequency can be roughly attributed to polarization loss and conduction loss. The polarization occurs through several mechanisms involving microscopic and/or macroscopic charge displacement such as space charge or interfacial polarizations. The conduction loss is attributed to the electrical

conductivity of the materials, representing the charge flow through the dielectric materials.^{10,11} The fraction of Ag, the more conductive element, in the Al/Ag-epoxy composites decreased with the increase of the Al filler loading. As such, a less Ag content leads to a lower conduction loss and thereby a lower total dielectric loss tangent up to 80 wt. % of the Al filler loading. In the case of 90 wt. % of Al/Ag-epoxy, the increase of interfacial loss induced by higher Al content might overwhelm the decrease of conduction loss due to the less Ag content, so the total dielectric loss tangent increased again.

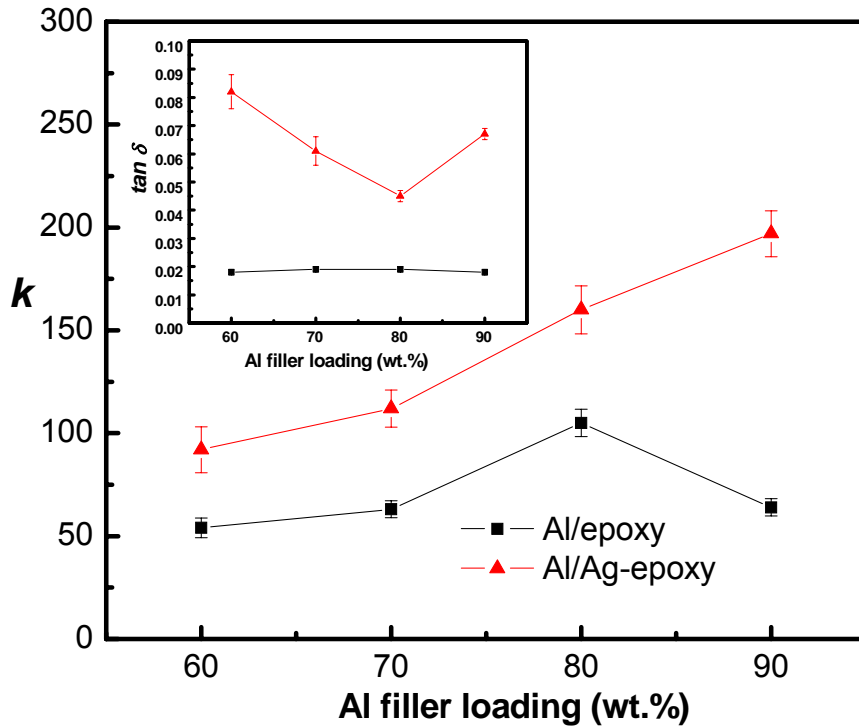


Figure 4-4. Dielectric constant (k) values of Al/epoxy and Al/Ag-epoxy composites as a function of Al filler loading (@ 10 kHz). Dielectric loss tangent ($\tan \delta$) values of Al/epoxy and Al/Ag-epoxy composites are displayed in the inset.

The frequency dependence of the dielectric properties was investigated as well. Figure 4-6 (a) and Figure 4-6 (b) depict the change of k and $\tan \delta$ values for Al/epoxy composites and Al/Ag-epoxy composites with different Al filler loading as a function of

frequency of the applied alternating fields ranging from 10 kHz to 1 MHz at room temperature, respectively. It can be observed that the frequency dependence of k as well as the dielectric loss tangent is stronger in the composite with higher filler loadings. The k values gradually decrease with the increase of the frequency for all the composites, which is mainly attributed to interfacial polarization in the composite. At higher frequency the dipole fails to respond rapidly to follow the field and dipole polarization decrease, so dielectric values tend to decrease. For the dielectric loss, the $\tan\delta$ values for Al/epoxy increase monotonically with the increase of the frequency, but the $\tan\delta$ values for Al/Ag-epoxy decrease initially then increase after 100 kHz. The reason could be that the contribution from interfacial polarization mechanism becomes more evident while the ac conduction contributes less as the frequency increases. Elemental Ag induces far more conduction loss than polarization loss as compared to the Al.

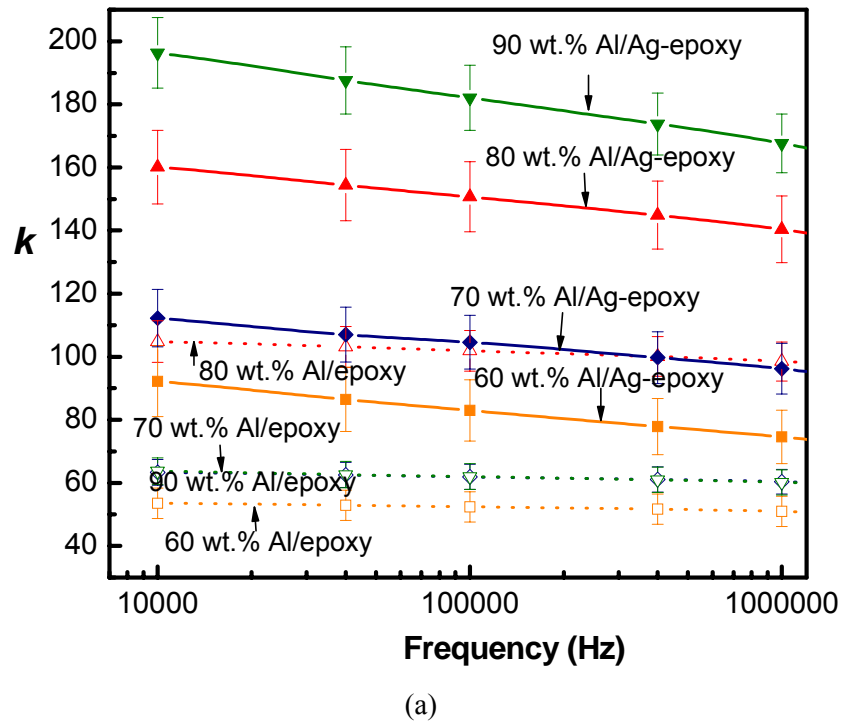
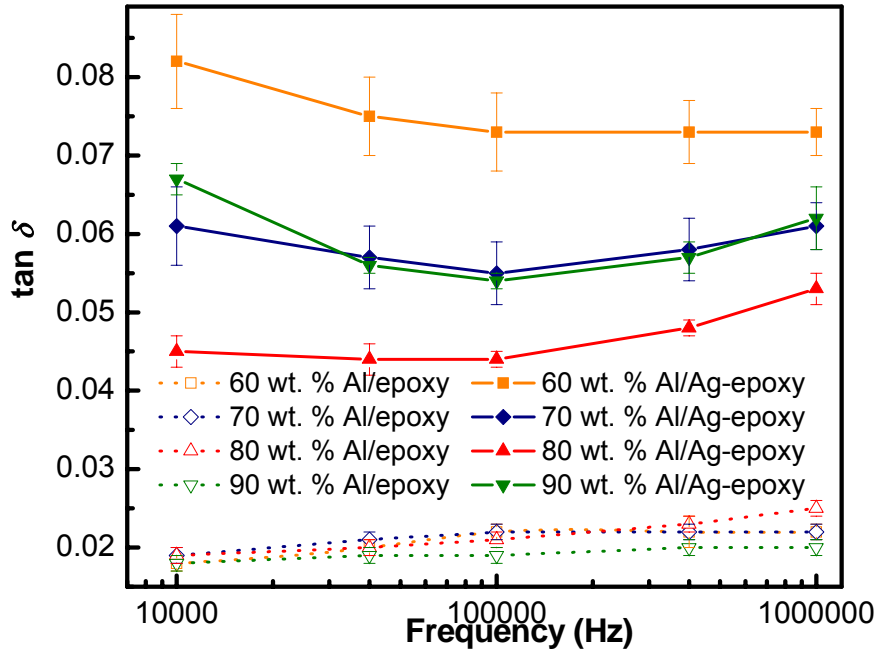


Figure 4-5. (a) k and (b) $\tan\delta$ values Al/epoxy composites and Al/Ag-epoxy composites with different Al filler loadings as a function of frequency.



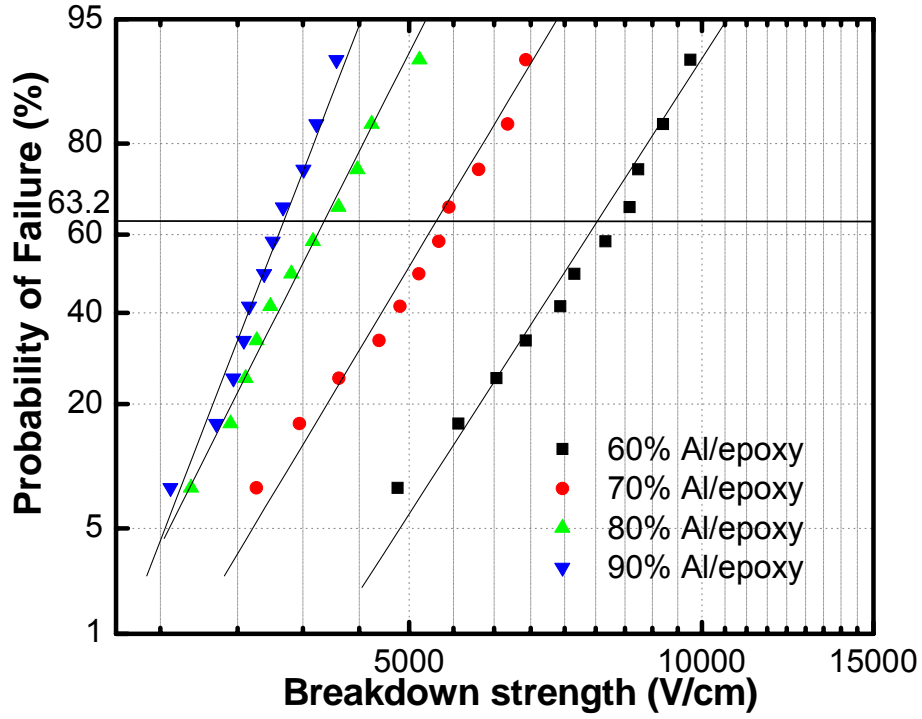
(b)

Figure 4-6 continued.

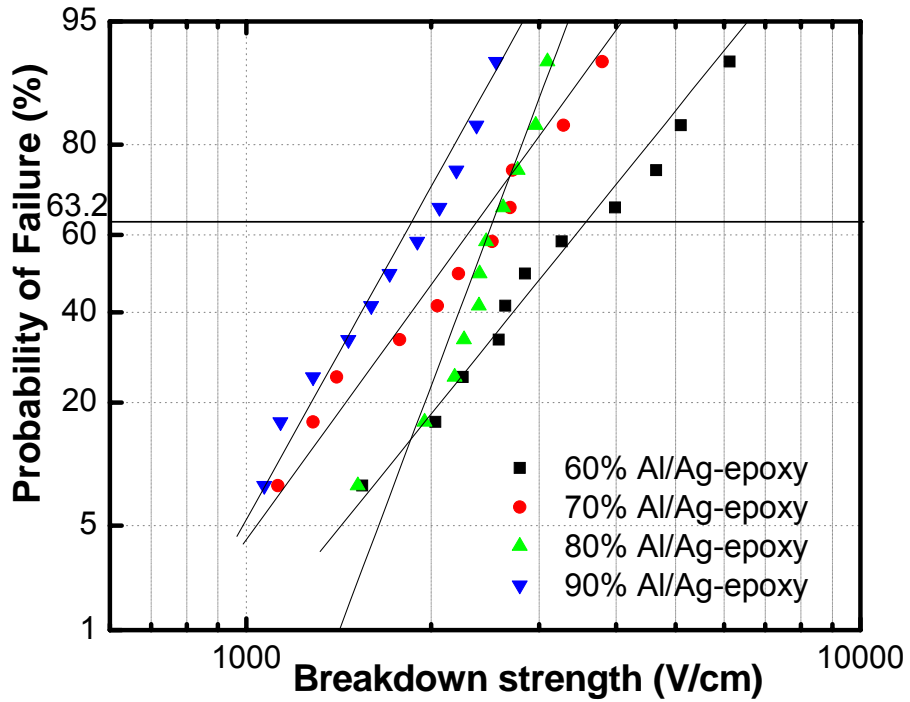
DC dielectric breakdown characteristics of Al/epoxy and Al/Ag-epoxy composites with different Al filler loadings were investigated and compared. A conventional 2-parameter Weibull distribution was used to analyze the dielectric breakdown strength for samples as displayed in Figure 4-7.^{105,106} Weibull statistics is considered as a popular and useful statistical method for dielectric breakdown strength analysis. The cumulative probability of electrical failure P can be described as:

$$P = 1 - \exp\left[-\left(\frac{E}{E_0}\right)^\beta\right] \quad \text{Equation 4-2}$$

where β is a shape parameter and E_0 is a scale parameter that represents DC characteristic breakdown strength at 63.2 % failure probability.



(a)



(b)

Figure 4-7. Dielectric breakdown statistics of (a) Al/epoxy composites and (b) Al/Ag-epoxy composites with different Al filler loadings plotted as a Weibull distribution.

Table 4-1 lists E_0 values of Al/epoxy composites and Al/Ag-epoxy composites with different Al filler loadings. For Al/epoxy composites, the dielectric breakdown strength decreases substantially with the increase of the Al filler loading. The dielectric breakdown strength of the Al/Ag-epoxy composites generally decreases as well with increasing Al filler loading. The reduction in dielectric strength of composites with increasing Al filler loading is attributed to the increased space charge accumulation.¹⁰⁷ At the same Al filler loading, the dielectric breakdown strength of the Al/Ag-epoxy composites is lower than Al/epoxy composites. This can be explained from the Ag nanoparticles contained in the samples which might result in increased conduction electron density and/or carrier mobility. The altered charge and altered mobility has the potential for changes in the dielectric breakdown strength.^{108,109}

Table 4-1. DC characteristic breakdown strength at 63.2 % failure probability (E_0) of Al/epoxy composites and Al/Ag-epoxy composites with different Al filler loadings.

Al filler loading (wt. %)	E_0 of Al/epoxy composites (V/cm)	E_0 of Al/Ag-epoxy composites (V/cm)
60 %	7818	3566
70 %	5332	2380
80 %	4100	2530
90 %	3714	1862

4.4 Conclusions

An *in-situ* synthesis of Ag nanoparticles was successfully carried out in an epoxy matrix by using a photochemical method. The as-prepared Ag-epoxy nanocomposite was utilized as high- k polymer matrix to host fillers for preparation of Al/Ag-epoxy composites as embedded capacitor candidate materials. The dielectric constant values of

the Al/Ag-epoxy composites increased remarkably as compared with those of Al/epoxy composite at the same Al filler loading by introduction of Ag in the polymer matrix. Moreover, the dielectric loss of the Al/Ag-epoxy composites was below 0.1. The results suggested that the metal-polymer nanocomposites via an *in-situ* photochemical method can be employed as high- k polymer matrices to enhance the dielectric constant while maintaining the low dielectric loss of the high- k composites. Detailed dielectric property measurements revealed that the concentration of silver nanoparticles in the polymer matrix play a significant role in determining the electrical conduction and breakdown behaviors as well as the frequency dependence of the dielectric composites. At low Ag concentration, the dielectric behaviors of Al/Ag-epoxy composites are mainly determined by interfacial polarization, while conduction and electron transport of Ag dominate the Al/Ag-epoxy composites at higher Ag concentration.

CHAPTER 5

NANO-SCALE PARTICLE SURFACE MODIFICATION FOR TAILORING DIELECTRIC PROPERTIES OF POLYMER NANOCOMPOSITES

5.1 Introduction

As stated in previous sections, dramatic increase of dielectric constant close to the percolation threshold observed in the conductor-insulator percolative system arouses interest of developing conductive metal/polymer composites as high- k dielectric candidate materials. According to the scaling theory, the effective k of the percolative composite can be dramatically enhanced at filler loadings approaching but not exceeding the percolation threshold. And also this percolative approach requires a much lower volume concentration of the filler compared to the traditional approach of dispersing ferroelectric ceramic particles in polymer matrix to achieve high k . Therefore, this material option represents advantageous characteristics over the conventional ceramic/polymer composites, specifically, ultra-high k with balanced mechanical properties and good adhesion strength. However, incorporation of the conductive fillers which modify the dielectric property of interest usually increases the dielectric loss and the breakdown strength as well. The high dielectric loss and narrow processing window of this system have hindered the metal/polymer composites from real applications.

To address this issue, the inter-particle barrier layer, i. e. an insulating surface coating around the conducting metal core formed either intrinsically or extrinsically, could effectively reduce the dielectric loss of the conductive filler/polymer composites. For instance, Shen et al. reported a polymer composite with synthesized core/shell hybrid particles using metal Ag cores coated by organic dielectric shells.⁴⁸ These coating layer were formed *in-situ* during the synthesis of metal nanoparticle cores, which might confine the real applications of these approaches due to the limited production scale of the nanoparticles. Therefore, surface coating layer was targeted to the commercially available nanoparticles in this study.

More recently, a new class of dielectric material with nanofillers in a polymer matrix for improving specific electrical properties, nanodielectric, is emerging.⁷¹ The molecular structure and/or modification at the nanofiller surface in the particle-polymer interface region are found to significantly affect the performance of nanodielectrics. The accordingly affected behaviors by such changes including charge (electrons/protons/molecular ions) transport, extended double layer structure, and space charge distribution are likely to be responsible for some of the unusual dielectric and electrical properties observed.^{109,110,111,112} However, few studies have elucidated the effect of metal filler surface chemistry and interfacial region in high- k nanocomposites on the dielectric and electrical properties such as dielectric constant, dielectric loss, dielectric breakdown strength, and few investigations have employed surface modification to tailor these properties. Therefore, fundamental studies of interface and its modification with organic molecules are of great significance to understand their effect on the dielectric and electrical behaviors of metal/polymer nanocomposites.

Functionalization or grafting of organo-silane molecules on a metal oxide surface is typical modification method, simple yet effective. For instance, the surface modification of TiO₂ nanoparticles by a polar silane coupling agent could effectively improve both the dielectric breakdown strength and space charge distribution of polyethylene composites.^{113,114,115} The modification is based on the chemical bonding between the silane group and the hydroxyl groups presented on these metal oxide particle surfaces. However, the effectiveness of these coupling agents on modifying metal nanoparticles is doubtful due to the lack of hydroxyl groups on some metal particle surface such as Ag prepared by certain methods. As an alternative, the atom coordination of certain elements in coupling agent to the metal nanoparticle surface might be hypothesized as an approach for chemical modification of the metal nanoparticles. Accordingly, it is of interest to investigate the applicability of the coupling agent to the metal nanoparticles and its mechanism.

In this study, surface modification of nanoparticles was employed with aim to change the surface chemistry and electrical state of nanoparticles and thereby to tailor the dielectric and electrical properties of corresponding polymer nanocomposites. Ideally, the surface passivation layer coated on the nanoparticles is expected to improve the performance of the conventional metal/polymer composites by decreasing the dielectric loss, enhancing the dielectric breakdown strength and expanding the processing window. The surface modification agents are supposed to attach to metal filler surfaces by atom coordination/chemical bonding and adsorption to form a multi-layer or oligomer film on the metal filler surfaces. Infrared spectrum measurement of the absorption band of functional groups on nanoparticles was used to determine the existence of chemical

bonding after surface modification. High resolution transmission electron microscopy (HRTEM) was used to characterize the morphology of surface modified nanoparticles (SMN) and investigate the existence and thickness of the surface coating layer.

Then the SMN/epoxy nanocomposites were prepared by dispersing different loadings of SMN into an epoxy matrix. A set of dielectric and electrical tests were performed to characterize the as-prepared nanocomposites and study the effect of surface modification on the dielectric and electrical properties of nanocomposites. It was found that the dielectric properties of the nanocomposites could be tailored by varying surface modifications of nanoparticles prior to the filler incorporation. The percolation-like increase of k value with the increase of filler loading was observed. Different surface modification conditions such as type and concentration of surface modification agent, solvent media etc. may play complex roles to the degree of surface modification which impact the changes of k and dielectric loss tangent values of SMN/polymer composites dramatically. Significant improvement in the dielectric breakdown strength was observed as well. More importantly, resistor-like behavior was shifted to be more capacitor-like behavior as the linearity in the current-voltage behavior of these composites. The improvement can be attributed to the interparticle electrical barrier layer formed via surface modification which prevents the metal cores from direct contact.

5.2 Experimental

5.2.1 Materials

A cycloaliphatic epoxy resin ERL-4221E (Shell Chemicals Co.), an anhydride type curing agent hexahydro-4-methylphthalic anhydride (Lindau Chemical Co.) and an

imidazole type catalyst 1-methylimidazole (Aldrich Chemical Co.) were used. γ -aminopropyltrimethoxy silane (APS, Crompton Co.) and γ -glycidoxypropyltrimethoxy silane (GPS, Crompton Co.) as surface modification agents were used as received without further purifications. The Ag nanoparticles synthesized by the combustion chemical vapor condensation (CCVC) method (nGimat Co.) were used as received. The ethanol (J. T. Baker) and toluene (EMD Chemicals) were used as solvents without further purifications.

5.2.2 Surface Modification of Ag Nanoparticles

The Ag nanoparticles were surface modified by different surface modification agents in various ratio of Ag to these agents. Aqueous ethanol (ethanol : DI water = 95 : 5 in volume) and dry toluene were used as solvent media for the surface modification process. The mixture of the nanoparticles and surface modifiers in different solvents was sonicated for 3 hrs and followed by centrifuge to obtain the nanoparticle solids. The treated nanoparticles were rinsed by solvent to remove the unreacted surface modifiers and then centrifuged repeatedly. Finally, the as-obtained SMNs were dried in a vacuum chamber for 24 hrs at room temperature. The SMNs with Ag nanoparticle to APS in molar ratio as 4:1, and 10:1, respectively, were noted as APS4-SMN, and APS10-SMN, respectively.

5.2.3 Preparation of SMN/Epoxy Composites

The SMN/epoxy composites were prepared by mixing the SMN particles in the epoxy resin and sonicating for 1 hr. The Al/epoxy composites and the Al/Ag-epoxy composites were cured under a two-step curing profile: 95 °C for 15 min then 150 °C for additional 90 min.

5.2.4 Material Characterization

Fourier transform infrared (FTIR) spectra of Ag nanoparticles with and without surface treatment via varied modification agents in different solvent media were recorded on a Nicolet Magna-IR 560 spectrometer.

A Hitachi 2000K high resolution transmission electron microscopy (HRTEM) was used for observing the morphology and the size of Ag nanoparticles as well as analyzing the result of surface modification. Spatially resolved energy-dispersive X-ray spectroscopy (EDS) attached with the HRTEM was also used to confirm the presence and element composition of a thin layer of shell around the nanoparticles after surface modification.

X-ray powder diffraction (XRD) patterns of unmodified Ag nanoparticles and surface modified Ag nanoparticles by APS were recorded at a scanning rate of $0.04^\circ \text{ s}^{-1}$ in the 2θ range of $20\text{--}80^\circ$ using an X-ray power diffractometer (PW 1800, Philips Co.) with Cu-K α radiation ($\lambda \sim 0.154 \text{ nm}$).

To investigate the surface chemistry characteristics of the Ag nanoparticles after surface modification, X-ray photoelectron spectroscopy (XPS) and Raman spectroscopy studies of the samples were employed. The XPS experiments were carried out in the ultrahigh vacuum chamber. XPS analysis was performed on a Model 1600 XPS with 46.95 eV X-rays from an Al K α source with spectrometer resolution $\sim 1.0 \text{ eV}$ for the survey scans and $\sim 0.1 \text{ eV}$ for high-resolution scans. Raman spectrum of surface modified Ag nanoparticles by APS was obtained using Bruker Optics Equinox 55 FT-Raman with near infrared (NIR) lasers ($\lambda = 1064 \text{ nm}$). In a typical measurement, the laser power at the sample position was 300-500 mW and the resolution is 2 cm^{-1} .

The glass transition temperatures (T_g s) of unmodified nanoparticle/epoxy nanocomposite and SMN/epoxy nanocomposites were studied by a modulated differential scanning calorimeter (DSC, TA Instruments model 2920) at a heating rate of 10 °C/min under a nitrogen atmosphere. The heat treatment process was also studied by DSC isothermally at 150 °C for 1 hr under a nitrogen atmosphere.

Scanning electron microscopy (SEM) measurements of the morphology of cured SMN/epoxy nanocomposite was carried out on a JEOL 1530 equipped with a thermally assisted field emission gun operated at 10 KeV.

5.2.5 Capacitor Prototype Fabrication and Dielectric Property Measurements

Parallel plate capacitors in MIM (Metal-Insulator-Metal) structure with the formulated high- k nanocomposite sandwiched between gold-coated glass substrates and gold top electrodes. The high- k nanocomposite films were spin-coated onto the gold-coated glass substrates and cured in a thermal oven. A thin layer of gold (about 3000 Å) as the top electrode was coated on the cured nanocomposite through a shadow mask by a DC sputtering. The capacitance and dissipation factor of the capacitor were then measured with a HP 4263A LCR meter. The leakage current and breakdown voltage was measured using a KEITHLEY 6517A high resistance meter. The thickness of the dielectric films was measured with a profilometer (Alpha-Step Co.) and used to calculate the dielectric constant and dielectric strength of the sample.

5.3 Results and Discussion

5.3.1 Characterization of Surface Modified Nanoparticles (SMN)

The metal nanoparticles were treated with different types and amounts of surface modification agents, which are supposed to react with metal filler surfaces by chemical bonding or complex coordination to form a monomolecular layer or multi-layers on the nanoparticle surfaces under appropriate conditions. Infrared spectrum measurement of the absorption band of functional groups on metal particles was used to determine the existence of chemical species after surface modification. Figure 5-1 shows the FTIR spectra of metal nanoparticles with and without surface treatment via varied modification agents in different solvent media. For spectrum of metal filler nanoparticles treated with APS in ethanol, the FTIR band recorded at 1090 cm^{-1} corresponds to Si–O stretching vibration, which could originate from the Si-O-Si linkages formed by the condensation occurring between silanol groups. The small FTIR band at 2930 cm^{-1} corresponds to stretching vibration of CH_2 in the silane chain. These results suggest the existence of organic layer on the SMN and/or the bond linkage between surface modification agent and the nanoparticle surface.

However, for nanoparticles treated by GPS with epoxide end group, the corresponding absorption peaks were hardly detected. These results indicate that the functional groups of the silane agents play an important role in the degree of surface modification. This provides indirect evidence that the coordination of nitrogen from the amino group in APS to the Ag nanoparticles might play a more important role in the formation of coating layer on the Ag nanoparticles than the chemical bonding between the Si atoms to the functional groups on the nanoparticle surface.

The effect of the solvent media on surface modification was also studied. Different from the aqueous ethanol solvent, in the case of APS treated nanoparticles in dry toluene solvent, the FTIR peaks of Si-O-Si and CH₂ groups were less obvious. It was likely that less amount of agents was coated on the nanofillers because less hydrolysis of silane agents took place in the dry solvent.

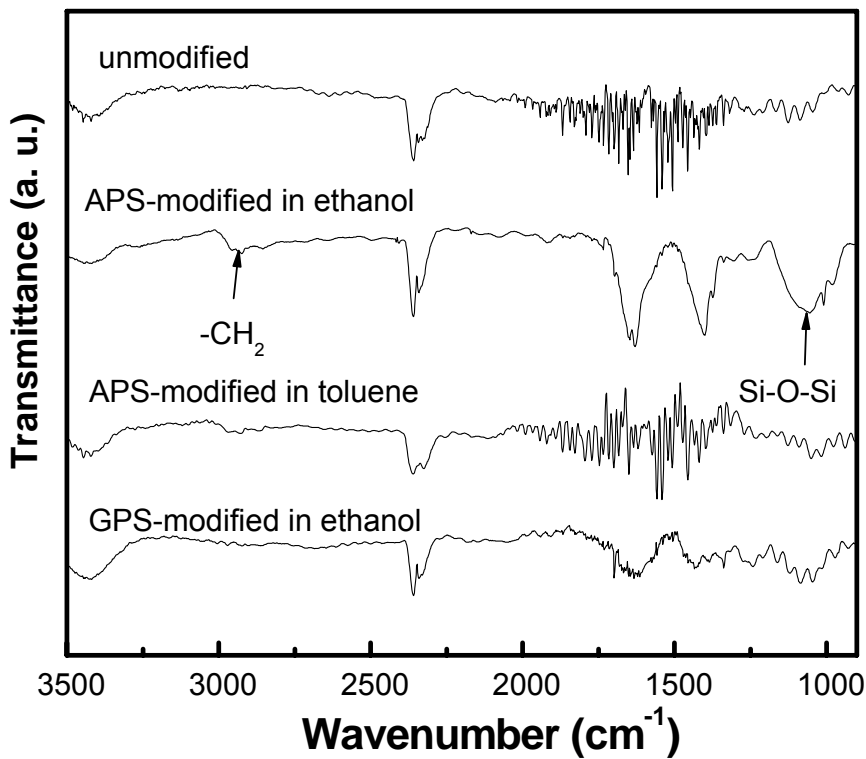


Figure 5-1. FTIR spectra of untreated nanoparticles and SMN treated in different conditions.

HRTEM was used to characterize the morphology of SMN and investigate the existence and thickness of the surface coating layer. Figure 5-2 shows the HRTEM micrograph of SMN. The size of nanoparticles was in the range of 20-50 nm. Well-defined lattice structure could be observed at higher magnification. A thin layer in 1-2 nm thickness could be observed on the surface of metal nanoparticles. A certain amount of coupling agent is distributed among the metal nanoparticles as well. This layer is

amorphous as no lattice structure could be detected even at higher magnification. The attached EDS indicated the presence of Si in the surface coating layer, which originates from the surface modification agent. These results indicate the successful formation of a thin coating layer on the nanoparticle surface, i.e. a core-shell structure formed by means of surface modification of nanoparticles via organic agent.

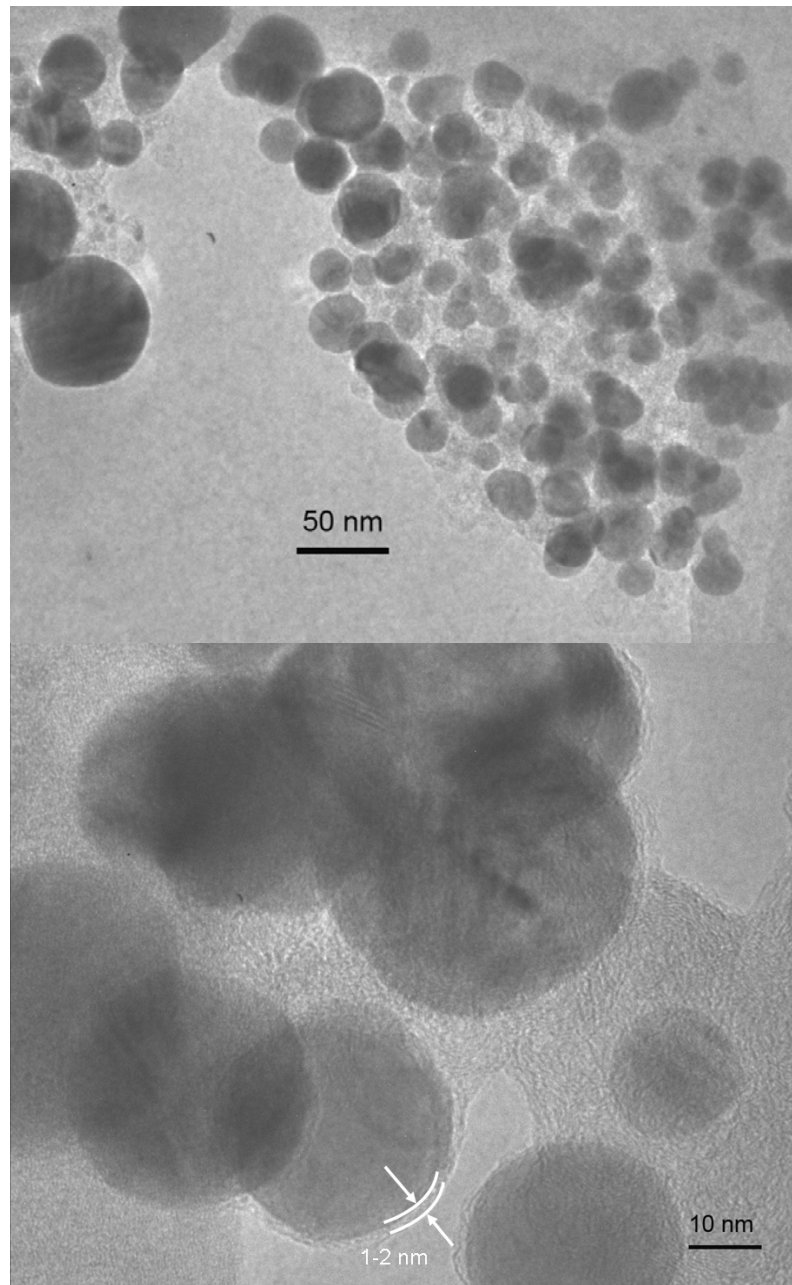


Figure 5-2. HRTEM micrographs of SMN.

XPS survey scan was conducted on the SMN. The spectrometer resolution was ~ 1.0 eV for the survey scans and ~ 0.1 eV for high-resolution scans. Figure 5-3 displays XPS survey scan which showed C 1s, O 1s, N 1s and Si 2p peaks besides Ag 3p and Ag 3d peaks. The assignment of the peaks at different binding energy (E_B) is listed in Table 5-1. The existence of oxygen and carbon, and traces of nitrogen and silicon which mainly originate from the silane moieties proves the presence of the APS coupling layer on the surface of Ag nanoparticles.

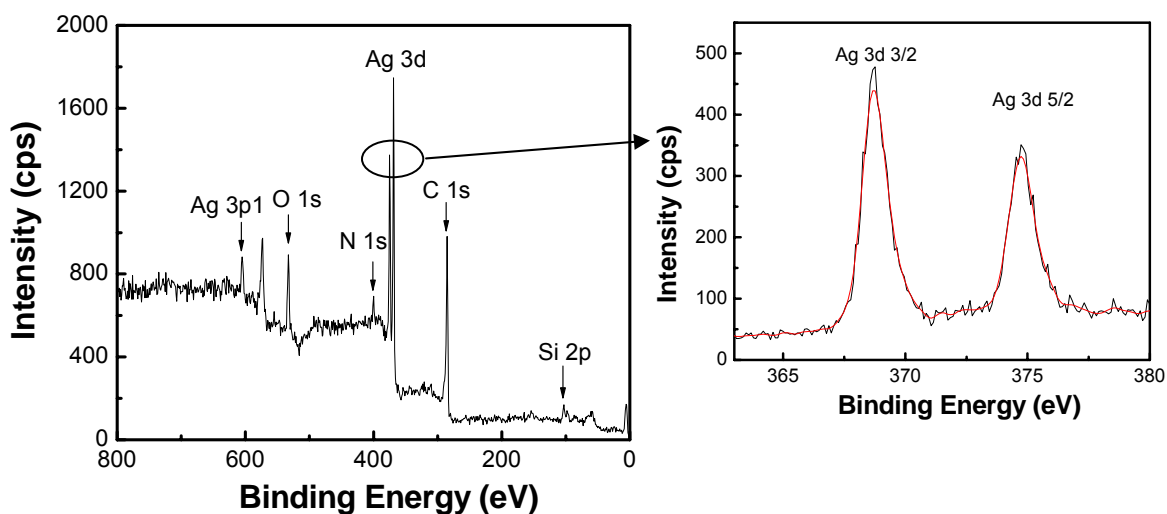


Figure 5-3. XPS general survey and high resolution scan spectra of SMN.

Table 5-1. Data analysis from XPS spectra of SMN.

B. E. (eV)	368.7	374.7	604	284	532	399	103
Element	Ag 3d 3/2	Ag 3d 5/2	Ag 3p1	C 1s	O 1s	N 1s	Si 2p
Atomic conc.	4.36 %	3.94 %	5.3 %	63 %	12.5 %	3.8 %	4.6 %

Figure 5-4 displays X-ray diffraction (XRD) patterns of unmodified Ag nanoparticles and SMN by APS. Both spectra show four well-defined strong peaks at $2\theta = 38.4, 44.3, 64.7$ and 77.6° , indexed as (111), (200), (220) and (311) planes,

respectively, of the face-centered cubic (fcc) Ag phase. No obvious change in the peak positions or width could be observed for the nanoparticles after treatment, indicating that neither crystal configuration nor grain size changed during the treating process. No occurrence of new peak suggests that the surface coating layer is amorphous, which is in agreement with the HRTEM result.

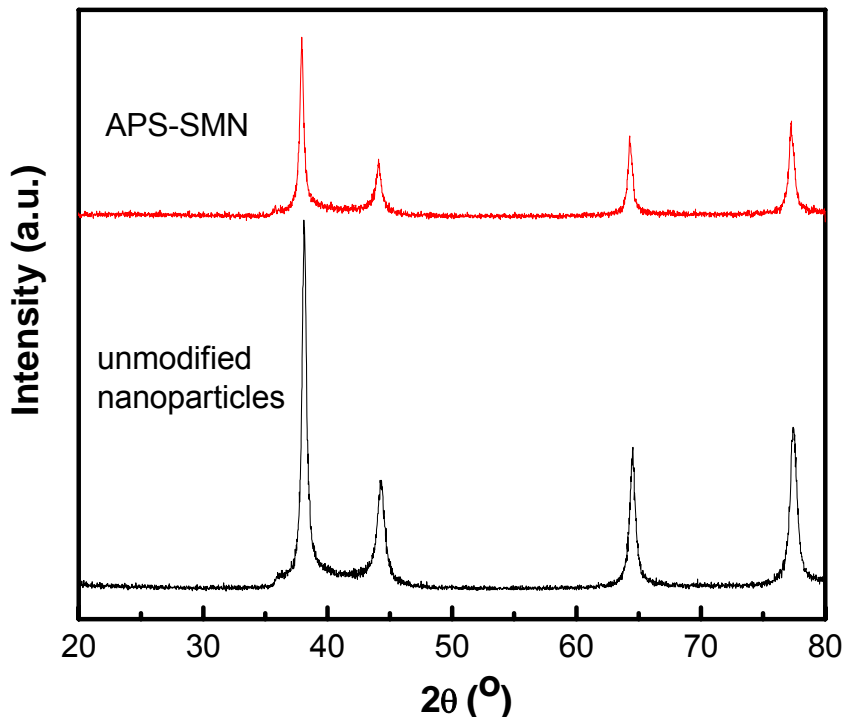


Figure 5-4. XRD spectra of unmodified nanoparticles and SMN.

Heat treatment at 150 $^{\circ}$ C for 1 hr was conducted on unmodified nanoparticles and SMN to investigate the effect of surface modification as well. From the DSC isothermal test results of unmodified nanoparticles and SMN as displayed in Figure 5-5, an additional reaction peak was observed for SMN. These results suggest that further condensation reaction might take place during the heat treatment process. The reaction heat was estimated as 16.4 kJ/mol (5 wt. % APS was assumed to be present in SMN). After heat treatment, the color of SMN remained black, while the color of unmodified Ag

nanoparticles changed from black to dark grey, which is indicative as a sintering effect. This difference also indicates the existence of the surface coating on the SMN which prevents the direct contact between the nanoparticles and thereby the sintering.

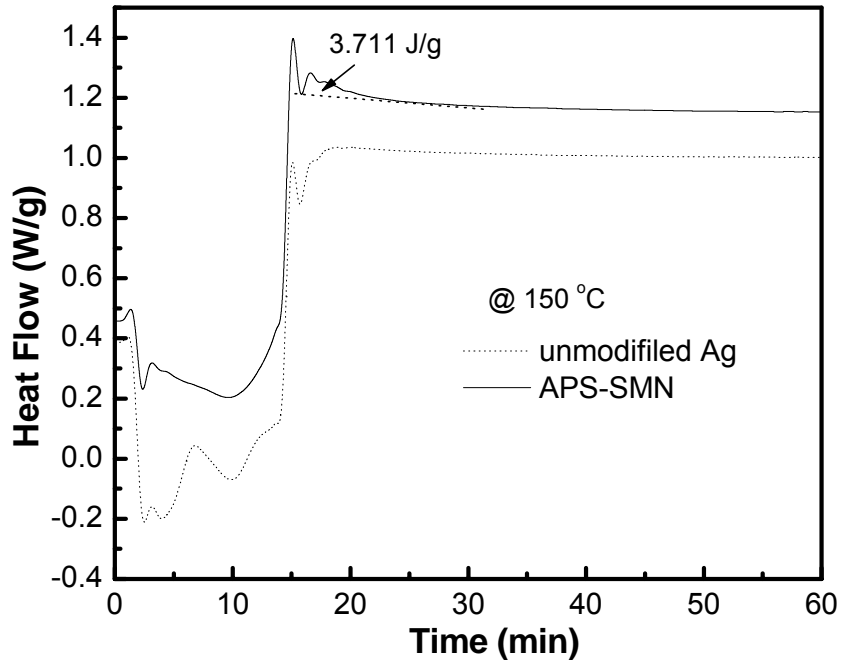


Figure 5-5. DSC isothermal curves of unmodified nanoparticles and SMN.

5.3.2 Characterization of Surface Modified Nanoparticles (SMN)/ Polymer Nanocomposites

The T_g s of unmodified nanoparticle/epoxy nanocomposite and SMN/epoxy nanocomposites with different SMN loadings were investigated by DSC as shown in Figure 5-6. The T_g s of SMN/epoxy nanocomposites are lower than that of unmodified nanoparticle/epoxy nanocomposite. This might be due to the enhancement of polymer-filler interaction around the filler resulted from the property change of the interface between nanoparticles and epoxy matrix after nanoparticle surface modification. The mobility of the polymer chains at the interfacial region were found to increase compared to the bulk material when the polymer-filler interactions are attractive, which might

explain the decrease of T_g of nanocomposites with SMN.^{109,116} Change in the free volume in the interfacial region after surface modification would also result in the change in T_g .¹¹⁷ Additionally, the reaction heat of these nanocomposites was investigated as well from the curing profiles because changes in crosslink density would complicate the T_g of crosslinked system as well. The normalized reaction heat for 20 wt. % unmodified Ag/epoxy, 20 wt. % APS1-SMN/epoxy, and 40 wt. % APS-SMN/epoxy nanocomposite are calculated as 315.8 J/g, 247.5 J/g, and 231 J/g, respectively. Compared to unmodified Ag/epoxy nanocomposite, crosslink density of nanocomposite containing surface modified fillers reduced, which could be another contributor to the decrease of T_g . And T_g of SMN/epoxy nanocomposites is further decreased with the increase of SMN loading.

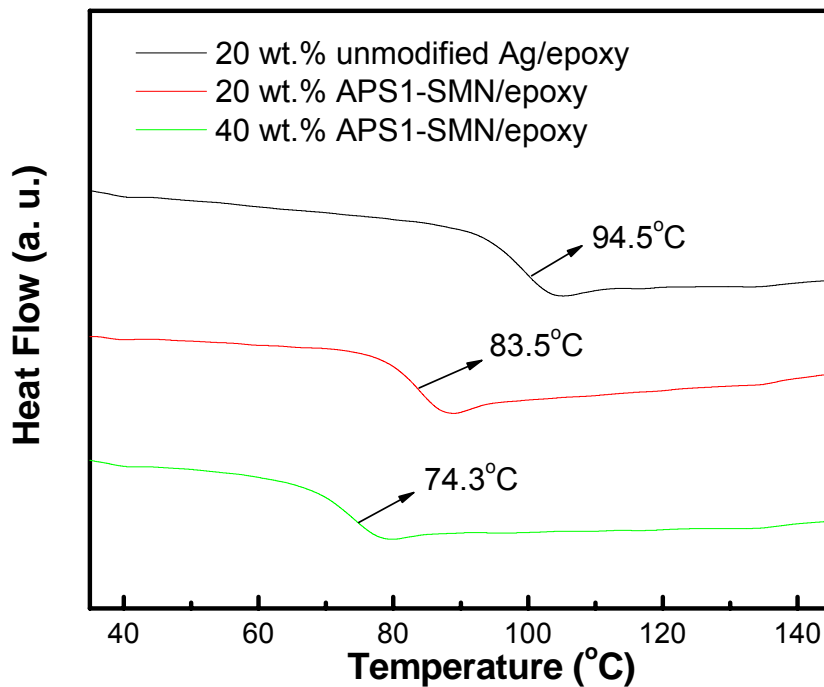


Figure 5-6. DSC curves and T_g s of cured unmodified nanoparticle/epoxy composite and SMN/epoxy composites with different SMN loadings.

The SEM image of a cured SMN/epoxy nanocomposite in Figure 5-7 showed that the nanoparticles in size of 30-50 nm were embedded in the polymer matrix. Compared

to the images of nanoparticles before incorporation into polymer matrix displayed in HRTEM micrograph (see Figure 5-2), the size of the nanoparticle was quite similar and no agglomeration was observed. This can be attributed to the effect of the surface coating which inhibits the direct contact of the nanoparticles and thus prevents the agglomeration which could lead to severe property degradation of nanocomposites.

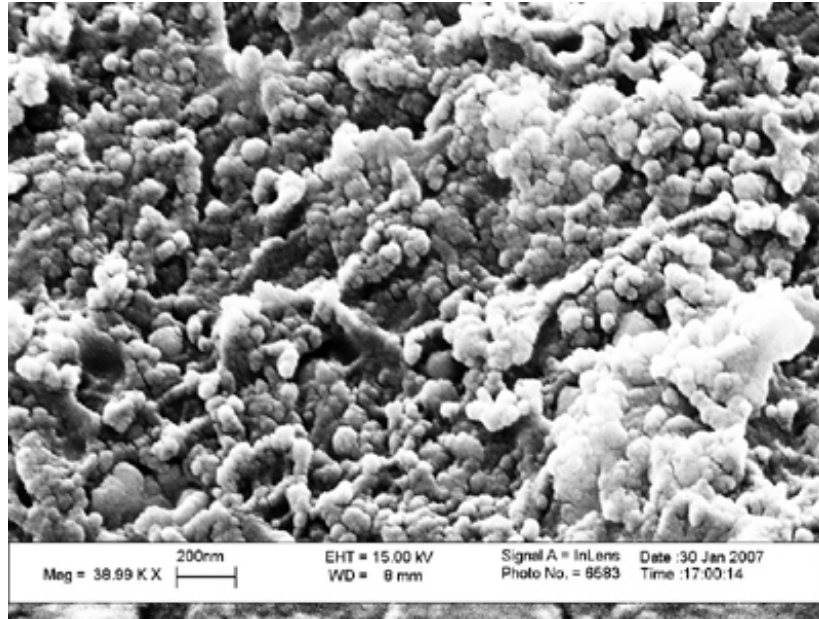


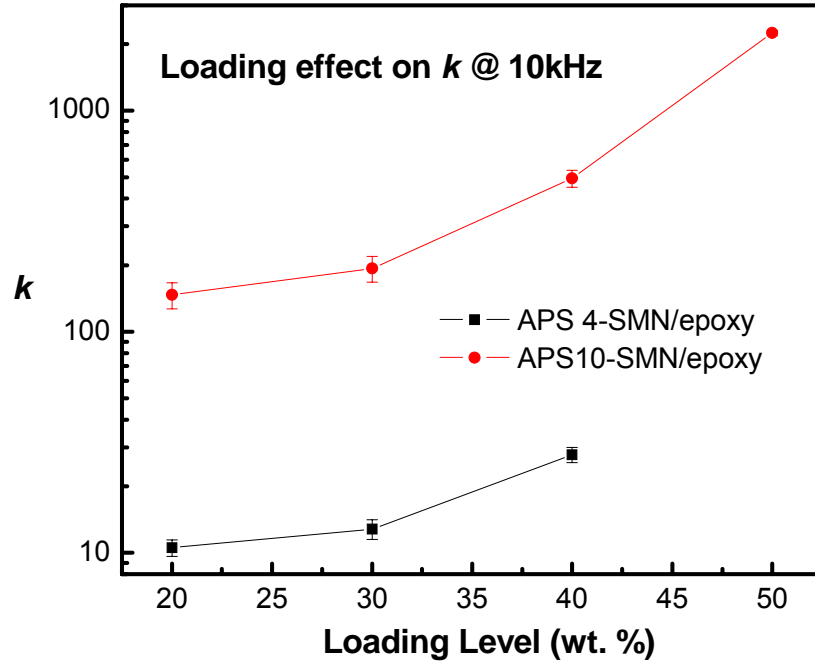
Figure 5-7. SEM image of cured SMN/epoxy nanocomposite.

5.3.3 Electrical and Dielectric Property Measurements

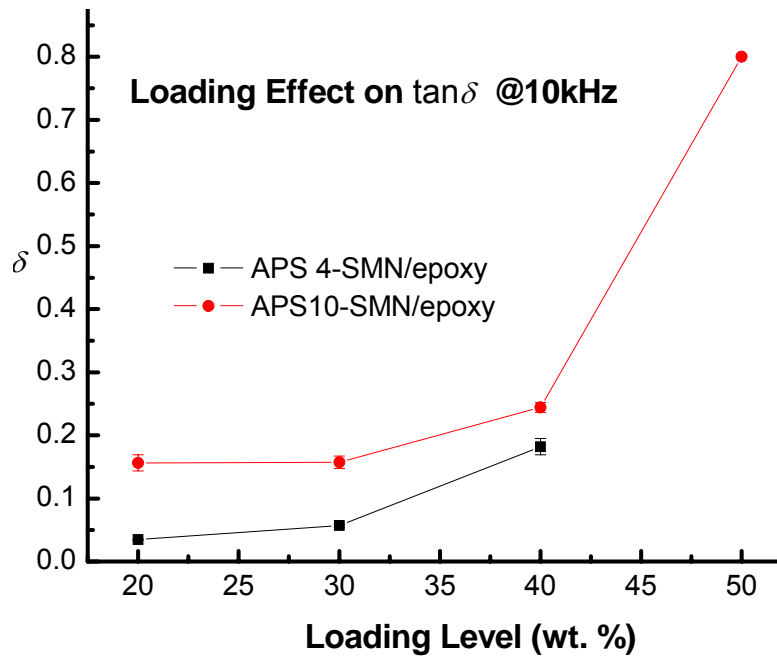
A set of dielectric and electrical tests were performed to characterize the SMN/epoxy nanocomposites and survey the effect of surface modification on the dielectric and electrical properties of these nanocomposites.

The dependence of the dielectric properties of the composite on both SMN loadings and frequency was investigated. Figure 5-9 (a) and Figure 5-9 (b) display the dielectric constant, k , and the dielectric loss tangent, $\tan\delta$, of the SMN/epoxy nanocomposites containing various loadings of SWN treated with different amounts of

APS. APS4-SMN/epoxy and APS10-SMN/epoxy refer to nanocomposites containing Ag nanoparticles treated with larger and smaller amounts of modification agent, respectively. In both cases, the k and $\tan\delta$ values increase as filler loading increases. In sharp contrast to the composites incorporating unmodified Ag nanoparticles for which 20 wt. % which is beyond the percolation, the SMN/epoxy nanocomposites didn't exhibit a sharp and narrow transition near percolation. Therefore, the processing window has been much expanded. Furthermore, with the decrease of treatment amount of modification agent, both of the k and $\tan\delta$ values increase significantly. The possible explanation might be that the treatment of fillers with larger amount of modification agent could render thicker coating layers on the conductive nanoparticle surface which prevent the direct contact and restrict the electron transfer between Ag nanoparticles. And also, the presence of Si-O-Si bonds and the nanoparticle surface can be treated as oxygen defects which act as the trap sites for charge carriers.^{105,114} These factors could lead to a decreased dielectric constant and dielectric loss of the nanocomposites. That is to say, the dielectric properties of the composites could be tailored by surface modification of incorporated nanoparticles. Generally speaking, the thicker the coating is, the lower the k and loss values the SWN/polymer composites are. Figure 5-9 (c) depicts the effect of frequency on the k values of SMN/epoxy composites. It shows that the k values decrease with the frequency for all loadings of SMN. And the composites containing higher loading of SMN showed the stronger frequency dependence of dielectric constant. The relatively strong frequency dependence resembles other percolative composites, which suggests that the lossy metal core is still dominant in determining the relaxation behavior of these SMN/epoxy composites.

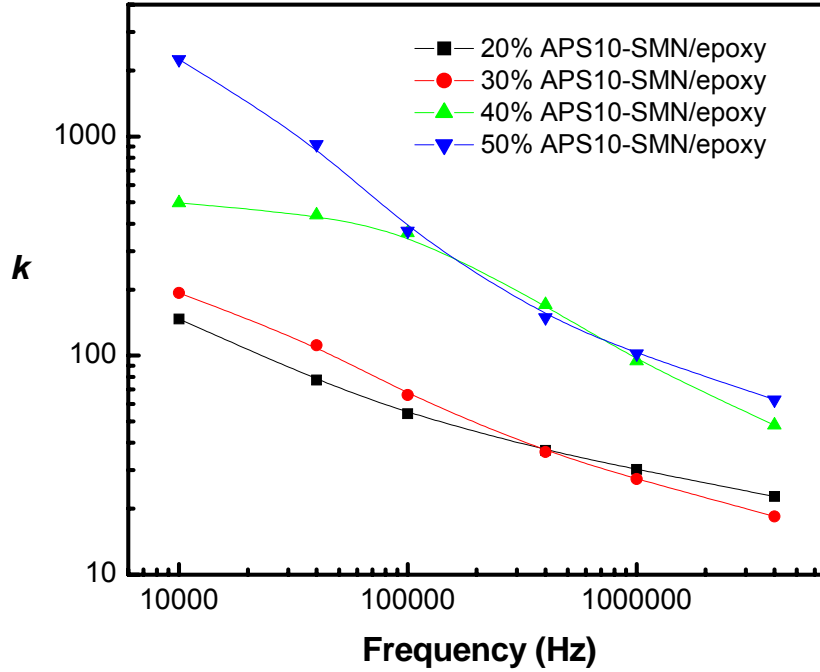


(a)



(b)

Figure 5-8. Dielectric properties of SMN/epoxy composites with different SMN loadings and different modification degree: (a) loading effects on k values, (b) loading effects on $\tan \delta$ values, and (c) frequency effects on k values.



(c)

Figure 5-9 continued.

The dielectric properties of SMN/epoxy nanocomposites containing SMN treated in different conditions were summarized in Table 5-2. Unlike the nanocomposites containing APS modified nanoparticles whose dielectric constant and dielectric loss was substantially decreased after surface modification, the dielectric behavior of nanocomposites containing GPS modified nanoparticles was more like composites containing nanoparticles without surface modification, i.e. high dielectric constant and high dielectric loss. With regard to the solvent media used in surface modification, the dielectric properties of composites containing nanoparticle treated by APS in dry toluene also exhibit relatively higher k and higher $\tan\delta$, indicate that the surface modification is more effective in aqueous media than the dry solvent. The nanocomposites incorporating SMN treated by APS in the aqueous solvent possess relatively lower dielectric constant and lower dielectric loss tangent, which is attributed to the passivation effect of the

coating layer on the nanoparticles incorporated in the composites. The conclusions inferred from the results of dielectric properties are in good agreement with those predicted from FTIR in terms of the effectiveness and degree of the surface modification. Accordingly, the possible mechanism of surface modification of Ag nanoparticles by APS is proposed as schematically represented in Figure 5-10. The effective surface coating layer on the Ag nanoparticles by APS might be due to the adsorption of APS onto Ag nanoparticle surface through atom coordination between nitrogen in the silane agent and the Ag, and the resulting layer after subsequent hydrolysis and condensation of the APS film.

Table 5-2. Dielectric properties of SMN/epoxy nanocomposites containing SMN treated in different conditions.

<i>wt. %</i>	<i>Agent</i>	<i>Solvent media</i>	<i>k</i>	<i>tan δ</i>
40	APS	aqueous ethanol	494	0.24
50	APS	aqueous ethanol	2247	0.80
40	GPS	aqueous ethanol	1233	1.76
50	GPS	aqueous ethanol	5035	3.47
40	APS	dry toluene	944	1.88
50	APS	dry toluene	3494	2.66

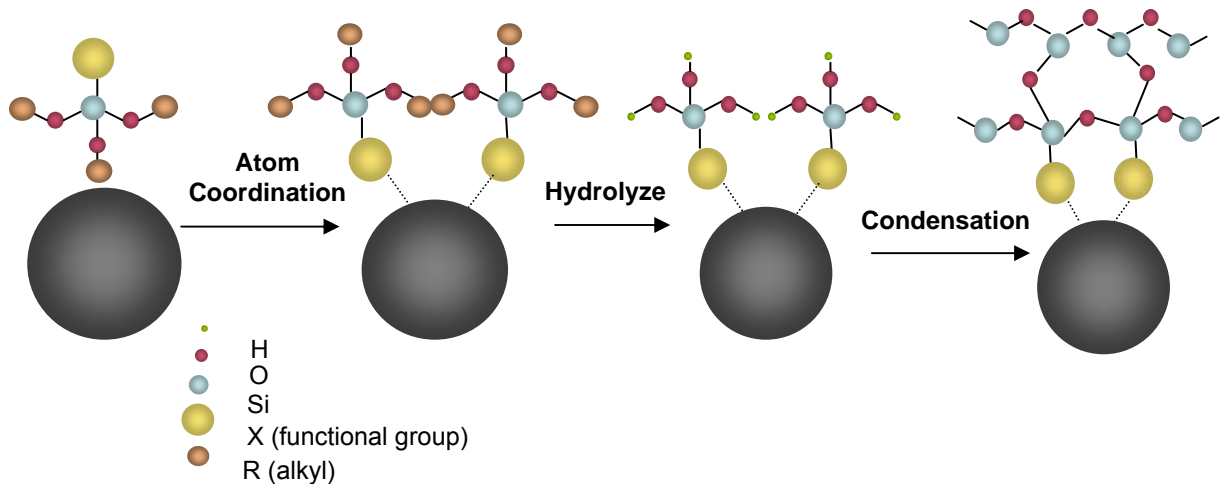


Figure 5-10. Schematic representation of proposed mechanism of surface modification of Ag nanoparticles by APS.

Dielectric breakdown strength of the nanocomposites, which is defined as the breakdown voltage (the highest voltage which samples can withstand before electrical failure) divided by sample thickness, was investigated as well. The effect of coating layer formed via surface modification can be confirmed by the current-voltage (I-V) characteristic measurements as displayed in Figure 5-11. Significant improvement in the dielectric breakdown strength was observed after the surface modification of the metal nanoparticles. The higher concentration of modification agents used, the thicker the coating layer on the nanoparticle surface, and correspondingly higher dielectric breakdown strength and lower leakage current at a given voltage. For the same 20 wt.% filler loading, the dielectric breakdown strength of APS4-SMN/epoxy nanocomposite and APS10-SMN/epoxy nanocomposite is 87 kV/cm and 17 kV/cm, respectively. Despite that the dielectric breakdown strength of APS4-SMN/epoxy nanocomposites substantially decreases from 87 kV/cm to 43 kV/cm as filler loading increases from 20 wt. % to 40 wt. %, the effect of coating is much more conspicuous than the filler loading effect. Because

the addition of surface coating layer may result in modifying the carrier trapping density and trapping depth in the polymer, and consequently modifying the space charge distribution in the nanocomposites.^{105,108,117} Furthermore, the surface coating layer can possibly serve as diffusion layer, so that the local electric field strength is reduced and the dielectric filed strength is increased.

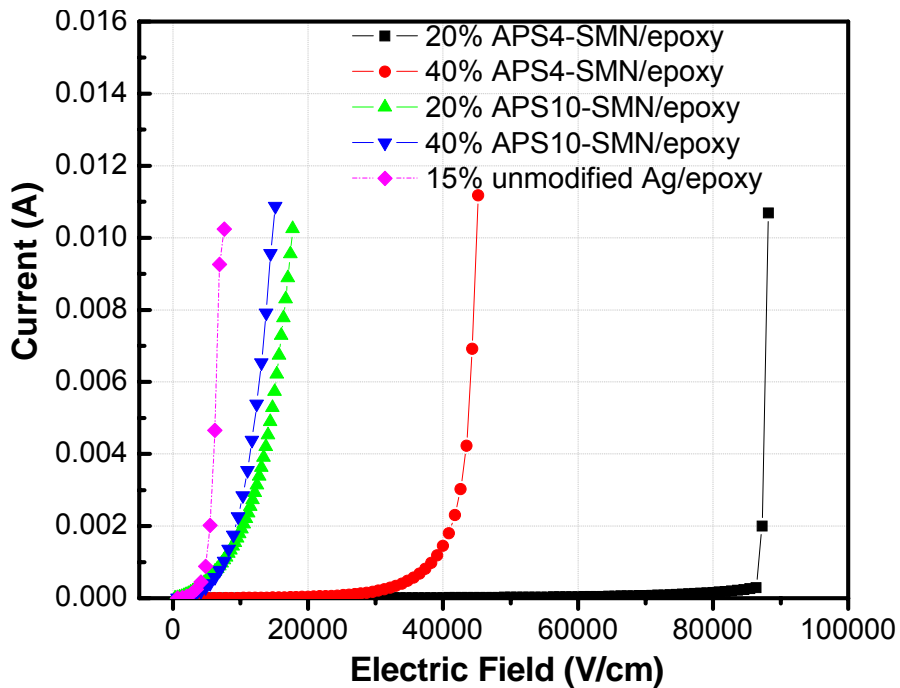


Figure 5-11. I-V characteristics of unmodified nanoparticle/epoxy nanocomposite and SMN/epoxy nanocomposites with different SMN loadings and different modification degree.

These dielectric and electrical property results of SMN/polymer composites are consistent with experimental evidence of SMN characterization. The surface passivation layer coated on the nanoparticles improves the performance of the conventional metal/polymer composites by decreasing the dielectric loss, enhancing the dielectric breakdown strength. Therefore, surface modification of nanofillers is believed to be an effective approach to adjust the electrical features at the nanofiller surface and the

interface between the nanofiller and the polymer matrix, and thereby tailor the corresponding property of interest of the nanocomposites. It is promising to achieve balanced dielectric properties of the nanocomposite by optimizing the degree of surface modification, the thickness and density of the nanoparticle surface coverage.

5.4 Conclusions

In this study, surface modification of nanoparticles was employed to change the surface chemistry and electrical state of nanoparticles and thereby tailor the dielectric and electrical properties of corresponding polymer nanocomposites. The surface coating layer coated on the nanoparticles via surface modification improves the performance of the metal nanoparticle/polymer composites by decreasing the dielectric loss, enhancing the dielectric breakdown strength. These performance improvements can be attributed to the interparticle electrical barrier layer formed via surface modification of nanoparticles which prevents the metal cores from direct contact, and/or the altered charge density and distribution around the interface of nanoparticles and polymer matrix. Surface modification of nanoparticles is believed to be an effective approach to adjust the electrical features at the nanoparticle surface and the interface between the nanoparticle and the polymer matrix, and thus tailor the corresponding property of interest of nanocomposites. It is also promising to achieve balanced dielectric properties of the nanocomposite by optimizing the degree of surface modification, the thickness and density of the coating layer on the nanoparticle surface.

CHAPTER 6

THE INFLUENCE OF CONNECTIVITY ON THE DIELECTRIC PROPERTIES OF NANOPARTICLE-BASED HIGH-K COMPOSITE MATERIALS

6.1 Introduction

To solve the problems of the conductive filler/polymer composites, currently much work has been directed to the control of the dielectric loss of this system to overcome the drawbacks of this system. It is well-known that the size, shape, distribution as well as the connectivity, i.e. the microstructure arrangement of the component phases in the composite, of the fillers possess great influence on the properties of the composite materials. Therefore, the manipulation of the conductive filler properties has been an important approach to achieve this target.

The electrical properties in terms of the percolation effects and transport phenomena in composite system are complicated. In specific, the type, shape and size of the filler in the composites are crucial, additionally, the connectivity and the resulting pathway and mean distance between particles or clusters also directly influence the charge carriers.⁵² The employment of nanofillers in the composites further increases the complexity because the change in the size of a simple nanocrystalline material can lead to great changes in its physical properties. As to electrical properties of composites, the volume or mass fraction and the structural phenomena have a large bearing on the

composite's transport properties. Alternatively, the proximity (path length) and size of metal particles can be varied depending on the technique for adding them into the polymer matrix. Instead of the aggregation of metal clusters and therefore nucleation to form larger grain sizes, islands of metallic clusters can be formed by some deposition techniques. Therefore, the manner of deposition and the resulting pathway and mean distance between island or particles or colloids also directly influence the conduction process as well as the dimensionality of the charge carriers. For instance, the electrical conductivity of a very thin metal film can be much lower than in a bulk material caused by a discontinuous structure, where the metal appears as cluster of island, in the thin films. However, work in the field of electrical properties of the nanocomposite is still inadequate for in-depth knowledge and complete understanding of percolation effects and dimensionality when nanofilers are used in composites.¹¹⁸

Similarly, it is anticipated that the feature of the fillers delivers a huge impact on the dielectric properties of the nanocomposites as well. However, there are even more deficiency in the research of this field. The effects of the size, size distribution, and surface property of the metal nanoparticles on the dielectric properties of the nanocomposites have been discussed in Chapter 3 and Chapter 5. The objective of this work is to investigate the impact of connectivity of nanoparticles and thereby to find an efficient way to enhance the dielectric performance of the high- k nanocomposites by the incorporation of appropriate metal nanoparticles.

There are usually three types of geometric morphologies of the phase distribution in a two-phase material because the microstructure of the material changes with the volume fraction of one phase, i.e. dispersed structure, aggregated structure, percolation-

like cluster structure.¹¹⁹ Before the volume fraction of the minor phase reaches percolation threshold to form a percolation-like interconnected cluster structure, dispersed structure and aggregated structure as shown in Figure 6-1 will be formed.

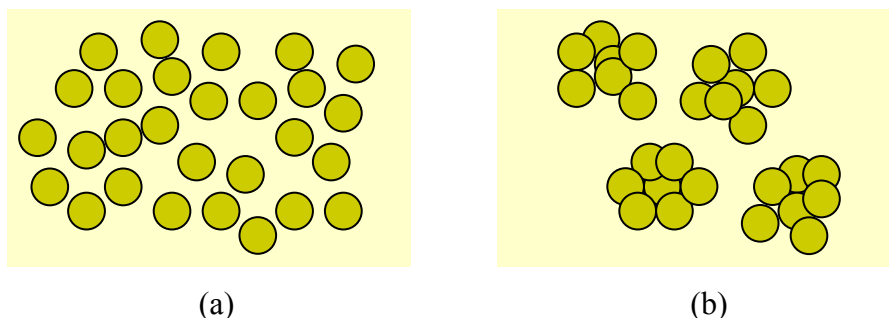


Figure 6-1. Schematic representation of geometric morphologies of the nanofiller distribution in a two-phase material in (a) dispersed structure and (b) aggregated structure.

Different degree of assembly and connectivity of phases in the nanocomposite might affect the interfacial polarization and conducting property and thereby have great impact on the dielectric constant, dielectric loss tangent and percolation of the final nanocomposites. Unfortunately, it is not easy to demonstrate due to other parameters of nanoparticles such as size, size distribution, surface property and so on might influence the properties of the nanocomposites and cannot be distinguished from the effect of connectivity. Therefore, in this work efforts were made to synthesize Ag nanoparticles of similar size, size distribution and surface property but with different connectivity in terms of aggregation status. The dielectric properties of the Ag/epoxy nanocomposites containing these nanoparticles were then studied to investigate this effect. The results revealed that aggregation status of the nanoparticles impacts the dielectric performance of the nanocomposite greatly.

6.2 Experimental

6.2.1 Materials

Epoxy of diglycidyl ether of bis-phenol A (Shell Chemicals Co.), an anhydride type curing agent (Lindau Chemical Co.) and an imidazole type catalyst (Shikoku Chemical Co.) were used as received. A low aggregate structure carbon black (Columbia Chemical Co.) was used. The silver nitrate (AgNO_3), resorcinol and sodium hydroxide (NaOH) were purchased from Aldrich and used without further purifications.

6.2.2 Preparation of Ag Nanoparticles with Different Morphology

Ag nanoparticles were prepared by a method similar to those previous reported.¹²⁰ Ag nanoparticles were synthesized by the wet chemical reduction of silver nitrate using resorcinol in alkaline medium. Resorcinol serves as the reducing agent as well as the capping agent. Variation of the pH value of the reaction solution through adjustment of the concentration of alkaline medium was employed to prepare Ag nanoparticles with different connectivity in terms of aggregation status. Centrifuging the resulting suspension allows the solvent to be decanted and powders of nanoparticles to be isolated. These powders consist of the desired nanoparticles and their intimate capping layer and can be re-dispersed in a variety of solvents.

6.2.3 Preparation of Ag/Epoxy Nanocomposites

The as-prepared Ag nanoparticles were dispersed in ethanol first and then mixed with a certain amount of the epoxy resin and hardener via ultrasonication.

6.2.4 Materials Characterization

A JEOL 100C transmission electron microscopy (TEM) was used for observing the morphology and analyzing the size of Ag nanoparticles prepared.

Fourier Transform Infrared (FTIR) was recorded on a Nicolet Magna-IR 560 spectrometer.

X-ray photoelectron spectroscopy (XPS) study of the samples was employed to characterize the surface of the Ag nanoparticles. The XPS data was collected on a Model 1600 XPS with 46.95 eV X-rays from an Al K α source (1486.6 eV) with spectrometer resolution \sim 1.0 eV for the survey scans.

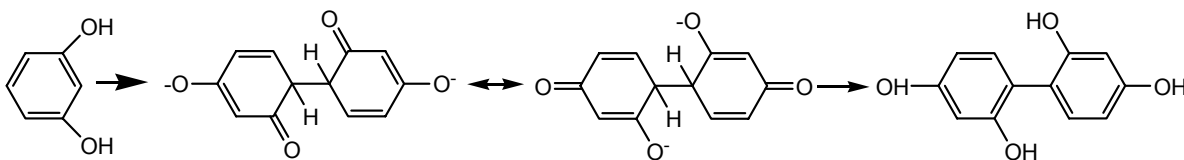
Thermogravimetric analysis (TGA) of the synthesized Ag nanoparticles was conducted on a TGA (TA Instruments 2050) at a heating rate of 10 °C/min under a nitrogen atmosphere.

Parallel plate capacitors of the nanocomposites were fabricated on glass substrate with DC sputtering copper layers as top and bottom electrodes. Capacitance and loss tangent measurements were carried out on a HP 4291A Multi-Frequency LCR meter over frequency range from 10 kHz to a few MHz. The thickness of the dielectric films was measured with a profilometer (Alpha-Step Co.) and was used to calculate the dielectric constant of the samples.

6.3 Results and Discussion

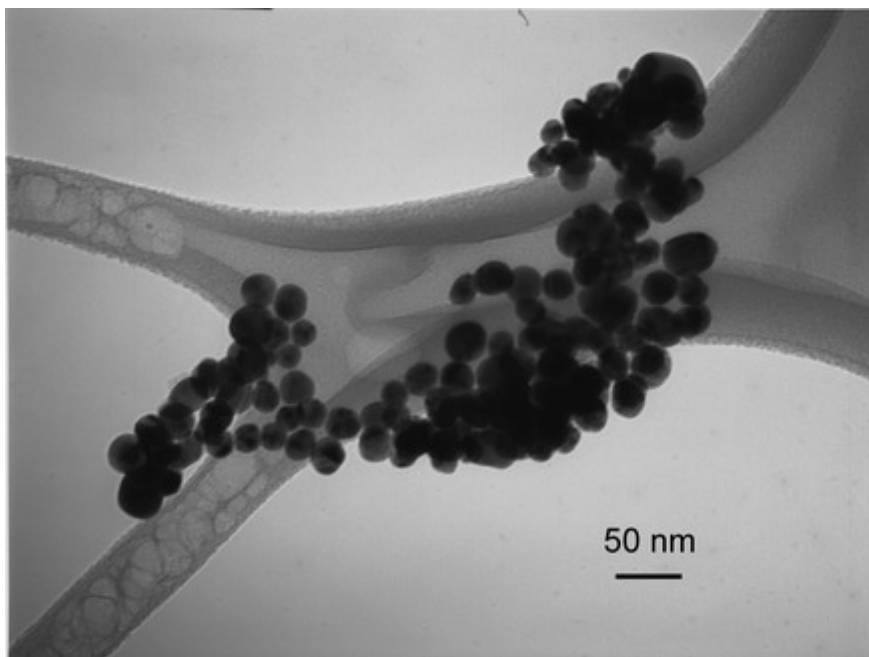
6.3.1 Synthesis of Ag Nanoparticles with Varied Connectivity

The synthesis of the Ag nanoparticles with different connectivity of interest was achieved by adjusting the pH of the reaction, which was found to play an important role in assembling the nanoparticles.¹²⁰ In this study, different concentration of NaOH was applied to prepare Ag nanoparticles with varied aggregation status. The TEM images of the Ag nanoparticles synthesized with different concentrations of alkaline medium are shown in Figure 6-2. The average size of the Ag nanoparticles is around 25 nm. At a high concentration of [NaOH] (1 mM), small primary Ag nanoparticles form more aggregated structure (denoted as Ag_a). In the case of a lower concentration of [NaOH] (0.3 mM), the Ag nanoparticles (denoted as Ag_d) are more discrete. The formation of Ag nanoparticle aggregates are brought about by a hydrogen-bonding interaction of the resorcinol and its dimer, tetrahydroxybiphenyl (see Scheme 6-1).¹²⁰

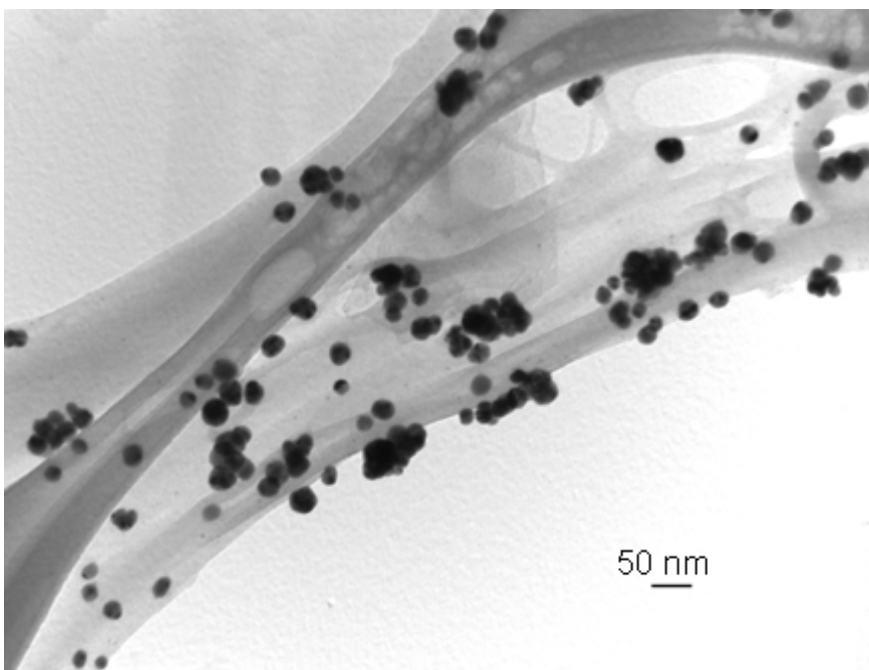


Scheme 6-1. Schematic presentation of the evolution of resorcinol to its dimer.

Resorcinol can act as weak acids and undergo deprotonation. Deprotonation of the hydroxyl group occurs more easily at higher concentration of NaOH and facilitates the formation of a close-pack assembly of nanoparticles.



(a)



(b)

Figure 6-2. TEM images of Ag nanoparticles with different morphology: (a) Ag_a and (b) Ag_d.

6.3.2 Characterization of Synthesized Ag Nanoparticles

Figure 6-3 displays FTIR spectra of pure resorcinol and Ag nanoparticles synthesized with resorcinol as both reducing agent and capping agent. The peak at ~ 1606 cm^{-1} and ~ 1387 cm^{-1} can be attributed to the C=C stretching on the phenyl ring and O-H vibration of the phenol moiety of resorcinol. The results revealed that the Ag nanoparticles are capped by the resorcinol moiety.

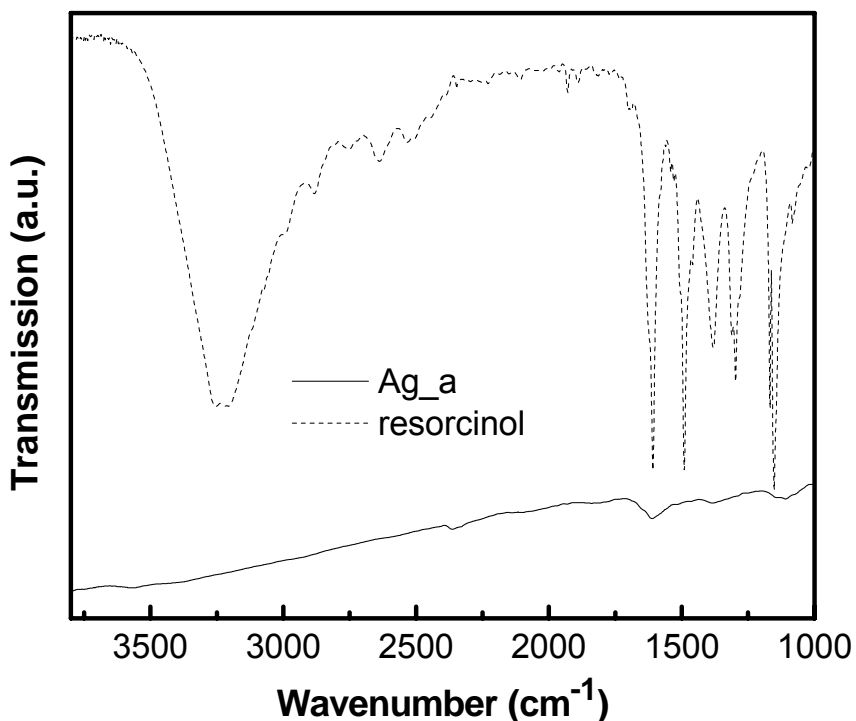


Figure 6-3. FTIR spectra of synthesized nanoparticles Ag_a (solid line) and pure resorcinol (dashed line).

XPS survey scan was conducted on the synthesized Ag nanoparticles Ag_a. Figure 6-4 display XPS survey scan which showed evidence for the C 1s and O 1s peaks besides Ag 3p and Ag 3d peaks. The results revealed that the Ag nanoparticles are capped by the resorcinol moiety.

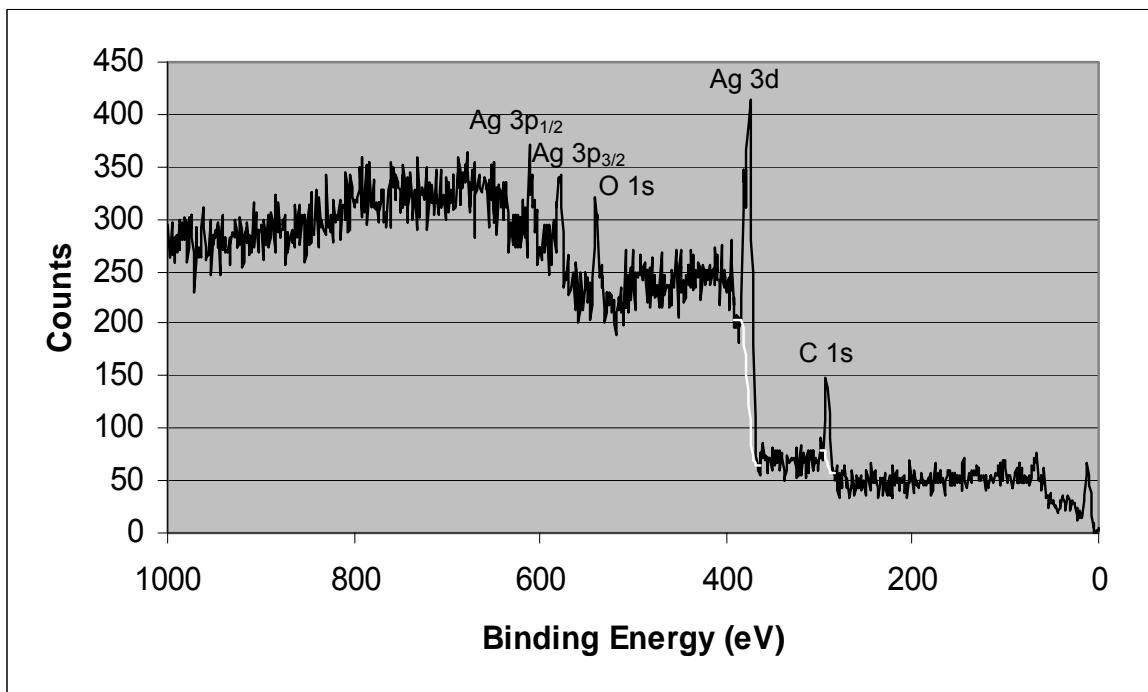


Figure 6-4. General survey XPS spectrum of Ag nanoparticle.

The TGA curves of the Ag nanoparticles prepared with different morphology were displayed in Figure 6-5. The weight loss for the Ag nanoparticles could be attributed to the resorcinol capping layer on the Ag nanoparticle surface, which accounts for around 7.1 wt. % and 6.5 wt. % of the total weight of Ag nanoparticles with more aggregated morphology and more discrete morphology, respectively.

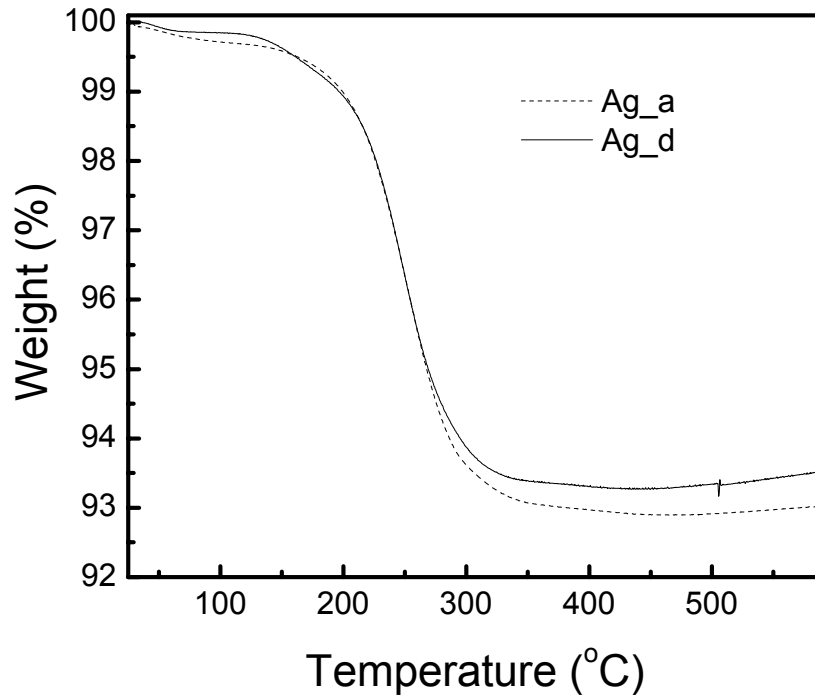


Figure 6-5. TGA curves of Ag nanoparticles with different morphology.

6.3.3 Dielectric Properties of Epoxy Nanocomposites Based on the Ag Nanoparticles with Varied Connectivity

The nanocomposites based on the as-synthesized Ag nanoparticles were prepared and the dielectric properties of these nanocomposites were investigated. Figure 6-7 shows the k and $\tan\delta$ values of the nanocomposite containing Ag nanoparticles with different connectivity at 10 kHz as a function of the filler loading. A moderate increase in k was observed when the Ag loading was below 60 wt. %. The increase of k became pronounced when Ag loading was beyond 63 wt. %. All these nanocomposites exhibit low dielectric loss tangent values below 0.06. The possible reasons contribute to the low dielectric loss for the composites could be the resorcinol moiety on the Ag nanoparticle surface inhibits the formation of a conducting filler network. As expected, the

connectivity of the Ag nanoparticle has great influence on the dielectric properties of final nanocomposite materials. There is not much difference in the k values of the nanocomposite containing Ag nanoparticles with different aggregation status, while the nanocomposite containing Ag nanoparticle with more discrete structure rendered much lower dielectric loss tangent. The dielectric loss mechanism in the nanocomposites is complicated but, in general, occurs via two main mechanisms, that is, interfacial loss and conduction loss. There are higher conduction loss and interfacial loss involved in more aggregated structures of Ag nanoparticles in the nanocomposites, which results in the behavior of the final nanocomposites more resistive rather than capacitive. Therefore, the Ag nanoparticles with more discrete structure are desirable as conductive filler in the nanocomposite system. For a 65 wt. % Ag_d/epoxy nanocomposite, the k value reaches 96 and the $\tan\delta$ value remains as low as 0.036.

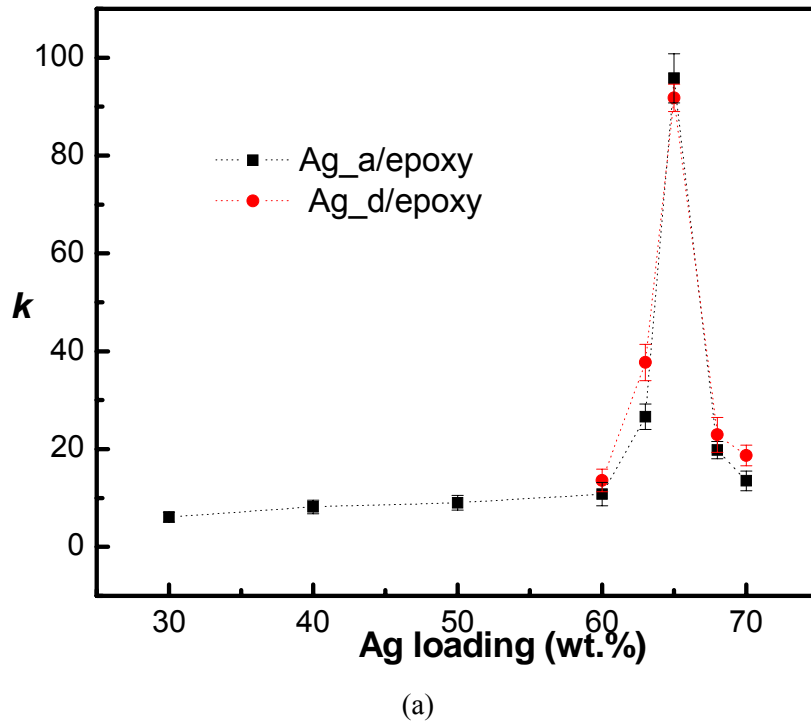
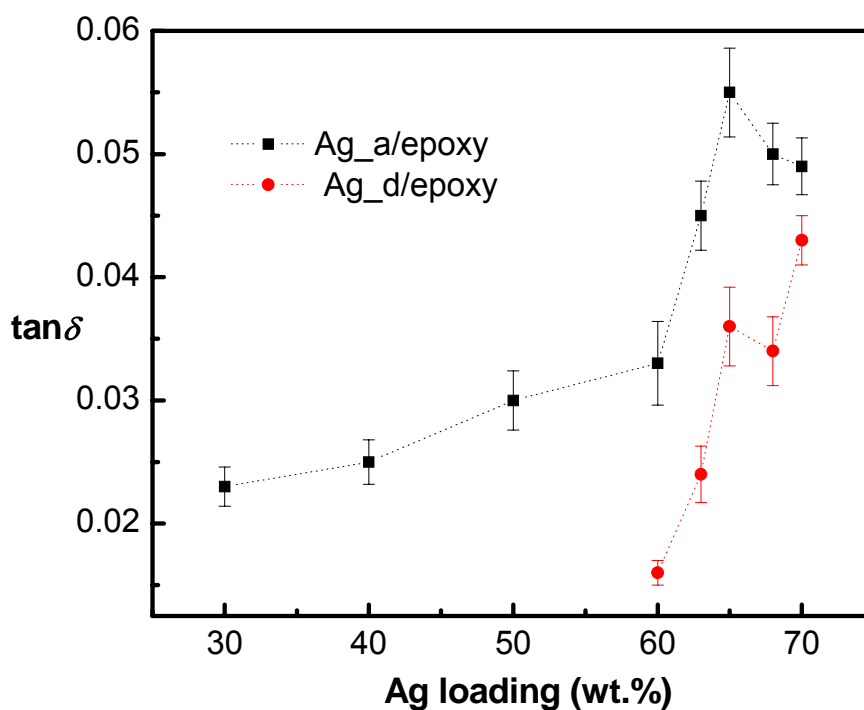


Figure 6-6. (a) k and (b) $\tan\delta$ values of Ag/polymer composites containing Ag nanoparticles with more aggregated structure (Ag_a) and more discrete structure (Ag_d).



(b)

Figure 6-7 continued.

6.4 Conclusions

In this study, the effect of the connectivity of the metal nanoparticle phase on the dielectric properties of the nanocomposites was investigated. The synthesis of the Ag nanoparticles with varied connectivity of interest was achieved by adjusting the pH of the reaction, which was found to play an important role in assembling the nanoparticles. Using this approach, NaOH of different concentrations was used to prepare Ag nanoparticles with varied aggregation status. The nanocomposites based on the as-synthesized Ag nanoparticles were prepared and the dielectric properties of these composites were investigated. The Ag/epoxy nanocomposites based on Ag nanoparticles capped with organic moiety showed very low dielectric loss tangent (<0.06). Assembly of

the nanoparticles impacts the dielectric performance of the nanocomposite greatly in terms of the interfacial polarization and conducting properties. There is not much difference in the k values of the nanocomposite containing Ag nanoparticles with different aggregation status, while the nanocomposite containing Ag nanoparticle with more discrete structure rendered much lower dielectric loss tangent compared to the nanocomposites with Ag nanoparticles of more aggregated structure.

CHAPTER 7

ALL-ORGANIC HIGH-*K* POLYANILINE/EPOXY COMPOSITES VIA AN *IN-SITU* POLYMERIZATION

7.1 Introduction

Dramatic increase of dielectric constant close to the percolation threshold observed in the conductor-insulator percolative system arouses interest of developing conductive filler/polymer composites as candidate materials for embedded capacitor applications. Various inorganic conductive fillers, such as metals like silver, aluminum, nickel, and carbon black have been used to prepare the two-phase or three-phase percolative composite system. This material option represents advantageous characteristics over the conventional ceramic/polymer composites, specifically, ultra-high k with balanced mechanical properties including the adhesion strength. The composites fabricated by dispersing an organic filler material possessing very high dielectric constant in a polymer matrix were found to exhibit high- k as well. Electrically conductive polymers such as polythiophenes, polypyrrole, polyaniline (PANI), and poly(p-phenylene vinylene) might be used as organic conductive element in such all-organic composites. In this work, the possibility of all-organic composites as candidate high- k material for embedded capacitor applications has been investigated.

PANI and its derivatives are regarded as one of the most promising conducting polymers because of its high polymerization yield, controllable electrical conductivity,

good environmental stability and relatively low cost.^{121,122,123,124,125,126} PANI/polymer composites have attracted considerable attention because low concentration of PANI can make the material achieve conductive or semiconductive capabilities which enable the development of thin, light, flexible and inexpensive organic electronics applied in display, sensor, and solar technologies.^{27,51,127,128,129,130,131} For instance, PANI/polyurethane (PU) composite containing 8.4 wt.% of PANI was reported with a conductivity of $2.17 \times 10^{-10} \text{ S cm}^{-1}$.¹²⁷ The electrical conductivity of PANI/PU-epoxy composites with 1 wt. % to 5 wt. % of PANI was in the range of 10^{-9} to $10^{-3} \text{ S cm}^{-1}$.¹²⁸ PANI nanorod/liquid crystal epoxy composites showed electrical conductivity varied from 10^{-5} to $10^{-3} \text{ S cm}^{-1}$.¹²⁹ The conductivities for PANI/epoxy-amine system was in the range of 10^{-12} to $10^{-6} \text{ S cm}^{-1}$, which was lower due to the deprotonation effect of amine.¹³⁰ Oligomeric PANI/epoxy resin composites cured with amine could be doped with protonic acids to achieve the electrical conductivity in the range of 10^{-5} to $10^{-3} \text{ S cm}^{-1}$.¹³¹

Besides the electrical behaviors, dielectric properties of PANI and its composites have been of interest as well. PANI was reported to possess a k value larger than 104 in a partially crystalline system for which an inhomogeneous disorder model was proposed. High k values ranging from 200 to 1000 were reported for a PANI/polyvinyl alcohol composite, where the dispersed PANI particles of submicron size were suspended in the insulating polyvinyl alcohol matrix.¹²⁴ A PANI/polyurethane composite with a k value around 1120 at 1 kHz and 433 at 10 kHz was also reported.¹²⁵ But no data about dielectric loss of this system was found. For electroactive applications, 23 vol% of insulating polymer coated PANI particulates in a poly(vinylidene fluoride-trifluoroethylene-chlorotrifluoroethylene) terpolymer matrix can reach a k value more

than 2000 and a dielectric loss tangent around 1.75 at 100 Hz.⁵¹ These results suggest the possibility of using conducting polymer as conductive elements instead of the metal fillers to achieve ultra-high dielectric constant and the worthwhileness of further study.

Epoxyes have been of particular interests for embedded capacitor applications because of its compatibility with PCB manufacturing process. However, there is limited information concerning PANI composites prepared within thermoset polymer matrix. Therefore, it is worthwhile to explore the feasibility of incorporate high-loading level PANI into the epoxy matrix and the properties of PANI/epoxy composites. In this study, camphorsulfonic acid (CSA) was chosen as a protonating agent because the PANI protonated with CSA has relatively high crystallinity, high electrical conductivity and high miscibility with another polymer matrix.^{132,133} Additionally, *in-situ* polymerization of protonated aniline in the epoxy matrix was employed to prepare PANI/epoxy composites. Compared with traditional simple solution blending method by mixing the doped PANI and epoxy resin,^{130,133,134,135} the *in-situ* polymerization method rendered the possibility of better miscibility between PANI and epoxy resins and the higher PANI loading.^{136,137,138}

The influence of PANI loading levels and the hardener type on dielectric properties of PANI/epoxy composites was discussed. Frequency dependency of dielectric properties for PANI/epoxy composites was also presented in the range of 10 kHz to 10 MHz. Scanning electron microscopy (SEM) was used to characterize the morphology of PANI/epoxy composites. The correlation of the microstructure with the corresponding dielectric properties was discussed.

7.2 Experimental

7.2.1 Materials

EPON 828 (Shell Chemicals Co.) was used as a matrix resin. Hexahydro-4-methylphthalic anhydride (HMPA, Lindau Chemical Co.), Ancamine 2167 (Air Product) and Anchor 1040 (Air Product) were selected as anhydride, amine and amine complex types hardeners, respectively. 1-methylimidazole (Aldrich Chemical Co.) was employed as a catalyst. Polyaniline protonated with p-toluene sulfonic acid (PANI_PTSA complex), aniline, camphor sulfonic acid (CSA) and ammonium persulfate (APS) were purchased from Aldrich Chemical Co.

7.2.2 Preparation of PANI/Epoxy Composites by Simple Solution Mixing Method

Firstly, polyaniline protonated with p-toluene sulfonic acid (PANI_PTSA complex)/epoxy composites were prepared by simple solution mixing method. PANI_PTSA was first dissolved in formic acid using ultrasonication. Then epoxy resin was added and the blends treated by ultrasonication again.

7.2.3 Preparation of PANI/Epoxy Composites by *In-situ* Polymerization Method

Preparation of PANI/epoxy composites by *in-situ* polymerization method was carried out in two steps as displayed in Figure 7-1, i. e. syntheses of aniline salt monomer Ani-CSA and PANI/epoxy composites via *in-situ* polymerization of Ani-CSA in the epoxy matrix.

7.2.3.1 Preparation of Aniline Salt Monomer

4.6565 g (0.05 mol) of aniline and 11.515 g (0.05 mol) of CSA were dissolved in a mixture of methanol and water by stirring. The aniline salt monomer Ani-CSA was obtained as a tan-white solid by recrystallization.

7.2.3.2 An *In-situ* Polymerization of Aniline Salt within Epoxy Matrix

1.537 g of Ani-CSA in 10 ml of chloroform was mixed with 3.5 g of epoxy in 5 ml of chloroform. An aqueous solution of 1.426 g of APS was added into the mixture dropwise with stirring over 1.5 hr. The resulting mixture was stirred for another 5 hr in an ice bath, and then washed with distilled water until the system neutralized to remove the excess amount of CSA and APS. A dark green viscous 20 wt. % PANI/epoxy composite was obtained after storing in a vacuum oven overnight. The 8 wt. %, 15 wt. % and 25 wt. % PANI/epoxy composites were prepared in the same manner.

After the addition of a hardener (if not specified, HMPA by default), the composites were cured at 100 °C for 0.5 hr and at 125 °C for 1 hr.

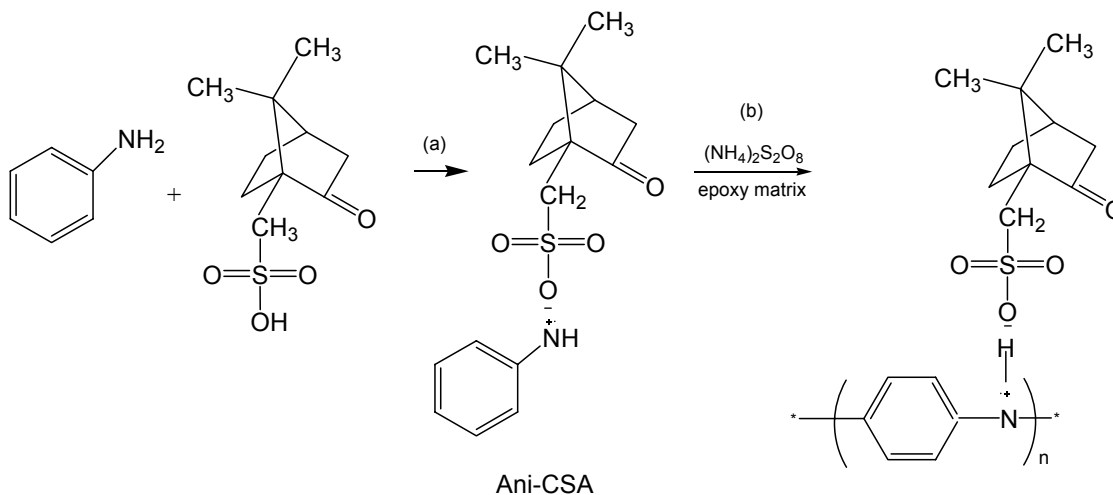


Figure 7-1. Syntheses of aniline salt monomer Ani-CSA and PANI/epoxy composites via an *in-situ* polymerization of Ani-CSA in the epoxy matrix.

7.2.4 Instrumental Analysis

Fourier Transform Infrared (FTIR) and Ultraviolet-visible (UV-Vis) spectra were recorded on a Nicolet Magna-IR 560 spectrometer and a Beckman DU 520 General purpose UV-Vis spectrophotometer, respectively.

The ^1H NMR Spectrum of aniline salt Ani-CSA monomer was obtained on a 300 MHz Varian Mercury Vx 300 NMR spectrometers.

The glass transition temperatures (T_g s) of materials were determined by a modulated differential scanning calorimeter (DSC, TA Instruments model 2920) at a heating rate of 5 °C/min under a nitrogen atmosphere.

Thermogravimetric analysis was conducted on a TGA (TA Instruments model 2050) at a heating rate of 5 °C/min under a nitrogen atmosphere.

Scanning electron microscopy (SEM) measurements were carried out on a JEOL 1530 equipped with a thermally assisted field emission gun operated at 10 KeV.

Parallel plate capacitors of the formulated high k composite materials were fabricated on a copper clad FR-4 board and copper top electrodes were coated by DC sputtering. The capacitance and dissipation factor of the capacitor were then measured with a HP 4263A LCR meter. The thickness of the dielectric films were in the range of 55 μm to 88 μm measured with a profilometer (Alpha-Step Co.) and used to calculate the dielectric constant of the sample. Electrical measurements were conducted at room temperature by the four-probe technique using a KEITHLEY 2000 Multimeter.

7.3 Results and Discussion

7.3.1 PANI/Epoxy Composites Prepared by Simple Solution Mixing Method

Initially, PANI-PTSA/epoxy composites were prepared by simple solution mixing method in cosolvent of PANI-PTSA and epoxy. Although macroscopic phase separation upon curing of the resin didn't occur and the film prepared by spin-coating remained transparent upon thermal curing, the agglomeration of PANI salt in the epoxy matrix could be observed in the SEM image as shown in Table 7-3. Figure 7-2 displays the dielectric properties of PANI-PTSA/epoxy composites with different PANI contents at 10 kHz. The dielectric constants of the blends remain at a low level due to the low concentrations of PANI-PTSA (less than 10 wt. %). Because of the limited solubility of the PANI-PTSA, more solvents are required to incorporate higher loading level of PANI-PTSA and this may cause more brittleness and poorer mechanical properties of the samples. As such, higher concentration of PANI-PTSA is difficult to achieve using this approach. An alternative method to prepare PANI/epoxy composites by an *in-situ* polymerization of aniline in the presence of epoxy resin was tried.

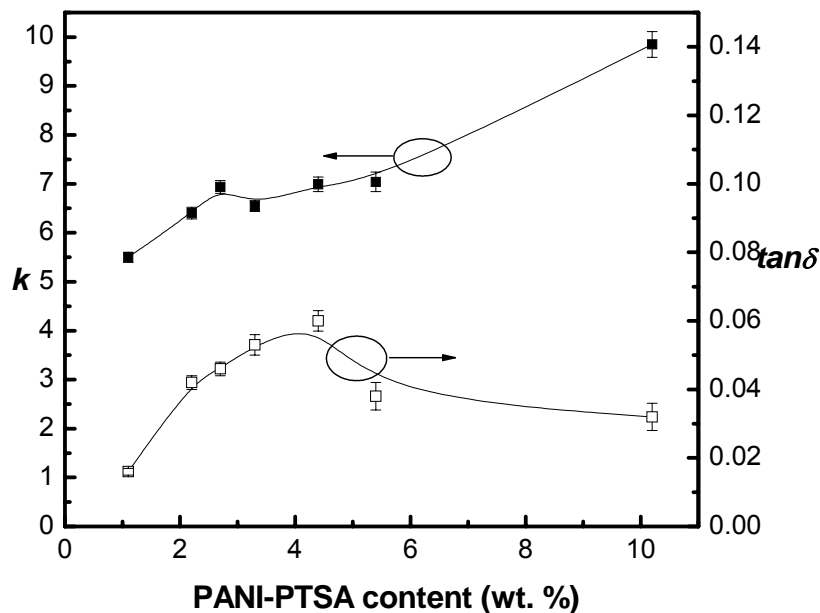


Figure 7-2. Dielectric properties of PANI-PTSA/epoxy composites with different PANI contents @ 10 kHz.

7.3.2 PANI/Epoxy Composites Prepared by an *In-situ* Polymerization Method

Preparation of PANI/epoxy composites by an *in-situ* polymerization method was carried out in two steps. Firstly, aniline salt monomer Ani-CSA was synthesized by aniline with protonating agent CSA, followed by the preparation of PANI/epoxy composites via an *in-situ* polymerization of Ani-CSA in the epoxy matrix.

7.3.2.1 Characterization of Aniline Salt Monomer

Figure 7-3 (a) shows FTIR spectrum of the Ani-CSA monomer. Aromatic C=C ring stretching observed at 1600 cm^{-1} and C-N stretching of benzenoid amine at 1509 cm^{-1} are consistent with the presence of the aniline ring. A peak at 1745 cm^{-1} is assigned to the C=O stretch of the carbonyl group in the camphor moiety. Peaks at 2640 cm^{-1} (N-H stretch), 1302 cm^{-1} and 1180 cm^{-1} (S=O symmetric stretch) are also consistent with the

presence of the secondary sulfonamide in the Ani-CSA monomer. These results confirm that CSA has been successfully attached to aniline.

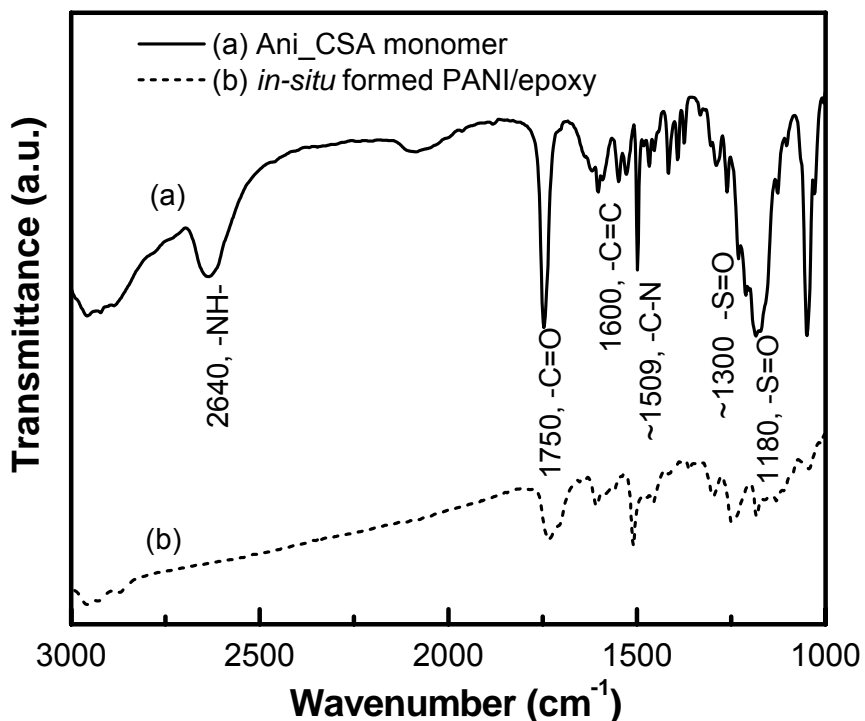


Figure 7-3. FT-IR spectra of (a) Ani-CSA monomer and (b) *in-situ* formed PANI/epoxy composite.

Figure 7-4 presents the ¹H NMR spectrum of the Ani-CSA in CDCl₃ which is found to be fully consistent with the proposed structure. The aryl proton is observed at 7.6-7.2 ppm, as expected for the presence of the aniline moiety. The integration of other hydrogen is also consistent with the structure as listed in Table 7-1. It is another strong evidence for the successful preparation of the Ani-CSA monomer.

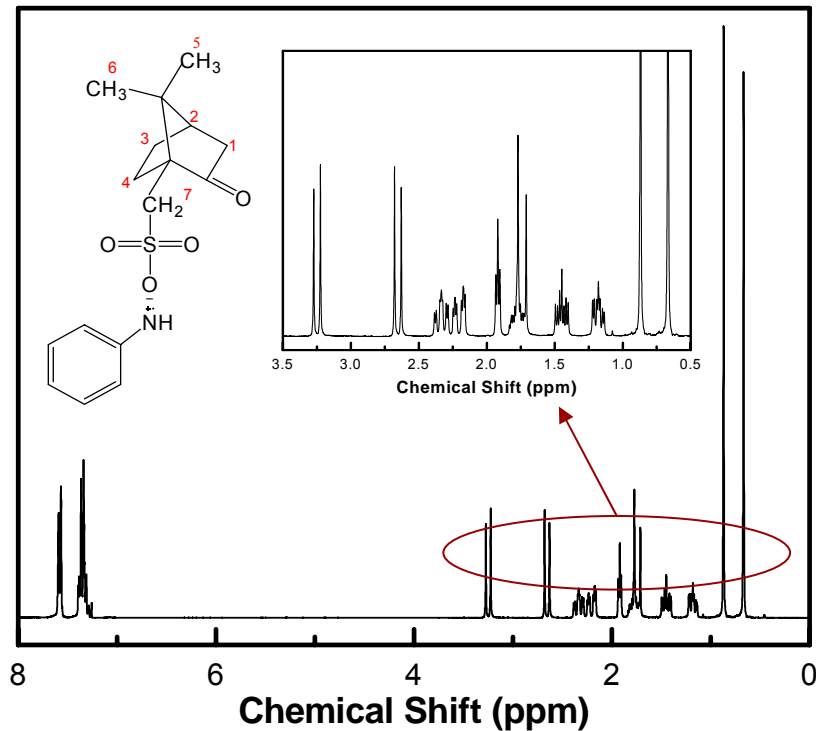


Figure 7-4. ^1H NMR spectrum of Ani-CSA monomer in CDCl_3 .

Table 7-1. ^1H NMR data for Ani-CSA monomer in CDCl_3 .

<i>Hydrogen</i>	<i>Chemical Shift (ppm)</i>	<i>Peak Multiplicity</i>	<i>Integration</i>
Aryl	7.6-7.2	m	5H
H^{10}	3.2, 2.65	dd	2H
H^5, H^6	2.35, 1.5	Overlapping m	4H
H^4	1.9	m	1H
H^3	1.8	dd	2H
Geminal CH_3	0.87, 0.68	s	6H

s = singlet, dd = doublet of doublets, m = multiplet

7.3.2.2 Characterization of *In-situ* Formed PANI/epoxy composites

The FT-IR result of the *in-situ* formed PANI/epoxy composite is displayed in Fig. 1(b). The peak at 2640 cm^{-1} attributed to N-H stretching is not visible in the spectra,

giving the evidence of the in-situ polymerization of PANI within the epoxy matrix. Peaks at 1750 cm^{-1} assigned to the C=O stretching of the carbonyl group in the camphor moiety and at $1180/1300\text{ cm}^{-1}$ due to S=O symmetric stretching can be observed, indicating that the CSA is still attached to the PANI within the epoxy matrix.

The UV-Vis spectrum of the green solution of an *in-situ* formed PANI/epoxy composite in dimethylsulfoxide (DMSO) is shown in Figure 7-5. An intense peak at ca. 330 nm is attributed to the transition from π band to π^* band, while the shoulder at ca. 435 nm is the typical transition between polaron band and π^* band which is generally observed for emeraldine salts. The broad absorption band at ca. 900 nm is assigned to the combination of transition from π band to polaron band and “free-carrier tail” which is resulted from the formation of delocalized polarons. The results indicate that the PANI remains its doped state and adopts a mixture of compact and expanded coil-like conformations in the composites.¹³⁹

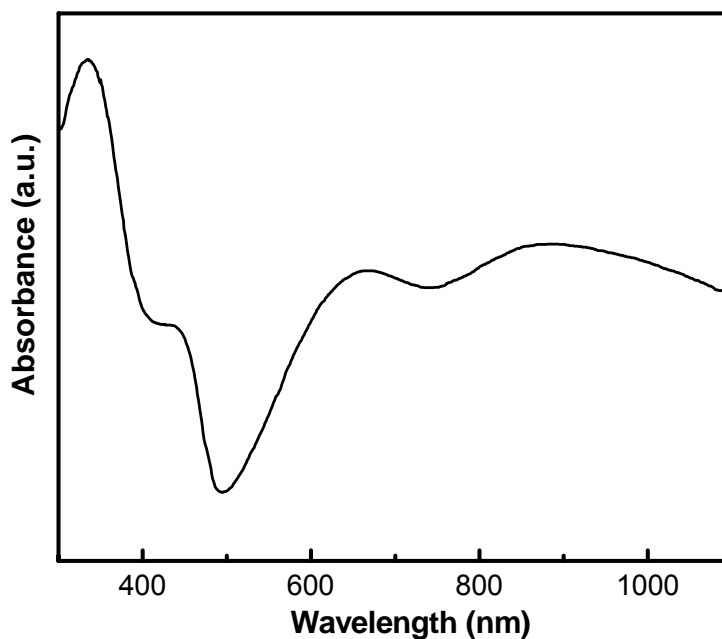


Figure 7-5. UV-Vis spectrum of an *in-situ* formed PANI/epoxy in DMSO.

The DSC thermograms of cured neat epoxy and *in-situ* formed PANI/epoxy composites with different PANI contents are shown in Figure 7-6. The T_g of the neat PANI is difficult to be detected by DSC. As compared to the neat epoxy, a slight decrease of T_g is observed for various *in-situ* PANI/epoxy composites with increasing PANI content, indicating that no obvious phase separation occurred in the composites.

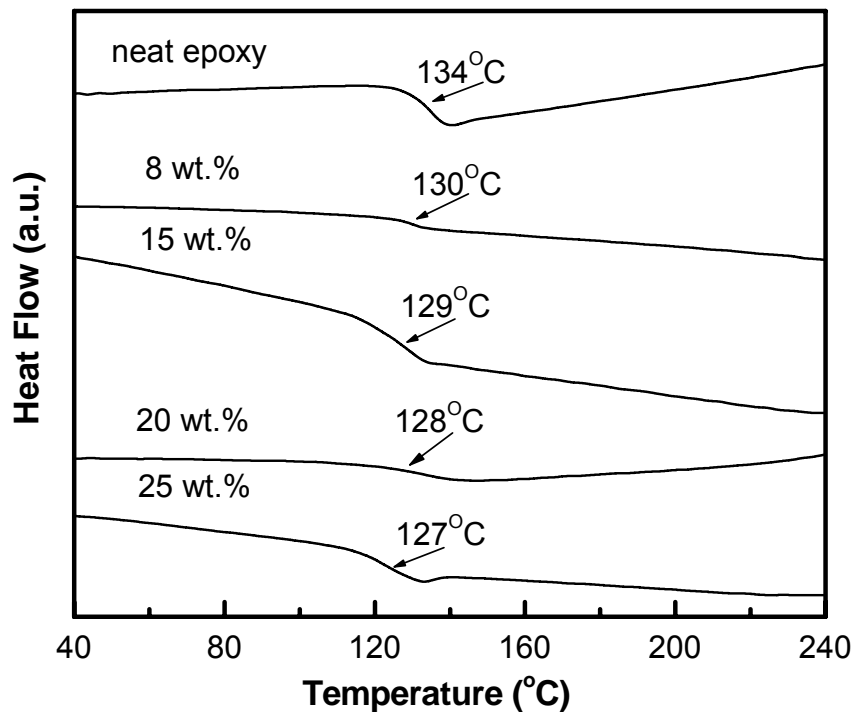


Figure 7-6. DSC curves of neat epoxy and *in-situ* formed PANI/epoxy composites with different PANI contents.

The thermal stability behavior of neat PANI and an *in-situ* formed PANI/epoxy with different PANI contents is shown in Figure 7-7. The TGA diagram of the neat PANI shows a certain weight loss below 200 °C, which is attributed to the loss of water and oligomers. The weight loss between 220 °C and 320 °C may correspond to the loss of the

bound CSA. This can explain the weight loss in the same temperature range for all the in-situ formed PANI/epoxy composites.

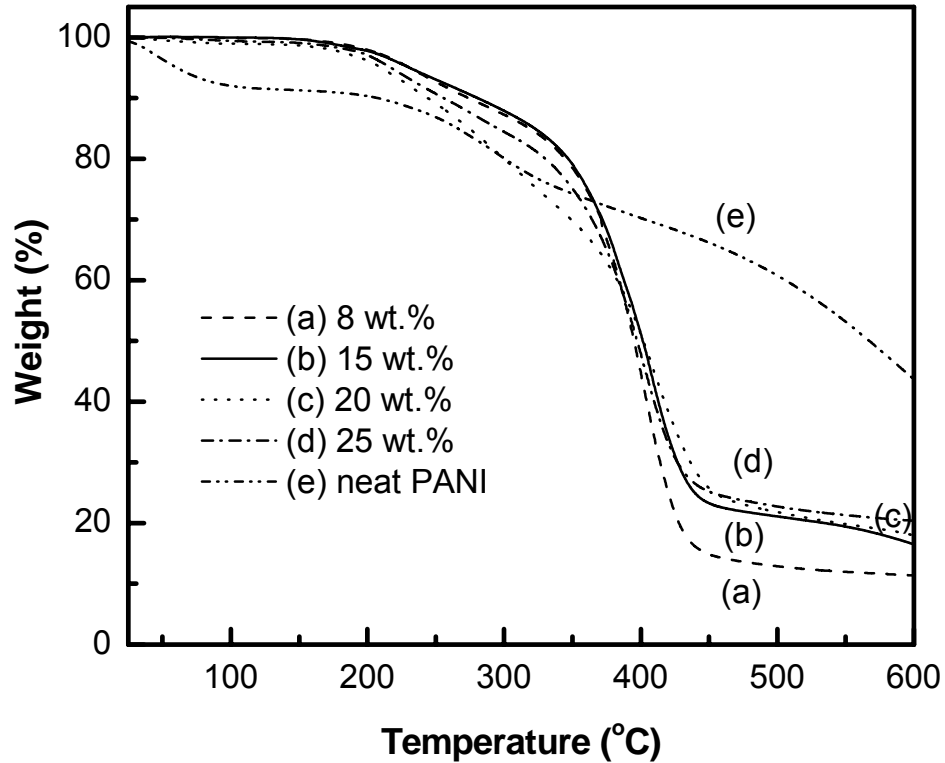


Figure 7-7. TGA diagrams of *in-situ* formed PANI/epoxy composites with different PANI contents and neat PANI.

7.3.3 Morphological Study of *In-situ* Formed PANI/epoxy Composites

Morphologies of the composites were observed by SEM. Figure 7-8 displays SEM micrographs of *in-situ* formed PANI/epoxy composites with different PANI contents. In contrast to the composites prepared by simple mixing in which the agglomeration of PANI occurred, no obvious phase separation is observed in the in-situ formed PANI/epoxy composites and this observation is consistent with the DSC results. The fracture surface of the PANI/epoxy composite with 8 wt. % PANI resembles that of a

typical neat epoxy fracture surface with a few different structures as conductive salt-rich regions.¹²³ The existence of the conductive salt clusters is more obvious in composites with higher concentrations of PANI. The morphological study suggested that the in-situ polymerization method to prepare the PANI/epoxy composites is useful to achieve good dispersion and high miscibility of PANI with the epoxy matrix.

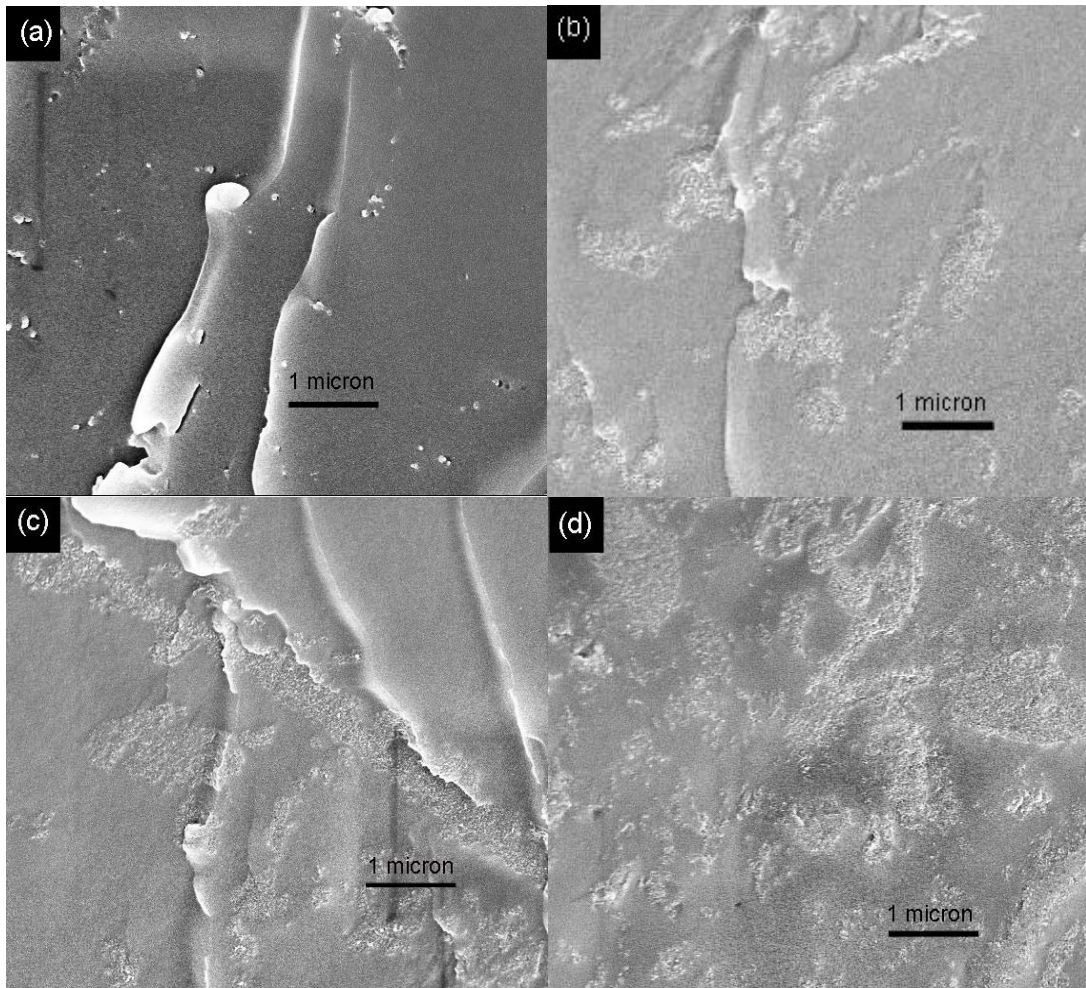


Figure 7-8. SEM micrographs of *in-situ* PANI/epoxy composites with (a) 8 wt. %, (b) 15 wt. %, (c) 20 wt. %, and (d) 25 wt. % PANI.

7.3.4 Dielectric and Electrical Property Study of *In-situ* Formed PANI/Epoxy Composites

Dielectric and electrical properties of in-situ formed PANI/epoxy composites with different PANI contents were studied on samples with parallel plate capacitor configuration. The electrical conductivity of the composite containing 25 wt. % PANI was $5 \times 10^{-6} \text{ S cm}^{-1}$. While the resistance of the other composites with lower contents of PANI was beyond the range of the equipment (over $10^7 \Omega$), demonstrating conductivity values below $10^{-7} \text{ S cm}^{-1}$. Compared to the values ranging from 10^{-10} to $10^{-3} \text{ S cm}^{-1}$ reported for other PANI/polymer composites, the conductivity values of these in-situ formed PANI/epoxy composites are reasonable as the conductive properties of these composites vary considerably resulting from the differences in PANI loading, doping state and level, molecular organization of the conductive clusters with respect to the polymer matrix and so on.

The values of k and dielectric loss tangent, $\tan \delta$, at 10 kHz are listed in Table 7-2. The k values increase significantly with the increase of PANI contents in the composites. As revealed from the data, the k value increases about 300-fold from ~ 10 with 8 wt. % PANI to ~ 2980 with 25 wt. % PANI. The enhancement of dielectric constant of the composites by PANI is related to interfacial polarization as well as the easy displacement of the electrons under electric fields through the highly highly conjugated structure which leads to a high dielectric response. While another polarization mechanism, electrode polarization arising from the accumulation of free charges at the blend/electrode interface, might also contribute to the high dielectric constant of the composite. An increase in composite conductance due to the incorporation of conductive polymer may enhance the

electrode polarization effect. The elimination of PANI agglomerates and the formation of a fine PANI network surrounded by epoxy matrix lead to enhanced dielectric properties of the composites. The relatively high dielectric loss tangent is due to the motion of free charge carriers and interfacial polarization relaxation attributed to the conductive salt clusters within the composites.

Table 7-2. Dielectric properties of *in-situ* formed PANI/epoxy composites with different PANI contents @ 10 kHz.

<i>PANI Content</i>	<i>8 wt. %</i>	<i>15 wt. %</i>	<i>20 wt. %</i>	<i>25 wt. %</i>
<i>k</i>	10	192	916	2980
<i>tanδ</i>	0.08	0.48	0.55	0.48

Morphological difference is obvious between the PANI/epoxy composites prepared by a simple solution mixing method and an *in-situ* polymerization method as shown in Table 7-3. Using an *in-situ* polymerization method, agglomerates surrounded by insulating matrix were eliminated. Homogeneous phase structure, instead of inhomogeneous phase segregated with PANI particulates, was achieved. And the formation of a fine network leads to better miscibility of PANI with epoxy matrix. Therefore, PANI content introduced into epoxy matrix was able to be effectively increased. Together with the decreased size of PANI particulates and thereby increased interfacial polarization effect, significantly enhanced *k* was observed in the PANI/epoxy composites prepared by an *in-situ* polymerization method. However, aggregation of PANI is still inevitable, which explained its higher dielectric loss tangent with respect to copolymer matrix.

Table 7-3. Comparison of the morphology of PANI/epoxy composites prepared by simple solution mixing method and *in-situ* polymerization method.

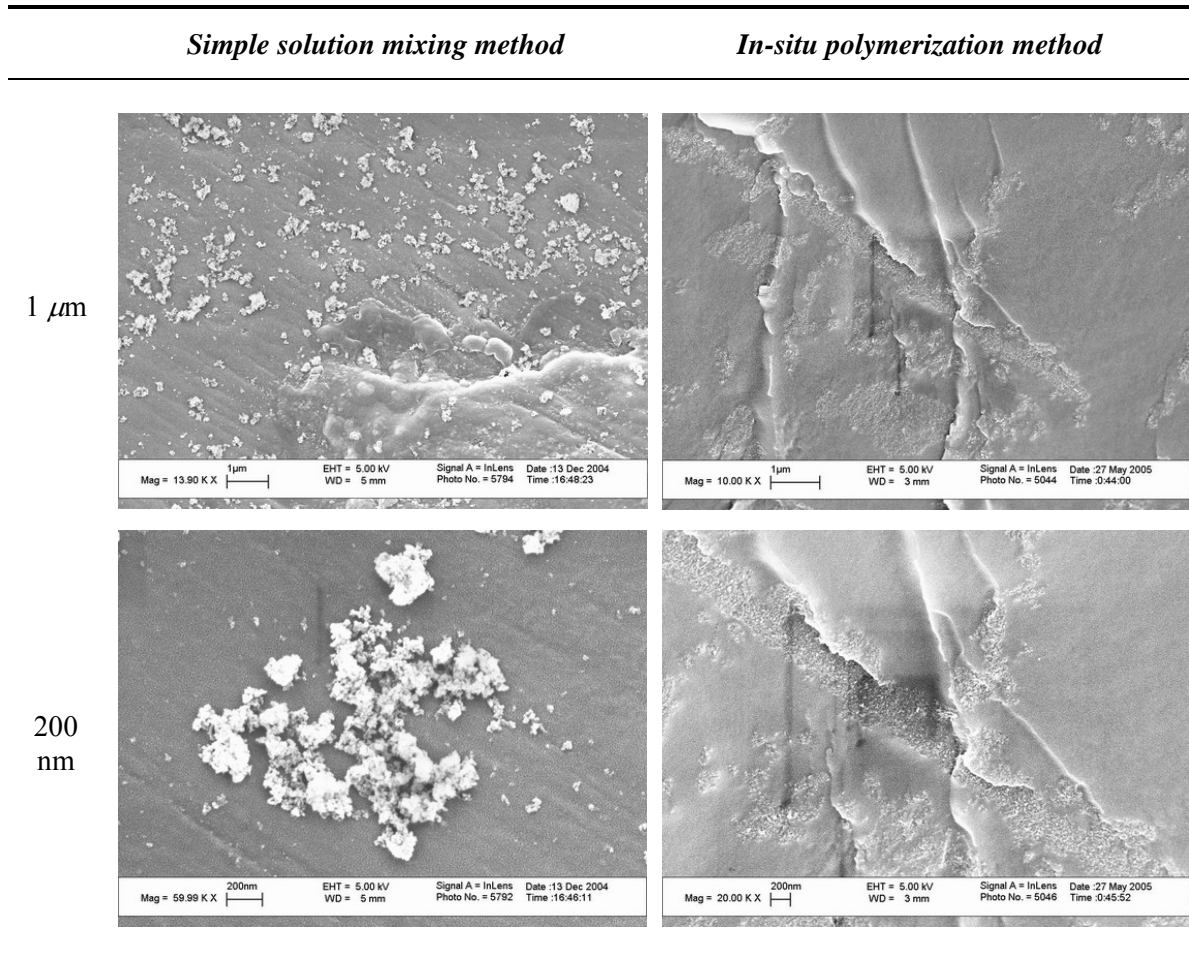


Figure 7-9 depicts the effect of the ac frequency on the values of k and $\tan\delta$ of *in-situ* formed PANI/epoxy composites with different PANI contents. It shows that the k values decrease with the AC frequency for all the composites, which is expected phenomenon as reported in other PANI/polymer composites.^{124,125,127} The results indicate that more PANI dipoles and charge carriers within the composites fail to keep up with the electric field of the increasing frequency. Another effect might contribute to this relaxation process is that the ac-conductivity exhibited at higher frequency will increase with frequency and thus decrease charge storing capability.¹²⁸ The composite containing

the largest amount of PANI showed the strongest frequency dependency of dielectric properties, which might be due to its highest conductivity. In Figure 7-9 (b) which shows the frequency dependence of dielectric loss tangent in the experimental frequency range, the peaks are possibly related to interfacial polarization relaxation effects, which correspond to the relaxation of k value as shown in Figure 7-9 (a).

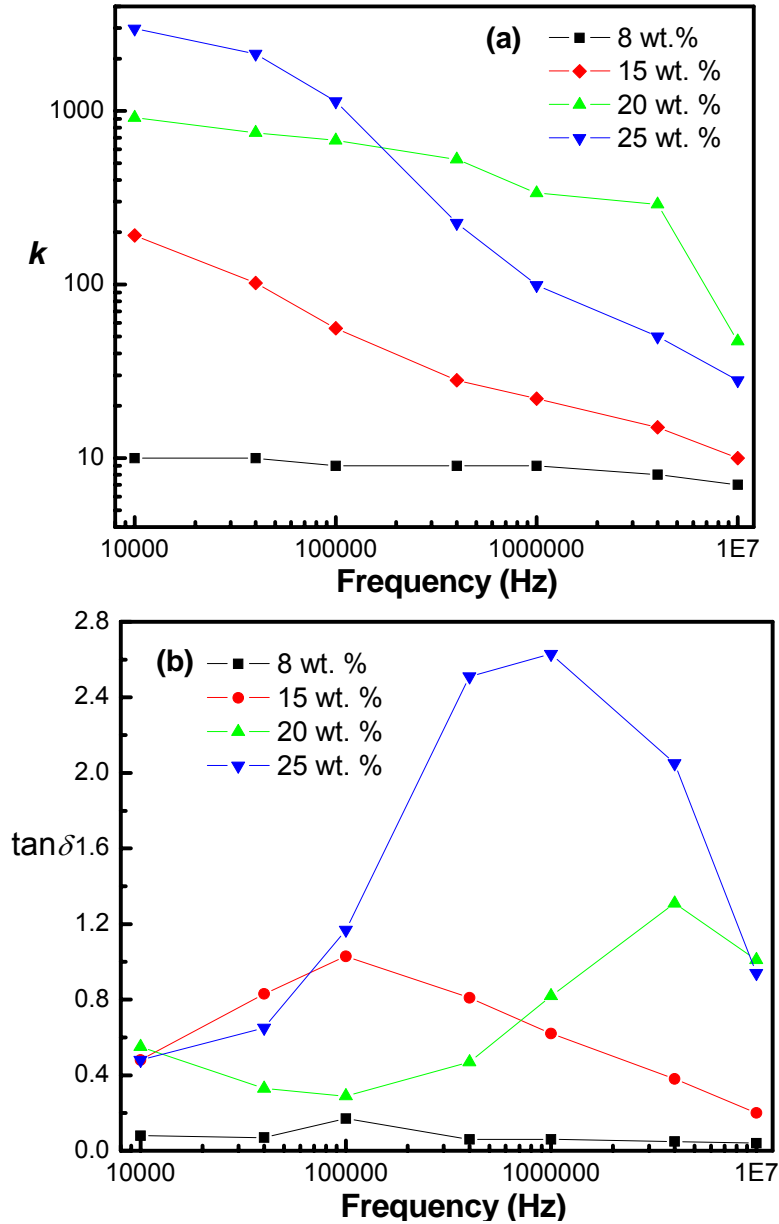


Figure 7-9. Frequency dependence of (a) k and (b) $\tan \delta$ of *in-situ* formed PANI/epoxy composites with different PANI contents.

The hardener type was also found as a critical parameter for the dielectric properties of PANI/epoxy composites. Table 7-4 lists the dielectric properties of in-situ formed PANI/epoxy composites with 15 wt. % PANI cured with different types of hardeners. The composites cured with alkaline type hardener (amine) showed a low dielectric constant, and this may be due to the dedoping effect of PANI salt by amine, which can react with the dopant of PANI and thus leads to the deprotonation of the conductive salt. The color change from green to blue by the addition of alkaline hardener was observed for the composites throughout the mixing procedure, suggesting that a conversion from a conductive PANI-CSA emeraldine salt to a nonconductive PANI emeraldine base occurred due to the basic character of the alkaline hardener. While using acidic type hardeners such as anhydride and amine complex, which retain the doping state of the PANI salt, led to a much higher dielectric constant. The results are consistent with the finding that the acidic curing agents support the conductive character of PANI, while alkaline hardeners conflict this property.¹⁴⁰

Table 7-4. Dielectric properties of 15 wt. % *in-situ* formed PANI/epoxy composites cured with various hardeners @ 10 kHz.

<i>Hardener</i>	<i>Anhydride</i>	<i>Amine</i>	<i>Amine Complex</i>
<i>k</i>	192	8.1	200
$\tan\delta$	0.48	0.03	0.39

7.4 Conclusions

The *in-situ* polymerization of an aniline salt within epoxy matrices was successful to prepare PANI/epoxy composites with various PANI contents. A PANI/epoxy composite prepared in this fashion exhibited a high dielectric constant close to 3000, a dielectric loss tangent less than 0.5 at 10 kHz and room temperature. The morphological study by SEM suggested that the *in-situ* polymerization method to prepare the PANI/epoxy composites was useful to achieve good dispersion and high compatibility of PANI with the epoxy matrix. The elimination of agglomerates surrounded by insulating matrix and the formation of a fine network led to enhanced dielectric properties of the composites. The hardener type was also found as a critical parameter for the dielectric properties of PANI/epoxy composites. Accordingly, the dielectric properties of the composites could be tailored by the doping level and the appropriate hardener selection.

CHAPTER 8

CONCLUSIONS AND SUGGESTED DIRECTIONS FOR FUTURE WORK

8.1 Conclusions

Materials design, development and processing of high dielectric constant nanocomposites for embedded capacitor applications are challenging for realization of the embedded passive technology. This work focuses on the study on the design, development and property evaluation of conductive filler/polymer nanocomposites as candidate material for this applicaiton. Metal nanoparticles with controlled parameters including size, size distribution, aggregation and surface properties were synthesized, and the impact of varied parameters on the dielectric properties of the high- k nanocomposites incorporated with these metal nanoparticles were investigated. The dielectric behavior of the nanocomposites was studied systematically over a range of frequencies to determine the dependence of dielectric constant, dielectric loss tangent and dielectric strength on these parameters.

Firstly, the Ag nanoparticles were *in-situ* formed in a polymer matrix and then incorporated into high- k composite materials. The size and size distribution of nanoparticles were controlled by the appropriate selection of capping agents and the ratio of capping agent to Ag precursor. The increased dielectric constant and decreased dissipation factor were observed by the incorporation of Ag nanocomposites. The increased dielectric constant is due to the piling of charges at the extended interface

which normally results in increased conductivity and higher loss. However, the reduced dielectric loss was observed in the high- k composite materials containing Ag nanoparticles, presumably in virtue of Coulomb blockade effect, the well-known quantum effect of nanoparticles, which reduces the electron tunneling. As such, it reduces the conduction loss part from the total dielectric loss of the high- k composite systems. The size, size distribution and a loading level of Ag nanoparticles in the nanocomposite have significant influence on the dielectric properties of the composite system and supply different effects at different frequency range as well.

In addition, an *in-situ* photochemical method was explored to prepare metal nanoparticle-polymer composite as high- k polymer matrix in which metal nanoparticles were generated by photochemical reduction of a metallic precursor within the polymer matrix. The high- k polymer matrix can be used to host various fillers such as conductive metal or ferroelectric ceramic fillers to achieve both high k and relatively low dielectric loss tangent. For example, the as-prepared Ag-epoxy nanocomposite was utilized as high- k polymer matrix to host fillers for preparation of Al/Ag-epoxy composites as embedded capacitor candidate materials. The dielectric constant values of the Al/Ag-epoxy composites increased remarkably as compared with those of Al/epoxy composite at the same Al filler loading by introduction of Ag elements in the polymer matrix. Moreover, the dielectric loss of the Al/Ag-epoxy composites was below 0.1, which meets the requirement for embedded decoupling capacitors. The results suggested that the metal-polymer nanocomposites via an *in-situ* photochemical method can be employed as a high- k polymer matrix to enhance the dielectric constant while maintaining the low dielectric loss of the high- k composites. The detailed dielectric property measurements

revealed that the concentration of silver nanoparticles in the polymer matrix play a significant role in determining the electrical conduction and breakdown behaviors as well as the frequency dependence of the dielectric composites. At low Ag concentration, the dielectric behaviors of Al/Ag-epoxy composites are mainly determined by interfacial polarization, while conduction and electron transport of Ag dominate the Al/Ag-epoxy composites at higher Ag concentration.

Surface modification of nanoparticles was employed with aims to change the surface chemistry and electrical state of nanoparticles and thereby tailor the dielectric and electrical properties of corresponding polymer nanocomposites. The surface coating layer coated on the nanoparticles via surface modification improves the performance of the metal nanoparticle/polymer composites by decreasing the dielectric loss, enhancing the dielectric breakdown strength. These performance improvements can be attributed to the interparticle electrical barrier layer formed via surface modification of nanoparticles which prevents the metal cores from direct contact, and/or the altered charge density and distribution around the interface of nanoparticles and polymer matrix. Surface modification of nanoparticles is believed to be an effective approach to adjust the electrical features at the nanoparticle surface and the interface between the nanoparticle and the polymer matrix, and thus tailor the corresponding properties of nanocomposites. It is also promising to achieve balanced dielectric properties of the nanocomposite by optimizing the degree of surface modification, the thickness and density of the coating layer on the nanoparticle surface. The experiments also provided information about different surface modification conditions such as surface modification agent type and

concentration, solvent media etc., which play complex roles in the quality and degree of the surface modification and allow for effective manipulation of the dielectric properties.

Apart from the size, size distribution and surface property effect, the effect of connectivity of the metal nanoparticles on the dielectric properties of the nanocomposites was investigated as well. The synthesis of the Ag nanoparticles with morphology of interest was achieved by adjusting the pH of the reaction, which was found to play an important role in assembling the nanoparticles. Using this approach, NaOH of different concentrations was applied to prepare Ag nanoparticles with varied degree of aggregation. The composites based on the as-synthesized Ag nanoparticles were prepared and the dielectric properties of these composites were investigated. The Ag/epoxy nanocomposites based on Ag nanoparticles capped with organic moiety showed very low dielectric loss tangent (<0.06). Assembly of the nanoparticles impacts the dielectric performance of the nanocomposite greatly in terms of the interfacial polarization and conducting properties. There is not much difference in the k values of the nanocomposite containing Ag nanoparticles with different degree of aggregation, while the nanocomposite containing Ag nanoparticle with more discrete structure rendered much lower dielectric loss tangent compared to the nanocomposites with Ag nanoparticles of more aggregated structure.

In addition to the metal conductive filler, the composites fabricated by dispersing an organic filler material possessing very high dielectric constant in a polymer matrix were found to exhibit high- k as well. The possibility of all-organic composites as candidate high- k material for embedded capacitor was investigated. The *in-situ* polymerization of an aniline salt within epoxy matrices was successful to prepare

PANI/epoxy composites with various PANI contents. A PANI/epoxy composite prepared in this fashion exhibited a high dielectric constant close to 3000, a dielectric loss tangent less than 0.5 at 10 kHz and at room temperature. The morphological study by SEM suggested that the in-situ polymerization method to prepare the PANI/epoxy composites was useful to achieve good dispersion and high compatibility of PANI with the epoxy matrix. The elimination of agglomerates surrounded by insulating matrix and the formation of a fine network led to enhanced dielectric properties of the composites. The hardener type was also found as a critical parameter for the dielectric properties of PANI/epoxy composites. Accordingly, the dielectric properties of the composites could be tailored by the doping level and the appropriate hardener selection.

In summary, the research explored various approaches to reduce the dielectric loss sufficiently while maintain the high k of the nanocomposites, and correlations were sought between the metal nanoparticles parameters including size, size distribution, aggregate extent, surface properties and the dielectric properties of nanocomposites with these metal nanoparticles incorporated. Study results suggest that the size and size distribution of metal nanoparticles in the nanocomposite have significant influence on the dielectric properties of the conductive filler/polymer composite systems and supply different effects at different frequency range as well. Smaller size and narrower size distribution of Ag nanoparticles result in lower dielectric loss tangent. Furthermore, Ag nanoparticles with more discrete morphology render much lower dielectric loss tangent compared to the nanocomposites with Ag nanoparticles of more aggregated morphology.

8.2 Suggested Directions for Future Work

This research work mostly focuses on the experimental trials to seek the relationship between the parameters of metal nanoparticles including size, size distribution, connectivity, surface properties and the dielectric properties of the nanocomposites with these metal nanoparticles incorporated. There are several topics of future work which may extend to improve the performance of high- k nanocomposites for embedded capacitor applications. To address the problems of the conductive filler/polymer nanocomposites as feasible candidate high- k materials, one may artificially passivate the metal nanoparticles to form core-shell structured nanofillers. With tailored thicknesses and characteristics of the shell layer, the dielectric constant, dielectric loss, and other electrical properties of the conductive filler/polymer nanocomposites can be adjusted.

8.2.1 Modeling of Structure and Dielectric Properties of High- k Materials

The dielectric characteristics of a composite material can be controlled by adjusting the material parameters of the individual phases. It is suggested to set up a numerical model that can precisely predict the dielectric properties of the high- k polymer nanocomposites and relate to the detailed structure and material parameters of the nanofiller including the geometry of particles, size of filler core and thickness of coating layer, permittivity and conductivity values of the individual phases, including core, shell, and polymer matrix. The modeling methodology will be of significance to serve to support the design, processing of the high- k nanocomposites in: (1) predicting the critical properties of the high- k nanocomposites such as dielectric constant, dielectric loss etc.; (2)

identifying and optimizing the parameters of nanofillers to enhance the dielectric properties of composites.

For a system of coated, spherical filler particles dispersed in a matrix, there are several models can be referred to study the bulk permittivity of a composite material. First one is the dipole model which assumes that the particles are sufficiently well separated that the electric potential in the neighbourhood of any one particle is not influenced by the presence of the others.¹⁴¹ Another one is the multipole model which accounts for perturbation of the electric potential in the vicinity of a particle due to its neighbours. This leads to greater accuracy in the result by taking interactions between the filler particles into consideration. Bowler reported a theoretical investigation on how factors such as particle shape, orientation with respect to the applied electric field, thickness of coating and permittivity value of the individual phases influences the bulk permittivity of the composite material by the multipole model in which the filler particles are replaced mathematically by electric multipole sources located at their centers.^{142,143}

Additionally, interaction zones, an interfacial layer of several tens nm surrounded the nanoparticles which play a significant role in properties of nanocomposites, should be taken into consideration.^{8,117} For instance, Li et al. constructed a dielectric nanocomposite as a three-phase material, consisting of a polymer matrix, an interfacial phase of fixed thickness, and nanoparticle fillers.

8.2.2 Core-shell Structure via Layer-by-Layer (LbL) Assembly

A multi-layer structure can be achieved by self-assembled polymer layers using layer-by-layer (LbL) colloid templating strategy.^{70,144} Electrostatic attraction between oppositely charged molecules can be a good driving force for multi-layer buildup. For

instance, polyanion-polycation LbL deposition process using the cyclic alternating adsorption of sodium salt of poly(styrene sulfonate) and poly(allyamine hydrochloride) is typical as schematically represented in Figure 8-1.¹⁴⁵

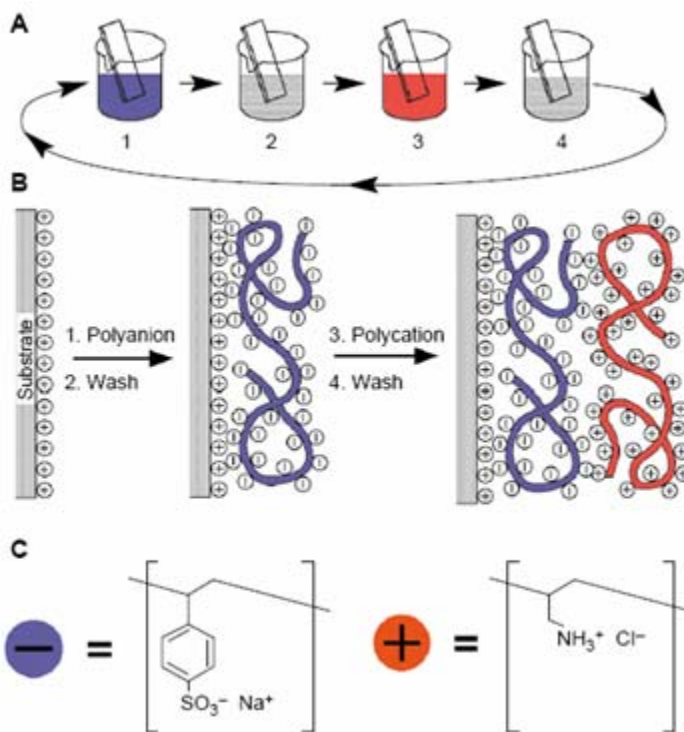


Figure 8-1. Schematic of the LbL film deposition process using two typical polyions, the sodium salt of poly(styrene sulfonate) and poly(allyamine hydrochloride).¹⁴⁵

LbL assembly possesses the advantages of simplicity, universality, thickness control in nanoscale, low cost and being environmentally friendly. Uniform multilayers can be formed by this approach on a number of 3D objects due to the conformal nature of the polyelectrolyte adsorption process besides the 2D surfaces. A frequently utilized method to create thin film coatings on colloidal particles is via LbL assembly of a polyelectrolyte preformed on an opposite surface charge. The buildup of polyelectrolyte multilayers on colloidal surfaces ranging in size from several micrometers down to

nanometers has been demonstrated.^{146,147,148} This approach provides a simple route to creating core-shell structures as schematically shown in Figure 8-2.

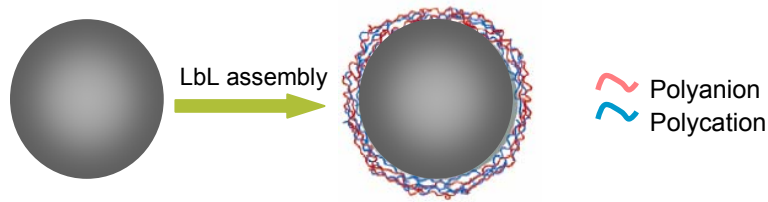


Figure 8-2. Schematic presentation of core-shell nanoparticle system formed via LbL assembly.

The chemical and physical properties like film thickness, degree of interpenetration between layers of PEMs are particularly sensitive to the pH and the concentration of the supporting polyelectrolyte solution during LbL multilayer assembly.^{149, 150, 151} Using this approach, the thickness of coating layer could be manipulated and optimized to tailor the dielectric properties of the high- k nanocomposites according to desired core-shell structure of fillers suggested by modeling work.

On the other hand, composite films can also be constructed by assembling multi-layer films of prefabricated nanoparticles and other inorganic materials with polyelectrolytes using LbL deposition. Several groups synthesized dendrimer-,^{152,153} citrate,^{154,155} or polyelectrolyte-stabilized¹⁵⁶ gold/platinum nanoparticles and then formed colloid/polyelectrolyte films by alternating adsorption of these properly charged and stabilized colloids and polymeric electrolytes. Furthermore, with *in-situ* synthesis methodology, both the concentration and size of the nanoparticles would be possible to be varied by manipulating the multi-layer processing conditions.^{157, 158} Smaller nanoparticles could be obtained at higher pHs during multi-layer assembly process and lower concentration of bould silver cations. Cyclic repetition of the ion exchange and

reduction of silver cations to zerovalent Ag nanoparticles can increase metal concentration in the film.¹⁵⁷ These approaches may provide more versatility of the coating layer characteristics and thereby find an efficient way to enhance the dielectric performance of the high- k nanocomposites by incorporation of nanofiller with appropriate structure and property.

Appendix A

AUTHOR'S AWARDS, PATENTS, AND PUBLICATIONS

A.1 Awards

- [1] Intel Best Student Paper Award for paper titled “Tailored Dielectric Properties of High-k Polymer Composites via Nanoparticle Surface Modification for Embedded Passives Applications” at the 57th Electronic Component & Technology Conference (ECTC), IEEE Components, packaging & Manufacturing Technology (CPMT) Society and Intel Inc., 2007.
- [2] Finalist for the 15th Motorola-IEEE/CPMT Fellowship at the 57th Electronic Component & Technology Conference (ECTC), IEEE Components, packaging & Manufacturing Technology (CPMT) Society and Motorola Inc., 2007.
- [3] Research Initiation Award, School of Materials Science & Engineering, Georgia Institute of Technology, 2006.

A.2 Publications

1. Journal papers

- [1] J. Lu, C. P. Wong, “Nano-scale Particle Surface Modification for Tailoring Dielectric Properties of Polymer Nanocomposites”, Chemistry of Materials, submitted, 2008.
- [2] J. Lu, K. S. Moon, C. P. Wong, “Silver/Polymer Nanocomposites as High-k Polymer Matrix for Dielectric Composites with Improved Dielectric Performance”, Journal of Materials Chemistry, DOI: 10.1039/B807566B, 2008.
- [3] Y. Sun, L. Zhu, H. Jiang, J. Lu, W. Wang, and C.P.Wong, “A Paradigm of Carbon Nanotube Interconnects in Microelectronic Packaging”, Journal of Electronic Material, DOI: 10.1007/s11664-008-0533-1, 2008.
- [4] J. Lu, C.P. Wong, “Recent Advances in High-k Composite Materials for Embedded Capacitor Applications”, IEEE Transactions on Dielectrics and Electrical Insulation, accepted, 2008.

- [5] J. Lu, K. S. Moon, B.-K. Kim, C. P. Wong, "High Dielectric Constant Polyaniline/epoxy Composites via In-situ Polymerization for Embedded Capacitor Applications", *Polymer*, 48 (6), 1510-1516, 2007.
- [6] J. Lu, K. S. Moon, J. Xu and C. P. Wong, "Synthesis and dielectric properties of novel high-K polymer composites containing *in-situ* formed silver nanoparticles for embedded capacitor applications", *Journal of Materials Chemistry*, 16 (16), 1543-1548, 2006.
- [7] J. Lu, K. S. Moon, J. Xu and C. P. Wong, "Novel High-K Polymer Composites with *in-situ* Formed Silver Nanoparticles for Embedded Capacitor Applications", *PMSE Preprints*, 94, 871-872, 2006.
- [8] H. Jiang, K. S. Moon, J. Lu and C.P. Wong, "Conductivity Enhancement of Nano Silver-Filled Conductive Adhesives by Particle Surface Functionalization", *Journal of Electronic Materials*, 34 (11), pp. 1432-1439, 2005.

2. Proceeding papers

- [1] C. P. Wong, W. Lin, H. Jiang, R. Zhang, Q. Liang, J. Lu, Y. Xiu, K. Moon, O. Hildreth, "Nano Materials for Microelectronic and Photonic Packaging", the 10th Electronics Packaging Technology Conference (EPTC 2008), Singapore, December 9-12, 2008.
- [2] J. Lu, C. P. Wong, "Polymer Nanocomposites with High Dielectric Strength and High Frequency Performance for Embedded Passive Applications", the 7th IEEE Conference on Polymers & Adhesives in Microelectronics & Photonics (Polytronic 2008), Garmisch-Partenkirchen, Germany, August 17-20, 2008.
- [3] J. Lu, C. P. Wong, "Dielectric Performance Enhancement of Nanoparticle-Based Materials for Embedded Passive Applications", *IEEE Proceedings of the 58th Electronic Components & Technology Conference*, pp. 736-741, 2008.
- [4] J. Lu, K. S. Moon, C. P. Wong, "High-k Polymer Nanocomposites for Gate Dielectric Applications", *Proceedings of the 12th International Symposium on Advanced Packaging Materials: Processes, Properties and Interfaces*, San Jose/Silicon Valley, CA, Oct. 3-5, 2007.
- [5] J. Lu and C. P. Wong, "Tailored Dielectric Properties of High-*k* Polymer Composites via Nanoparticle Surface Modification for Embedded Passives Applications", *IEEE*

- Proceedings of the 57th Electronic Components and Technology Conference, pp.1033-1039, 2007.
- [6] J. Lu, K. S. Moon and C. P. Wong, "High-*k* Polymer Nanocomposites as Gate Dielectrics for Organic Electronics Applications", IEEE Proceedings of the 57th Electronic Components and Technology Conference, pp. 453-457, 2007.
- [7] J. Lu, K. S. Moon and C. P. Wong, "Development of Novel Silver Nanoparticles/Polymer Composites as High K Polymer Matrix by In-situ Photochemical Method", IEEE Proceedings of the 56th Electronic Components and Technology Conference, San Diego, CA, pp. 1841-1846, 2006.
- [8] J. Xu, S. Bhattacharya, K. S. Moon, J. Lu, B. Englert, P. Pramanik, "Large-Area Processable High-*k* Nanocomposite-Based Embedded Capacitors", IEEE Proceedings of the 56th Electronic Components and Technology Conference, San Diego, CA, pp. 1520-1532, 2006.
- [9] J. Lu, K. S. Moon and C. P. Wong, "In-situ Photochemical Synthesis of Novel Silver Nanoparticles-Polymer Composites as High K Polymer Matrix for Embedded Passives Applications", Proceedings of 11th International Symposium on Advanced Packaging Materials, pp.184-188, 2006.
- [10] J. Lu, K. S. Moon and C. P. Wong, "Novel All Organic High Dielectric Constant Polyaniline/epoxy Composites for Embedded Capacitor Applications", Proceedings of 11th International Symposium on Advanced Packaging Materials, pp. 88-92, 2006.
- [11] J. Lu, K. S. Moon, J. Xu and C. P. Wong, "Novel High-K Polymer Composites with *in-situ* Formed Silver Nanoparticles for Embedded Capacitor Applications", 231st American Chemical Society Meeting, Atlanta, GA, March 26-30, 2006.
- [12] J. Lu, K. S. Moon, J. Xu and C. P. Wong, "Development of novel silver nanoparticles/polymer composites by in-situ photochemical method for embedded capacitor applications", 231st American Chemical Society Meeting, Atlanta, GA, March 26-30, 2006.
- [13] J. Lu, K. S. Moon, J. Xu, and C. P. Wong, "All organic high dielectric constant polyaniline/epoxy composites for embedded capacitor applications", 231st American Chemical Society Meeting, Atlanta, GA, March 26-30, 2006.

- [14] J. Lu, K. S. Moon, J. Xu and C. P. Wong, "Dielectric Loss Control of High-K Polymer Composites by Coulomb Blockade Effects of Metal Nanoparticles for Embedded Capacitor Applications", Proceedings of 10th International Symposium on Advanced Packaging Materials, Irvine, CA, March 16-18, 2005.
- [15] H. Jiang, K. S. Moon, L. Zhu, J. Lu and C. P. Wong, "The Role of Self-Assembled Monolayer (SAM) on Ag Nanoparticles for Conductive Nanocomposite", Proceedings of 10th International Symposium on Advanced Packaging Materials, Irvine, CA, March 16-18, 2005.
- [16] C. P. Wong, J. Xu, L. Zhu, Y. Li, H. Jiang, Y. Sun, J. Lu, H. Dong, "Recent Advances on Polymers and Polymer Nanocomposites for Advanced Electronic Packaging Applications", the 7th International IEEE Symposium on High Density Packaging and Component Failure Analysis in Electronics Manufacturing (HDP'05), Shanghai, China, June 27-30, 2005.
- [17] J. Xu, F. Xiao, J. Lu, C.P Wong, "Study of Core-Shell Structured Nanoparticles for High-k Embedded Capacitor Dielectrics", 2nd International Workshop in Nano Bio-Packaging, Atlanta, GA, March 2005.

3. Book Chapter

- [1] J. Lu, and C. P. Wong, "Nanoparticle-based High-k Dielectric Composites: Opportunities and Challenges", Nanopackaging: Nanotechnologies and Electronics Packaging, Ed. J. Morris, D. Mallik, Springer-Verlag New York Inc., 2008.
- [2] J. Lu, and C. P. Wong, "High-k Dielectric Materials for Embedded Capacitor Applications", Materials for Advanced Packaging, Ed. D. Lu, C. P. Wong, Springer-Verlag New York Inc., 2009.

REFERENCES

- ¹ R. R. Tummala, E. J. Rymaszewski, A. G. Klopfenstein, "Microelectronics Packaging Handbook", 2nd Edition, Massachusetts: Kluwer Academic Publishers, 1999.
- ² W. T. Chen, A. Tseng, "Overview of recent developments in microelectronic packaging", International Symposium on Electronic Materials and Packaging, pp. 15-16, 2001.
- ³ J. H. Lau, "Chip on Board Technologies for Multichip Modules", New York: Van Nostrand Reinhold, 1994.
- ⁴ J. Prymark, S. Bhattacharya, K. Paik, R. R. Tummala Ed., "Fundamentals of Microsystems Packaging", New York: McGraw-Hill, 2001.
- ⁵ R. K. Ulrich, W. D. Brown, "Advanced Electronic Packaging", 2nd Edition, New Jersey: IEEE Press, 2006.
- ⁶ R. K. Ulrich, L.W. Schaper, "Integrated Passive Component Technology", Hoboken, NJ: IEEE Press, Wiley-Interscience, 2003.
- ⁷ A. R. Blythe, "Electrical Properties of Polymers", Cambridge: Cambridge University Press, 1979.
- ⁸ J. Y. Li, L. Zhang, S. Ducharme, "Electric energy density of dielectric nanocomposites", Applied Physics Letters, Vol. 90, pp. 132901, 2007.
- ⁹ A. Dey, S. K. De, "Large dielectric constant in zirconia polypyrrole hybrid nanocomposites," Journal of Nanoscience and Nanotechnology, Vol. 7, pp. 2010-2015, 2007.
- ¹⁰ G. L. Johnson, "Solid State Tesla Coil", Ch.3 Lossy Capacitors, 2001, available at www.eece.ksu.edu/~gjohnson/.
- ¹¹ O. E. Gouda, A. M. Thabet, H. H. El-Tamaly, "How to get low dielectric losses in binary and multi-mixtures dielectrics at high frequency", 39th International Universities Power Engineering Conference, Vol. 3, pp.1237-1240, 2004.
- ¹² J. P. Shaffer, A. Saxena, S. D. Antolovich, T. H. J. Sanders, and S. B. Warner, "The Science and Design of Engineering Materials", Boston: McGraw-Hill, 1999.

-
- ¹³ N. Tohge, S. Takahashi, and T. Minami, "Preparation of PbZrO₃-PbTiO₃ ferroelectric thin films by the sol-gel process", *Journal of American Ceramic Society*, Vol 74 (1), pp. 67-71, 1991.
- ¹⁴ C. Pecharroman, F. Esteban-Betegon, J. F. Bartolome, S. Lopez-Esteban, J. S. Moya, "New percolative BaTiO₃-Ni composites with a high and frequency-independent dielectric constant (epsilon(r) approximate to 80,000)," *Advanced Materials*, Vol. 13, pp. 1541-1544, 2001.
- ¹⁵ C. Pecharroman, J. S. Moya, "Experimental evidence of a giant capacitance in insulator-conductor composites at the percolation threshold", *Advanced Materials*, Vol. 12, pp. 294-297, 2000.
- ¹⁶ M. A. Subramanian, D. Li, N. Duan, B. A. Reisner, A. W. Sleight, "High Dielectric Constant in ACu₃Ti₄O₁₂ and ACu₃Ti₃FeO₁₂ Phases", *Journal of Solid State Chemistry*, Vol. 151, pp. 323-325, 2000.
- ¹⁷ L. He, J. B. Neaton, M. H. Choen, D. Vanderbilt, C. C. Homes, "First-principles study of the structure and lattice dielectric response of CaCu₃Ti₄O₁₂", *Physical Review B*, Vol. 65, pp. 214112, 2002.
- ¹⁸ J. Lia, A. W. Sleight, M. A. Subramanian, "Evidence for internal resistive barriers in a crystal of the giant dielectric constant material: CaCu₃Ti₄O₁₂", *Solid State Communications*, Vol. 135, pp. 260-262, 2005.
- ¹⁹ Y. Lin, L. jiang, R. Zhao, C.-W. Nan, "High-permittivity core/shell structured NiO-based ceramics and their dielectric response mechanism", *Physical Review B*, Vol. 72, pp. 0.14103, 2005.
- ²⁰ Y. Rao, C. P. Wong, "Material characterization of a high-dielectric-constant polymer-ceramic composite for embedded capacitor for RF applications," *Journal of Applied Polymer Science*, Vol. 92, pp. 2228-2231, 2004.
- ²¹ H. S. Nalwa, "Ferroelectric Polymers", New York: Marcel Dekker, 1995.
- ²² S. Yano, "Dielectric relaxation and molecular motion in poly(vinylidene fluoride)", *Journal of Polymer Science Part A-2: Polymer Physics*, Vol. 8, pp. 1057-1072, 1970.
- ²³ H. Kakutani, "Dielectric absorption in oriented poly(vinylidene fluoride)", *Journal of Polymer Science Part A-2: Polymer Physics*, Vol. 8, pp. 1177-1186, 1970.
- ²⁴ Q. M. Zhang, V. Bharti, X. Zhao, "Giant electrostriction and relaxor ferroelectric behavior in electron-irradiated poly(vinylidene fluoride-trifluoroethylene) copolymer", *Science*, Vol. 280, pp. 2101-2104, 1998.

-
- ²⁵ T. C. Chung, A. Petchsuk, "Synthesis and properties of ferroelectric fluoroterpolymers with Curie transition at ambient temperature," *Macromolecules*, Vol. 35, pp. 7678-7684, 2002.
- ²⁶ Z. Yu, C. Ang, L. E. Cross, A. Petchsuk, T. C. Chung, "Dielectric and electroactive strain properties of poly(vinylidene fluoride-trifluoroethylene-chlorotrifluoroethylene) terpolymers," *Applied Physics Letters*, Vol. 84, pp. 1737-1739, 2004.
- ²⁷ J. Joo, S. M. Long, J. P. Pouget, E. J. Oh, A. G. macDiarmid, A. J. Epstein, "Charge transport of the mesoscopic metallic state in partially crystalline polyanilines," *Physical Review B*, Vol. 57, pp. 9567-9579, 1998.
- ²⁸ R. Gregorio, M. Cestari, F. E. Bernardino, "Dielectric behavior of thin films of beta-PVDF/PZT and beta-PVDF/BaTiO₃ composites", *Journal of Materials Science*, Vol. 31, pp. 2925-2930, 1996.
- ²⁹ Y. Bai, Z. Y. Cheng, V. Bharti, H. S. Xu, Q. M. Zhang, "High-dielectric-constant ceramic-powder polymer composites", *Applied Physics Letters*, Vol. 76, pp. 3804-3806, 2000.
- ³⁰ K. Mazur, "Polymer-Ferroelectric Ceramic Composites in Ferroelectric Polymers: Chemistry, Physics, and Applications", H.S. Nalwa Ed., New York: Marcel Dekker Inc., 1995.
- ³¹ D. K. Dasgupta, K. Doughty, "Polymer-ceramic composite materials with high dielectric constants", *Thin Solid Films*, Vol. 158, pp. 93-105, 1988.
- ³² S. Liang, S. Chong, E. Giannelis, "Barium titanate/epoxy composite dielectric materials for integrated thin film capacitors", *Proceedings of 48th Electronic Components and Technology Conference*, pp. 171-175, 1998.
- ³³ H. Windlass, P. M. Raj, D. Balaraman, S. K. Bhattacharya, R. R. Tummala, "Processing of polymer-ceramic nanocomposites for system-on-package applications", *Proceedings of the 51st Electronic Components and Technology Conference*, pp. 1201-1206, 2001.
- ³⁴ Y. Rao, S. Ogitani, P. Kohl, C. P. Wong, "Novel polymer-ceramic nanocomposite based on high dielectric constant epoxy formula for embedded capacitor application", *Journal of Applied Polymer Science*, Vol. 83, pp. 1084-1090, 2002.
- ³⁵ Z. M. Dang, Y. H. Lin, C. W. Nan, "Novel ferroelectric polymer composites with high dielectric constants", *Advanced Materials*, Vol. 15, pp. 1625-1629, 2003.

-
- ³⁶ S. D. Cho, J. Y. Lee, J. G. Hyun, K. W. Paik, "Study on epoxy/BaTiO₃ composite embedded capacitor films (ECFs) for organic substrate applications", *Materials Science and Engineering B*, Vol. 110 (3), pp. 233–239, 2004.
- ³⁷ R. Popielarz, C. K. Chiang, R. Nozaki, J. Obrzut, "Dielectric properties of polymer/ferroelectric ceramic composites from 100 Hz to 10 GHz", *Macromolecules*, Vol. 34, pp. 5910-5915, 2001.
- ³⁸ M. Arbatti, X. B. Shan, Z. Y. Cheng, "Ceramic-polymer composites with high dielectric constant," *Advanced Materials*, Vol. 19, pp. 1369-1372, 2007.
- ³⁹ P. Kim, S. C. Jones, P. J. Hotchkiss, J. N. Haddock, B. Kippelen, S. R. Marder, J. W. Perry, "Phosphonic acid-modified barium titanate polymer nanocomposites with high permittivity and dielectric strength," *Advanced Materials*, Vol. 19, pp. 1001-1005, 2007.
- ⁴⁰ Y. Rao, C. P. Wong, J. Xu, "Ultra high k polymer metal composite for embedded capacitor application", US Patent 6864306, 2005.
- ⁴¹ J. Xu, C. P. Wong, "Low loss percolative dielectric composite", *Applied Physics Letters*, Vol. 87, pp. 082907, 2005.
- ⁴² Z. M. Dang, Y. Shen, C. W. Nan, "Dielectric behavior of three-phase percolative Ni-BaTiO₃/Polyvinylidene fluoride composites", *Applied Physics Letters*, Vol. 81, pp. 4814-4816, 2002.
- ⁴³ H. W. Choi, Y. W. Heo, J. H. Lee, J. J. Kim, H. Y. Lee, E. T. Park, Y. K. Chung, "Effects of BaTiO₃ on dielectric behavior of BaTiO₃-Ni-polymethylmethacrylate composites", *Applied Physics Letters*, Vol. 89, pp. 132910, 2006.
- ⁴⁴ P. M. Raj, D. Bahaman, V. Govind, L. Wan, R. Abothu, R. Gerhardt, S. Bhattacharya, M. Swaminathan, R. Tununala, "High frequency characteristics of nanocomposite thin film 'Supercapacitors' and their suitability for embedded decoupling", *Proceedings of the 54th IEEE Electronic Components and Technology Conference*, Las Vegas, NV, pp.154-161, 2004.
- ⁴⁵ J. Xu, C. P. Wong, "Super high dielectric constant carbon black-filled polymer composites as integral capacitor dielectrics", *Proceedings of the 54th IEEE Electronic Components and Technology Conference*, Las Vegas, NV, pp. 536-541, 2004.

-
- ⁴⁶ H. Xu, Z. Dang, M. Jiang, S. Yao, J. Bai, “Enhanced dielectric properties and positive temperature coefficient effect in the binary polymer composites with surface modified carbon black”, *Journal of Materials Chemistry*, Vol. 18, pp. 229-234, 2008.
- ⁴⁷ L. Qi, B. I. Lee, S. Chen, W. D. Samuels, G. J. Exarhos, “High-dielectric-constant silver-epoxy composites as embedded dielectrics”, *Advanced Materials*, Vol. 17, pp.1777-1781, 2005.
- ⁴⁸ Y. Shen, Y. Lin, M. Li, C.-W. Nan, “High Dielectric performance of polymer composite films induced by a percolating interparticle barrier layer”, *Advanced Materials*, Vol. 19, pp. 1418-1422, 2007.
- ⁴⁹ Q. M. Zhang, H. F. Li, M. Poh, F. Xia, Z. Y. Cheng, H. S. Xu, C. Huang, “An all-organic composite actuator material with a high dielectric constant”, *Nature*, Vol. 419, pp. 284-287, 2002.
- ⁵⁰ J. Wang, Q. Shen, C. Yang, Q. Zhang, “High dielectric constant composite of P(VDF-TrFE) with grafted copper phthalocyanine oligmer”, *Macromolecules*, Vol. 37, pp. 2294-2298, 2004.
- ⁵¹ C. Huang, Q. M. Zhang, J. Su, “High dielectric constant all polymer percolative composites”, *Appl. Phys. Lett.*, Vol. 82, pp. 3502-3504, 2003.
- ⁵² P. M. Ajayan, L. S. Schadler, P. V. Braun, “Nanocomposite Science and Technology”, Weinheim: Wiley-VCH, 2003.
- ⁵³ I. Capek, “Nanocomposite Structure and Dispersion: Science and Nanotechnology-Fundamental Principles and Colloidal Particles”, Amsterdam, the Netherlands: Elsevier, 2006.
- ⁵⁴ D. Gerion, W. J. parak, S. C. Williams, D. Zanchet, C. M. Micheel, A. P. Alivisatos, “Sorting fluorescent nanocrystals with DNA”, *Journal of the American Chemical Society*, Vol. 124, 7070-7074, 2002.
- ⁵⁵ S. Stankovich, D. A. Dikin, G. H. B. Dommett, K. M. Kohlhaas, E. J. Zimney, E. A. Stach, R. D. Piner, S. T. Nguyen, R. S. Ruoff, “Graphene-based composite materials”, *Nature*, Vol. 442, pp. 282-286, 2006.
- ⁵⁶ M. Sumita, Y. Tsukumo, K. Miyasaka, K. Ishikawa, “Tensile yield stress of polypropylene composites filled with ultrafine particles”, *Journal of Materials Science*, Vol.18, pp.1758-1764, 1983.

-
- ⁵⁷ J. I. Hong, K. S. Cho, C. I. Chung, L. S. Schadler, R. W. Siegel, "Retarded cross-linking in ZnO-low-density polyethylene nanocomposites", *Journal of Materials Research*, Vol.17 (5), pp.940-943, 2002.
- ⁵⁸ E. Petrovicova, R. Knight, L. S. Schadler, T. Twardowski, "Nylon 11/silica nanocomposite coatings applied by the HVOF process: I. microstructure and morphology", *Journal of Applied Polymer Science*, Vol. 77, pp. 1684-1699, 2000.
- ⁵⁹ F. Yang, Y. Ou, Z. Yu, "Polyamide 6/silica nanocomposites prepared by in situ polymerization", *Journal of Applied Polymer Science*, Vol. 69, pp. 355-361, 1998.
- ⁶⁰ Y. Zhang, G. Zhou., Y. Zhang, L. Li, L. Yao, C. Mo, "Preparation and optical absorption of dispersions of nano-TiO₂/MMA (methylmethacrylate) and nano-TiO₂/PMMA (polymethylmethacrylate)", *Materials Research Bulletin*, Vol. 34, pp. 701-709, 1999.
- ⁶¹ M. Avella, M. E. Errico, E. Martuscelli, "Novel PMMA/CaCO₃ nanocomposites abrasion resistant prepared by an in situ polymerization process", *Nano Letters*, Vol. 1, pp. 213-217, 2001.
- ⁶² A. B. R. Mayer, "Formation of noble metal nanoparticles within a polymeric matrix: nanoparticle features and overall morphologies", *Materials Science & Engineering C. Biomimetic Materials, Sensors and Systems*, Vol. 6, pp.155-166, 1998.
- ⁶³ A. Roescher, M. Möller, "Stabilization of gold nanoparticles in toluene by styrene/ethyleneoxide block copolymer II", *Polymeric Materials Science and Engineering*, Vol. 73, 156-159, 1995.
- ⁶⁴ M. Antonietti, E. Wenz, L. M. Bronstein, M. Seregina, "Synthesis and characterization of noble metal colloids in block copolymer micelles", *Advanced Materials*, Vol.7, pp. 1000-1005, 1995.
- ⁶⁵ M. Seregina, L. M. Bronstein, O. A. Platonova, D. M. Chernyshov, P. M. Valetsky, E. Wenz, M. Antonietti, "Preparation of noble-metal colloids in block copolymer micelles and their catalytic properties in hydrogenation", *Chemistry of Materials*, Vol. 9, pp.923-931, 1997.
- ⁶⁶ A. B. R. Mayer, J. E. Mark, R. E. Morris, "Palladium and platinum nanocatalysts protected by amphiphilic block copolymers", *Polymer Journal*, Vol. 30, pp.197-205, 1998.
- ⁶⁷ S. Wang, M. Wang, Y. Lei, L. Zhang, "'Anchor effect" in poly(styrene maleic anhydride)/TiO₂ nanocomposites", *Journal of Materials Science Letters*, Vol. 8, pp. 2009-2012, 1999.

-
- ⁶⁸ L. Quaroni, G. Chumanov, "Preparation of polymer-coated functionalized silver nanoparticles," *Journal of the American Chemical Society*, Vol. 121, pp. 10642-10643, 1999.
- ⁶⁹ T. von Werne, T. E. Patten, "Preparation of structurally well-defined polymer-nanoparticle hybrids with controlled/living radical polymerizations", *Journal of the American Chemical Society*, Vol. 121, pp. 7409-7410, 1999.
- ⁷⁰ P. T. Hammond, "Form and function in multilayer assembly: New applications at the nanoscale," *Advanced Materials*, Vol. 16, pp. 1271-1293, 2004.
- ⁷¹ M. F. Frechette, M. L. Trudeau, H. D. Alamdari, S. Boily, "Introductory remarks on nanodielectrics," *IEEE Transactions on Dielectrics and Electrical Insulation*, Vol. 11, pp. 808-818, 2004.
- ⁷² L. Nicolais and G. Carotenuto, "Metal-Polymer Nanocomposites", Hoboken, New Jersey: John Wiley & Sons, Inc., 2005.
- ⁷³ K. Uchino, E. Sadanaga, T. Hirose, "Dependence of the crystal-structure on particle-size in BaTiO₃", *Journal of the American Ceramic Society*, Vol. 72, pp.1555-1558, 1989.
- ⁷⁴ M. R. Leonard, A. Safari, "Crystallite and grain size effects in BaTiO₃", *Proceedings of the IEEE 10th International Symposium on Ferroelectric Applications*, 2, pp.1003-1005, 1996.
- ⁷⁵ S. K. Bhattacharya, R. R. Tummala, "Next generation integral passives: materials, processes, and integration of resistors and capacitors on PWB substrates", *Journal of Materials Science: Materials in Electronics*, Vol. 11, pp. 253-268, 2000.
- ⁷⁶ B. Ellis, "Chemistry and Technology of Epoxy Resins", Glasgow: Blackie Academic & Professional, 1993.
- ⁷⁷ C. A. May, "Epoxy Resins: Chemistry and Technology", 2nd Ed., New York: Marcel Dekker, Inc., 1988.
- ⁷⁸ J. J. Harris, S. C. Temin, "Proposed mechanism for the curing of epoxy resins with amine-lewis acid complexes or salts", *Journal of Applied Polymer Science*, Vol. 10, pp. 523-534, 1966.
- ⁷⁹ E. P. Plueddemann, "Silane Coupling Agents", New York: Plenum Press, 1982.
- ⁸⁰ D. Kumar, R. C. Sharma, "Advances in Conductive Polymers", *European Polymer Journal*, Vol. 34 (8), pp. 1053-1060, 1998.

-
- ⁸¹ Y. Wei, X. Tang, Y. Sun, W. W. Focke, "A Study of the Mechanism of Aniline Polymerization," *Journal of Polymer Science Part A-Polymer Chemistry*, Vol. 27, pp. 2385-2396, 1989.
- ⁸² A. J. Epstein, "Conductive polymers and plastics in industrial application", in: *Conductive Polymers and Plastics in Industrial Applications*, L. Rupprecht Ed., pp. 1-9, William Andrew Inc., 1999.
- ⁸³ M. G. Han, S. S. Im, "Processable conductive blends of polyaniline/polyimide", *Journal of Applied Polymer Science*, Vol. 67, pp. 1863-1870, 1998.
- ⁸⁴ Y. Cao, P. Smith, A. J. Heeger, "Counterion induced processibility of conducting polyaniline and of conducting polyblends of polyaniline in bulk polymers," *Synthetic Metals*, Vol. 48, pp. 91-97, 1992.
- ⁸⁵ M. Hu, X. Wang, G. V. Hartland, V. Salgueirino-Maceira, L. M. Liz-Marzan, "Heat dissipation in gold-silica core-shell nanoparticles", *Chemical Physics Letters*, Vol. 372, pp. 767-772, 2003.
- ⁸⁶ C. Querner, P. Reiss, J. Bleuse, A. Pron, "Chelating ligands for nanocrystals' surface functionalization", *Journal of the American Chemical Society*, Vol. 126, pp. 11574-11582, 2004.
- ⁸⁷ M. C. Schlamp, X. G. Peng, A. P. Alivisatos, "Improved efficiencies in light emitting diodes made with CdSe(CdS) core/shell type nanocrystals and a semiconducting polymer", *Journal of Applied Physics*, Vol. 82, pp. 5837-5842, 1992.
- ⁸⁸ W. J. Borland, S. Ferguson, "Embedded passive components in printed wiring boards: a technology review", *CircuiTree*, March 2001.
- ⁸⁹ D. K. Ferry, S. M. Goodnick, "Transport in Nanostructures", Longdon: Cambridge University Press, 1997.
- ⁹⁰ C. A. Berven, L. Clarke, J. L. Mooster, M. N. Wybourne, J. E. Hutchison, "Defect-tolerant single-electron charging at room temperature in metal nanoparticle decorated biopolymers", *Advanced Materials*, Vol.13, pp. 109-113, 2001.
- ⁹¹ Q. Feng, Z. Dang, N. Li, X. Cao, "Preparation and dielectric property of Ag/PVA nano-composite", *Materials Science & Engineering. B*, Vol. 99, pp. 325-328, 2003.
- ⁹² L. Tang, P. Du, Gao. Han, W. Weng, G. Zhao, G. Shen, "Effect of dispersed Ag on the dielectric properties of sol-gel derived PbTiO₃ thin films on ITO/glass substrate", *Surface & Coatings Technology*, Vol. 167, pp.177-180, 2003.

-
- ⁹³ S. Pothukuchi, Y. Li, C. P. Wong, "Development of a novel polymer-metal nanocomposite obtained through the route of in situ reduction for integral capacitor application", *Journal of Applied Polymer Science*, Vol. 93, pp. 1531-1538, 2004.
- ⁹⁴ Z. Zhang, L. Zhang, S. Wang, W. Chen, Y. Lei, "A convenient route to polyacrylonitrile/silver nanoparticle composite by simultaneous polymerization-reduction approach", *Polymer*, Vol. 42, pp. 8315-8318, 2001.
- ⁹⁵ L. Zhi, T. Zhao, Y. Yu, "Preparation of phenolic resin/silver nanocomposites via in situ reduction", *Scripta Mater*, Vol. 47, pp. 875-879, 2002.
- ⁹⁶ A. Taylor, "X-ray Metallography", New York: John Wiley & Sons, Inc, 1961.
- ⁹⁷ L. Clarke, M. N. Wybourne, L. O. Brown, J. E. Hutchison, M. Yan, S. X. Cai, J. F. W. Keana, "Room-temperature Coulomb-blockade-dominated transport in gold nanocluster structures," *Semiconductor Science and Technology*, Vol. 13, pp. A111-a114, 1998.
- ⁹⁸ C. A. Berven, L. Clarke, J. L. Mooster, M. N. Wybourne, J. E. Hutchison, "Defect-tolerant single-electron charging at room temperature in metal nanoparticle decorated biopolymers," *Advanced Materials*, Vol. 13, pp. 109-113, 2001.
- ⁹⁹ A. Facchetti, M. H. Yoon, T. J. Marks, "Gate dielectrics for organic field-effect transistors: New opportunities for organic electronics", *Advanced Materials*, Vol. 17, pp. 1705-1725, 2005.
- ¹⁰⁰ Z. M. Dang, C. W. Nan, D. Xie, Y. H. Zhang, S. C. Tjong, "Dielectric behavior and dependence of percolation threshold on the conductivity of fillers in polymer-semiconductor composites", *Applied Physics Letters*, Vol. 85, pp. 97-99, 2004.
- ¹⁰¹ T. K. Saul, T. Pal, "Size controlled synthesis of gold nanoparticles using photochemically prepared seed particles", *Journal of Nanoparticle Research*, Vol. 3, pp. 257-261, 2001.
- ¹⁰² S. K. Ghosh, T. Pal, "Evolution of gold nanoparticles in micelle by UV-irradiation: a conductometric study", *Current Science*, Vol. 84 (6), pp. 791-795, 2003.
- ¹⁰³ A. Pal, "Photoinitiated gold sol generation in aqueous Triton X-100 and its analytical application for spectrophotometric determination of gold", *Talanta*, Vol. 46, pp. 583-587, 1998.
- ¹⁰⁴ T. K. Sau, T. Pal, "Size regime dependent catalysis by gold nanoparticles for the reduction of eosin", *Journal of Physical Chemistry B*, Vol. 105 (38), pp. 9266-9272, 2001.

-
- ¹⁰⁵ M. Roy, J. K. Nelson, R. K. MacCrone, L. S. Schadler, "Polymer nanocomposite dielectrics-the role of the interface", IEEE Transactions on Dielectrics and Electrical Insulation, Vol. 125, pp. 629-642, 2005.
- ¹⁰⁶ E. Tuncer, I. Sauers, D. R. James, A. R. Ellis, M. P. Paranthaman, A. Goyal, K. L. More, "Enhancement of dielectric strength in nanocomposites", Nanotechnology, , 18, pp. 325704, 2007.
- ¹⁰⁷ J. K. Nelson, J. C. Fothergill, "Internal charge behavior of. nanocomposites", Nanotechnology, Vol. 15, pp. 586-595, 2004.
- ¹⁰⁸ J. J. O'Dwyer, "The Theory of Dielectric Breakdown of Solids", London, England: Oxford University Press, 1964.
- ¹⁰⁹ R. C. Smith, C. Liang, M. Landry, J. K. Nelson, L. S. Schadler, "The mechanisms leading to the useful electrical properties of polymer nanodielectrics", IEEE Transactions on Dielectrics and Electrical Insulation, Vol. 15, pp. 187-196, 2008.
- ¹¹⁰ M. F. Frechette, W. R. Clive, "On molecular dielectric in their role in shaping and controlling annodielectrics", IEEE Conference on Electrical Insulation and Dielectric Phenomena, pp. 333-337, 2006.
- ¹¹¹ M. F. Frechette, W. R. Clive, "The role of molecular dielectric in shaping the interface of polymer nanodielectrics", IEEE Conference on Electrical Insulation and Dielectric Phenomena, pp. 279-285, 2007.
- ¹¹² T. J. Lewis, "Interface and nanodielectric are synonymous", International Conference on Solid Dielectrics, Toulouse, France, July 5-9, 2004.
- ¹¹³ D. L. Ma, R. W. Siegel, J. I. Hong, L. S. Schadler, E. Martensson, C. Onneby, "Influence of nanoparticle surfaces on the electrical breakdown strength of nanoparticle-filled low-density polyethylene," Journal of Materials Research, Vol. 19 pp. 857-863, 2004.
- ¹¹⁴ D. L. Ma, T. A. Hugener, R. W. Siegel, A. Christerson, E. Martensson, C. Onneby, L. S. Schadler, "Influence of nanoparticle surface modification on the electrical behaviour of polyethylene nanocomposites," Nanotechnology, Vol. 16, pp. 724-731, 2005.
- ¹¹⁵ M. Roy, J. K. Nelson, R. K. MacCrone, L. S. Schadler, C. W. Reed, R. Keefe, W. Zenger, "Polymer nanocomposite dielectrics-The role of the interface," IEEE Transactions on Dielectrics and Electrical Insulation, Vol. 12, pp. 629-643, 2005.

-
- ¹¹⁶ T. Desai, P. Keblinski, S. K. Kumar, "Molecular dynamics simulations polymer transport in nanocomposites", *Journal of Chemical Physics*, Vol. 122, pp. 134910, 2005.
- ¹¹⁷ T. Tanaka, M. Kozako, N. Fuse, Y. Ohki, "Proposal of a multi-core model for polymer nanocomposite dielectrics", *IEEE Transactions on Dielectrics and Electrical Insulation*, Vol. 12, pp. 669-681, 2005.
- ¹¹⁸ I. J. Youngs, "Exploring the universal nature of electrical percolation exponents by genetic algorithm fitting with general effective medium theory", *Journal of Physics D: Applied Physics*, Vol. 35, pp. 3127-3137, 2002.
- ¹¹⁹ C. W. Nan, "Physics of inhomogeneous inorganic materials", *Progress in Materials Science*, Vol. 37, pp. 1-116, 1993.
- ¹²⁰ S. Panigrahi, S. Praharaj, S. Basu, S. K. Ghosh, S. Jana, S. Pande, T. Vo-Dinh, H. Jiang, T. Pal, "Self-assembly of silver nanoparticles: Synthesis, stabilization, optical properties, and application in surface-enhanced Raman scattering," *Journal of Physical Chemistry B*, Vol.110, pp. 13436-13444, 2006.
- ¹²¹ D. Kumar, R. C. Sharma, "Advances in conductive polymers", *European Polymer Journal*, Vol. 34, pp. 1053-1060, 1998.
- ¹²² P. Tsotra, K. Friedrich, "Thermal, mechanical, and electrical properties of epoxy resin/polyaniline-dodecylbenzenesulfonic acid blends," *Synthetic Metals*, Vol. 143, pp. 237-242, 2004.
- ¹²³ P. Tsotra, O. Gryshchuk, K. Friedrich, "Morphological studies of epoxy/polyaniline blends," *Macromolecular Chemistry and Physics*, Vol. 206, pp. 787-793, 2005.
- ¹²⁴ P. Dutta, S. Biswas, S. K. De, "Dielectric relaxation in polyaniline-polyvinyl alcohol composites," *Materials Research Bulletin*, Vol. 37, pp. 193-200, 2002.
- ¹²⁵ C. Chwang, C. Liu, S. Huang, D. Chao, S. Lee, "Synthesis and characterization of high dielectric constant polyaniline/polyurethane blends," *Synthetic Metals*, Vol. 142, pp. 275-281, 2004.
- ¹²⁶ W. C. Chiou, D. Y. Yang, J. L. Han, S. N. Lee, "Synthesis and characterization of composites of polyaniline and polyurethane-modified epoxy," *Polymer International*, Vol. 55, pp. 1222-1229, 2006.
- ¹²⁷ M. Tabellout, K. Fatyeyeva, P.-Y. Baillif, J.-F. Bardeau, A. A. Pud, "The influence of the polymer matrix on the dielectric and electrical properties of conductive polymer

-
- composites based on polyaniline”, *Journal of Non-Crystalline Solids*, Vol. 351, pp. 2835-2841, 2005.
- ¹²⁸ N. Kohut-Svelko, F. Dinant, S. Magana, G. Clisson, J. Francois, C. Dagron-Lartigau, S. Reynaud, "Overview of the preparation of pure polyaniline and conductive composites in dispersed media and by thermal processes: from laboratory to semi-industrial scale," *Polymer International*, Vol. 55, pp. 1184-1190, 2006.
- ¹²⁹ H. Deligoz, B. Tieke, "Conducting composites of polyurethane resin and polypyrrole: Solvent-free preparation, electrical, and mechanical properties," *Macromolecular Materials and Engineering*, Vol. 291, pp. 793-801, 2006.
- ¹³⁰ V. X. Moreira, F. G. Garcia, B. G. Soares, "Conductive epoxy/amine system containing polyaniline doped with dodecylbenzenesulfonic acid," *Journal of Applied Polymer Science*, Vol. 100, pp. 4059-4065, 2006.
- ¹³¹ X. Yang, T. Zhao, Y. Yu, Y. Wei, "Synthesis of conductive polyaniline/epoxy resin composites: doping of the interpenetrating network”, *Synthetic Metals*, Vol. 142, pp. 57-61, 2004.
- ¹³² W. Łuzny, E. Banka, "Relations between the structure and electric conductivity of polyaniline protonated with camphorsulfonic acid," *Macromolecules*, Vol. 33, pp. 425-429, 2000.
- ¹³³ M. G. Han, S. S. Im, "Morphological study of conductive polyaniline/polyimide blends. I. Determination of compatibility by small-angle X-ray scattering method," *Polymer*, Vol. 42, pp. 7449-7454, 2001.
- ¹³⁴ J. Jang, J. Bae, K. Lee, "Synthesis and characterization of polyaniline nanorods as curing agent and nanofiller for epoxy matrix composite," *Polymer*, Vol. 46, pp. 3677-3684, 2005.
- ¹³⁵ Q. H. Yang, S. G. Wei, G. X. Cheng, "Preparation of conductive polyaniline/epoxy composite," *Polymer Composites*, vol. 27, pp. 201-204, 2006.
- ¹³⁶ C. C. Han, W. Lawrence, "Process for forming dispersions or solutions of electrically conductive conjugated polymers in a polymeric or liquid phase”, US Patent 5378404, 1995.
- ¹³⁷ W. J. Bae, W. H. Jo, Y. H. Park, "Preparation of polystyrene/polyaniline blends by in situ polymerization technique and their morphology and electrical property”, *Synthetic Metals*, Vol. 132, pp. 239-242, 2003.

-
- ¹³⁸ Y. Fu, R. A. Weiss, "In situ polymerization of aniline within lightly sulfonated polystyrene", *Synthetic Metals*, Vol. 84, pp. 129-130, 1997.
- ¹³⁹ Y. Xia, A. G. MacDiarmid, "Camphorsulfonic acid fully doped polyaniline emeraldine salt: In situ observation of electronic and conformational changes induced by organic vapors by an ultraviolet/visible/near-infrared spectroscopic method," *Macromolecules*, Vol. 27, pp. 7212-7214, 1994.
- ¹⁴⁰ P. Tsotra, K. G. Gatos, O. Gryshchuk, K. Friedrich, "Hardener type as critical parameter for the electrical properties of epoxy resin/polyaniline blends," *Journal of Materials Science*, Vol. 40, pp. 569-574, 1995.
- ¹⁴¹ T. Hanai, "Electrical properties of emulsions", *Emulsion Science*, P. Sherman Ed., London: Academic, 1968.
- ¹⁴² N. Bowler, "Effects of lossy, layered filler particles on the bulk permittivity of a composite material", *Journal of Physics D.: Applied Physics*, Vol. 37, pp. 326-333, 2004.
- ¹⁴³ N. Hartfield, "Bulk permittivity of a composite with coated spheroidal filler particles", *Journal of Materials Science*, Vol. 35, pp. 5809-5816, 2000.
- ¹⁴⁴ D. Lee, M. F. Rubner, R. E. Cohen, "Formation of nanoparticle-loaded microcapsules based on hydrogen-bonded multilayers," *Chemistry of Materials*, Vol. 17, pp. 1099-1105, 2005.
- ¹⁴⁵ G. Decher, "Fuzzy nanoassemblies: Toward layered polymeric multicomposites," *Science*, Vol. 277, pp. 1232-1237, 1997.
- ¹⁴⁶ S. Y. Yang, D. Lee, R. E. Cohen, M. F. Rubner, "Bionert solution-cross-linked hydrogen-bonded multilayers on colloidal particles", *Langmuir*, Vol. 20, pp. 5978-5981, 2004.
- ¹⁴⁷ O. Crespo-Biel, B. Dordi, D. N. Reinhoudt, J. Huskens, "Self-assembled organic/inorganic multilayers via alternating adsorptions of guest- and host-functionalized molecules and particles using multivalent supramolecular interactions", *Journal of American Chemical Society*, Vol. 127, pp. 7594-7600, 2005.
- ¹⁴⁸ H. Chen, G. Zeng, Z. Wang, X. Zhang, M. Peng, L.-Z. Wu, C.-H. Tung, "To combine precursor assembly and layer-by-layer deposition for incorporation of single-charged species: nanocontainers with charge-selectivity and nanoreactors", *Chemistry of Materials*, Vol. 17, pp. 6679-6685, 2005.

-
- ¹⁴⁹ D. Yoo, S. S. Shiratori, M. F. Rubner, "Controlling bilayer composition and surface wettability of sequentially adsorbed multilayers of weak polyelectrolytes," *Macromolecules*, Vol. 31, pp. 4309-4318, 1998.
- ¹⁵⁰ S. S. Shiratori, M. F. Rubner, "pH-dependent thickness behavior of sequentially adsorbed layers of weak polyelectrolytes," *Macromolecules*, Vol. 33, pp. 4213-4219, 2000.
- ¹⁵¹ S. T. Dubas, J. B. Schlenoff, "Factors controlling the growth of polyelectrolyte multilayers," *Macromolecules*, Vol. 32, pp. 8153-8160, 1999.
- ¹⁵² M. Q. Zhao, R. M. Crooks, "Dendrimer-encapsulated Pt nanoparticles: Synthesis, characterization, and applications to catalysis," *Advanced Materials*, Vol. 11, pp. 217-220, 1999.
- ¹⁵³ J. A. He, R. Valluzzi, K. Yang, T. Dolukhanyan, C. M. Sung, J. Kumar, S. K. Tripathy, L. Samuelson, L. Balogh, D. A. Tomalia, "Electrostatic multilayer deposition of a gold-dendrimer nanocomposite," *Chemistry of Materials*, Vol. 11, pp. 3268-3274, 1999.
- ¹⁵⁴ W. Schrof, S. Rozouvan, E. Van Keuren, D. Horn, J. Schmitt, G. Decher, "Nonlinear optical properties of polyelectrolyte thin films containing gold nanoparticles investigated by wavelength dispersive femtosecond degenerate four wave mixing (DFWM)," *Advanced Materials*, Vol. 10, pp. 338-341, 1998.
- ¹⁵⁵ D. L. Feldheim, K. C. Grabar, M. J. Natan, T. E. Mallouk, "Electron transfer in self-assembled inorganic polyelectrolyte/metal nanoparticle heterostructures," *Journal of the American Chemical Society*, Vol. 118, pp. 7640-7641, 1996.
- ¹⁵⁶ Y. Liu, Y. Wang, R. O. Claus, "Layer-by-layer ionic self-assembly of Au colloids into multilayer thin-films with bulk metal conductivity", *Chemical Physics Letters*, Vol. 298, pp. 315-319, 1998.
- ¹⁵⁷ T. C. Wang, M. F. Rubner, R. E. Cohen, "Polyelectrolyte multilayer nanoreactors for preparing silver nanoparticle composites: Controlling metal concentration and nanoparticle size," *Langmuir*, Vol. 18, pp. 3370-3375, 2002.
- ¹⁵⁸ J. H. Dai, M. L. Bruening, "Catalytic nanoparticles formed by reduction of metal ions in multilayered polyelectrolyte films," *Nano Letters*, Vol. 2, pp. 497-501, 2002.